5-2012

Homogenization of Large-Scale Movement Models in Ecology with Application to the Spread of Chronic Wasting Disease in Mule Deer

Martha J. Garlick
Utah State University

HOMOGENIZATION OF LARGE-SCALE MOVEMENT MODELS IN ECOLOGY WITH APPLICATION TO THE SPREAD OF CHRONIC WASTING DISEASE IN MULE DEER

by

Martha J. Garlick

A dissertation submitted in partial fulfillment
of the requirements for the degree

of

DOCTOR OF PHILOSOPHY

in

Mathematical Sciences

Approved:

Dr. James A. Powell Co-Major Professor	Dr. Mevin B. Hooten Co-Major Professor
Dr. Brynja Kohler Committee Member	Dr. Nghiem Nguyen Committee Member
Dr. David Koons Committee Member	Dr. Mark R. McLellan Vice President for Research and Dean of the School of Graduate Studies

UTAH STATE UNIVERSITY
Logan, Utah

2012

ABSTRACT

Homogenization of Large-Scale Movement Models in Ecology
with Application to the Spread of Chronic
Wasting Disease in Mule Deer

by

Martha J. Garlick, Doctor of Philosophy
Utah State University, 2012

Co-Major Professors: Dr. James A. Powell and Dr. Mevin B. Hooten
Department: Mathematics and Statistics

A difficulty in using diffusion models to predict large-scale animal population dispersal is that individuals move differently based on local information (as opposed to gradients) in differing habitat types. This can be accommodated by using ecological diffusion. However, real environments are often spatially complex, limiting application of a direct approach. Homogenization for partial differential equations has long been applied to Fickian diffusion (in which average individual movement is organized along gradients of habitat and population density). In this work, we derive a homogenization procedure for ecological diffusion, which allows us to determine the impact of small-scale (10-100 m) habitat variability on large-scale (10-100 km) movement, and apply it to models for chronic wasting disease (CWD) in mule deer.

CWD is an infectious prion disease that affects members of the Cervidae family. It is a slow-developing, fatal disease, which is rare in the free-ranging deer population of Utah. We first present a simple spatial disease model to illustrate our homogenization procedure and the use of ecological diffusion as a way to connect animal movement with disease

spread. Then we develop a more disease-specific sex-structured model for the spread of CWD, incorporating both horizontal and environmental transmission pathways. We apply our homogenization technique to greatly reduce the computational load for a simulation of disease spread from the La Sal Mountains to the Abajo Mountains of Southeast Utah. We use the averaged coefficients from the homogenized model to explore asymptotic invasion speed and critical population size for portions of our study area. Lastly, we describe the estimation of motilities for the disease-specific model from GPS location data, using a continuous-time correlated random walk model.

(127 pages)

PUBLIC ABSTRACT

Homogenization of Large-Scale Movement Models in Ecology with Application to the Spread of Chronic Wasting Disease in Mule Deer

Chronic wasting disease (CWD) is a transmissible spongiform encephalopathy (TSE) that affects deer, elk, and moose. TSEs are prion diseases which include mad cow disease and scrapie in sheep and goats. The disease agent is a misshapen protein called a prion, which causes lesions in the brain, and to date, there is no cure. CWD is a slow-developing, fatal disease, which is rare in the free-ranging mule deer population of Utah. Infected deer shed prions into the environment through saliva, feces, and decaying carcasses. These prions remain infective in soils for many years and healthy deer may contract CWD by ingesting them while grazing, as well as through direct contact with infected deer. CWD positive deer shed prions into the environment for as long as two years before they appear visibly sick. This complicates detection and control of this potentially devastating disease.

Mathematical modeling is one of the tools used in analyzing how wildlife diseases spread across the landscape. Historically, diffusion models with constant coefficients have been used to predict spread. They are limited, however, in their ability to connect disease spread to how animals move across differing habitats. Individuals make movement decisions based on local information, i.e. they move quickly through areas that do not provide needed resources and linger in areas that do. Ecological diffusion is a form of spatially varying diffusion that accommodates this through a motility coefficient. In this work we develop two disease models with ecological diffusion: a simple, general disease model and a sex-specific CWD model. We use GPS location data gathered from collared mule deer in the La Sal mountains of Utah (2005-2006) to estimate the motility (a measure of how animals move) for each land cover type in Southeast Utah to use in our models.

Real environments are often spatially complex, limiting application of a direct approach to modeling with ecological diffusion. Here we derive a homogenization procedure for ecological diffusion, which allows us to determine the impact of small-scale (10-100 m) habitat variability on large-scale movement (10-100 km). Our homogenized models take 1/10000 the computational time to solve than small scale ecological diffusion models. Also the average coefficients in the homogenized equations can be used in analysis of speed of disease spread and critical population size necessary for the speed of spread to be zero. This work is important from a disease management point of view. Possible applications are identification of barriers or corridors for disease spread and estimation of population size needed to control spread from disease hotspots. These methods may also be applied to other dispersal problems, such as invasive species, insect invasions, and escaped genetically modified organisms.

Martha J. Garlick

ACKNOWLEDGMENTS

I would like to thank my co-advisors, James Powell and Mevin Hooten, for their guidance, patience, and insight. I also thank Leslie McFarlane for sharing her knowledge of chronic wasting disease and mule deer, the Utah Division of Wildlife Resources for providing telemetry data, and Ben Crabb and John Lowry for providing landcover data. This research was partially funded by USGS, grant number 1434-06HQRU15555.

Martha J. Garlick

CONTENTS

LIST OF TABLES

LIST OF FIGURES

CHAPTER 1

INTRODUCTION

Application of diffusion models to biological problems has a long history. Fisher pioneered their use in genetics [20], while Turing developed their use in modeling pattern formation [66, 94, 99]. Skellam combined the diffusive dispersal of organisms with population dynamics via reaction-diffusion equations of the form $\frac{\partial u}{\partial t} = D\nabla^2 u + f(u)$, where D is the rate of random movement (diffusion) of organisms across the landscape and the function, $f(u)$, describes the population density at a particular time and place [90]. Models of this type assume diffusion of organisms over a homogeneous landscape [108], and have been used to explore critical patch size [46] and biological invasions [2, 28, 90]. Patlak added biological realism by deriving the diffusion approximation for correlated and biased random walks [76] . Turchin and Thoeny facilitated the use of diffusion models in ecology with their work in analyzing data from mark-recapture experiments [98].

Because diffusion is based on a random walk, it has been considered only applicable to organisms with simple movement patterns [73]. However, when applied at a large enough scale, it has been useful in modeling more complex behavior such as coyote home range use [65]. Diffusion models with constant coefficients were first applied to epidemiology by Kendall [45] and have been used to study the spread of wildlife diseases for many years, such as rabies in fox [42, 67], foot and mouth disease in feral pigs [77], and conjunctivitis in house finches [34].

Realistically, landscapes are heterogeneous, requiring a connection between habitat type and animal movement [43]. The relationship between small-scale movement through heterogenous landscapes and large-scale dispersal of organisms is key to understanding the spatial spread of wildlife diseases [34]. In fact, environments can act as the principal organizers for spatial processes [5, 35, 82]. The effect of heterogeneous landscapes on the dispersal of populations and the spread of diseases has been studied in the movement of hispid cotton rats [9], the abundance of scarab beetles [3], and the spread of feline leukemia

virus [21]. Cantrell and Cosner examined the effect of fragmented landscapes on dispersal [10], and Ovaskainen and Cornell explored the need for diffusion processes to be discontinuous at habitat boundaries [75], necessitating the need to classify landscapes in order to determine habitat-specific diffusion coefficients [73]. Other approaches to connect landscape with spatial spread include circuit theory [55] and explicit network models [8].

In order for the dispersal of organisms to reflect heterogeneous landscapes, variable diffusion rates are needed [43]. Two types of diffusion with variable coefficients are Fickian diffusion and ecological diffusion [97]. Fickian diffusion, of the form $\frac{\partial u}{\partial t} = \nabla[D\nabla u]$, where D is the spatially varying diffusion coefficient, is derived from Fick's Law [51], which says flux is proportional to the gradient. It is used to model the distribution of organisms when they move from high densities to low densities at a rate proportional to the density gradient [29]. Fickian diffusion eventually distributes organisms evenly across the landscape regardless of habitat type, when a zero density gradient has been reached [97]. It has been widely used in ecological models [21, 47, 50].

Although Fickian diffusion may be appropriate in the case of simple organisms, most animals do not diffuse like particles in heterogeneous environments [70]. Rather they are much more likely to aggregate in habitats that provide needed resources and avoid or move quickly through areas that are inhospitable. Ecological diffusion, represented by $\frac{\partial u}{\partial t} = \nabla^2[\mu u]$, accommodates this variation in motility and is appropriate when organisms make local decisions regarding movement. The motility parameter, μ, represents the rate at which organisms choose to leave a habitat patch, irrespective of density gradients [97]. Thus ecological diffusion gives an eventual distribution of animals which is inversely proportional to the motility and allows for distinct population differences at habitat boundaries. A derivation of the ecological diffusion equation from a random walk is included in Turchin [97].

Even though diffusion equations with variable coefficients are recognized as necessary to reflect the heterogeneity of landscapes [70], they can be daunting to implement, especially at large spatial scales. This is chiefly due to the added mathematical complication

and lack of data to derive motility coefficients for each landscape type in an area of interest. Dobzhansky et al. [16] were the first to attempt to incorporate spatial heterogeneity into an ecological diffusion model. They divided a study area for the movement of fruit flies (*Drosophila pseudoobscura*) into cells, classified into six habitat types, and estimated a diffusion coefficient for each type. The limited computing capacity of the time kept them from obtaining reliable parameter estimates [73]. Today, increased computing power and homogenization techniques can help deal with the mathematical complication of using variable coefficients and advances in telemetry have enhanced data collection [72].

Homogenization of partial differential equations (PDEs) is a technique for facilely accommodating small-scale variability in diffusion coefficients for large-scale simulation [15]. It has been applied to Fickian diffusion models in engineering applications, such as heat transfer in composite materials, for decades. In ecology such techniques have been used to model seed dispersal [80], the spread of biofilms [14], the spread of feline leukemia [21], and the relationship between dispersal ability and habitat fragmentation [15]. Homogenization uses the method of multiple scales [30] to approximate PDEs with rapidly-varying coefficients with similar PDEs with averaged coefficients. One advantage of this technique is that the 'homogenized' PDE is framed on large spatial and temporal scales, while preserving the influence of the small scale variability in the averages. In this work we derive a homogenization procedure for ecological diffusion and apply it to the spread of chronic wasting disease (CWD) in mule deer.

CWD is a contagious transmissible spongiform encephalopathy (TSE) in North American cervids, namely mule deer (*Odocoileus hemionus*), white-tailed deer (*Odocoileus virginianus*), elk (*Cervus elaphus*), and moose (*Alces alces shirasi*) [4]. Like all other TSEs, a misfolded cellular prion protein is believed to be the disease agent [89]. However, CWD has the distinction of being the only TSE known to affect free-ranging species [106]. It is a slow-developing, always fatal disease; infected mule deer may live 12-24 months before showing outward signs of infection. Clinical symptoms include weight loss, excessive salivation, and behavioral changes, such as hyperexcitability, lack of awareness, and repetitive

walking [105].

CWD transmission has been established from empirical studies as being horizontal [12]. The disease may be contracted by direct contact with infected deer [61], potentially through saliva [52], as well as indirectly through contact with contaminated environments [37]. Prions shed into the environment through the feces, saliva, and decaying carcasses of infected deer may remain infective for many years [25, 62, 85, 102].

Data from captive mule deer studies indicate equal susceptibility of males and females to infection [62, 107]. However, observed CWD prevalence in free-ranging deer is 2-4 times higher in breeding-age males than in younger males or females [18, 57, 63]. This may be due to deer social structure and breeding behaviors [57]. Female deer form matrilinear groups that show strong fidelity to winter and summer ranges. Male deer wander more, especially during breeding season [53]. Mature male deer practice polygyny, covering a wide area searching for receptive females and testing them for receptiveness through extensive licking [24, 69]. Males also interact with each other in competition for females [49].

CWD was first discovered in Utah in 2002. There are three distinct areas where the disease has since been found, near Vernal, the La Sal mountains near Moab, and near Fountain Green. To date, there have been 54 mule deer and one elk that have tested positive. The highest prevalence rate is two percent in the buck population in the La Sal Mountains, where 38 of the 54 cases have been found [100].

Mathematical models are critical tools in assessing the impact of CWD on deer populations and analyzing different management strategies [86]. Existing mathematical models for CWD include discrete-time deterministic models [63], individual-based models [26], difference equation models [36], and SI epidemic models [58, 87, 104]. Models that incorporate the spatial aspect of disease spread have been statistical for the most part [13, 18, 41]. Statistical approaches require a large body of data, which is not available in areas where the disease is in its initial stages, such as Utah. A deterministic, process-based model does not need the same amount of data to be useful.

We present two spatial models for the spread of CWD in mule deer, using ecological

diffusion. The first model is a simple SI model with diffusion, which does not include environmental transmission. The main purpose of this model is to illustrate our homogenization technique and the connection between animal movement over heterogeneous landscapes and disease spread, using spatially varying motility coefficients. We simulate the spread of CWD in a small area of Utah including the La Sal Mountains where the disease was first detected and discuss the use of the coefficients from the homogenized model to analyze critical population size (i.e. the population size at which the speed of the wavefront of disease spread is zero) [23].

The second model is a disease-specific sex-structured model, incorporating both horizontal and environmental transmission pathways. Male and female deer are modeled separately to reflect distinct behavioral differences that may impact the spread of CWD. The motility coefficients for this model vary spatially and temporally (by season of the year), as well as by sex. Although this model is a system of partial differential equations, our homogenization procedure still applies. We use the homogenized system to simulate the spread of CWD from the La Sal Mountains to the Abajo Mountains (100 kilometers to the southwest). The parameters from the homogenized model can be used to analyze asymptotic invasive speed of spread from areas of interest, which can be important to disease management.

Motilities for the disease-specific model are estimated using landscape data and GPS movement data, collected at irregular time intervals. Traditional methods of determining motilities involve approximating mean-squared displacement over time by connecting data points with straight lines [44]. This means dividing or combining moves when data are collected at irregular time intervals, [96], which can obscure the underlying movement process [95]. To address this, we employ the methods of Johnson et al. [38, 39], which consider animal movement to be a continuous process regardless of how it is sampled.

CHAPTER 2

HOMOGENIZATION OF LARGE-SCALE MOVEMENT MODELS IN ECOLOGY [1]

2.1 Introduction

Diffusion models have been applied to biological problems for many years. Fisher [20] pioneered their use in genetics, while Turing [99], Swindale [94], and Murray [66] are among many to use them to model pattern formation. Skellam [90] greatly impacted mathematical modeling in ecology by combining the diffusive dispersal of organisms with population dynamics via reaction-diffusion equations of the form $\frac{\partial u}{\partial t} = D\nabla^2 u + f(u)$. Here D is the rate of random movement (diffusion) of organisms across the landscape and $f(u)$ is a function describing the population density at a particular time and place. This type of equation has been used to study critical patch size [46], biological invasions [2], and disease spread [42]. These models assume diffusion of organisms occurs over a homogeneous landscape [108].

Realistically, landscapes are heterogeneous, requiring diffusion rates to vary with habitat type [43]. Fickian diffusion, of the form $\frac{\partial u}{\partial t} = \nabla[D(x_1, x_2)\nabla u]$, models the distribution of organisms along habitat quality or population density gradients [29]. It is derived from Fick's Law, which states that the amount of substance that moves through a cross section of the domain at time t is proportional to its density gradient ∇u [51]. For u representing a population, organisms move from high densities to low densities at a rate proportional to the density gradient, and are advected at a speed proportional to habitat gradients. This means that the organisms are making nonlocal decisions (i.e. sensing spatial differences in either habitat or population density) as they move [97].

Fickian diffusion has been used widely in ecological models [21, 47, 50] and leads to a uniform population distribution at equilibrium, even when D varies spatially [97]. That is, according to a Fickian model (and neglecting birth and death processes), organisms are

[1] This chapter is reprinted from Martha Garlick, James Powell, Mevin Hooten, and Leslie McFarlane *Homogenization of large-scale movement models in ecology*, Bulletin of Mathematical Biology **73** (2011), 2088-2108.

just as likely to (eventually) be found in habitats that do not provide food and shelter as those which do, as well as on the boundaries of vastly different land cover types.

Although this may be appropriate for simple organisms at small scales, most animals do not diffuse like particles in heterogeneous environments [70]. They are greatly influenced by habitat type, moving slowly through landscapes that provide needed resources and more quickly through inhospitable regions and are therefore much more likely to be found some places than others. Ecological diffusion, represented by $\frac{\partial u}{\partial t} = \nabla^2[\mu(x_1, x_2)u]$, accommodates this variation in motility, predicting that animals eventually accumulate in desirable habitats and leave or avoid undesirable ones [97]. The motility parameter, μ, is analogous to the diffusion coefficient, D, in the Fickian diffusion equation, however, ecological diffusion gives an eventual distribution of animals which is inversely proportional to the motility. Ecological diffusion is appropriate when organisms make local decisions regarding movement, rather than nonlocal decisions as in the Fickian case, e.g. when their probability of moving or rate of movement depends entirely on the habitat within which they reside. Unlike Fickian diffusion, ecological diffusion supports discontinuous solutions, allowing for distinct population differences at habitat boundaries. A derivation of the ecological diffusion equation from a random walk is included in Turchin [97], and is known as the Fokker-Planck or Kolmogorov equation without an advection component [83]. A simple comparison of ecological diffusion with Fickian diffusion is shown in Figure 2.1, illustrating the aggregation of individuals in areas with low motilities (longer residence times).

Although diffusion equations with variable coefficients reflect the heterogeneity of landscapes, they can be daunting to implement in a model, particularly at large spatial scales. A technique for facilely accommodating small scale variability in diffusion coefficients for large scale simulation is homogenization. Homogenization techniques for partial differential equations (PDEs) with Fickian diffusion have been widely used in engineering applications, such as heat transfer in composite materials, for decades. In ecology they have been used in modeling such things as seed dispersal [80], the spread of biofilms [14], the spread of feline leukemia [21], and the relationship between dispersal ability and habitat fragmentation

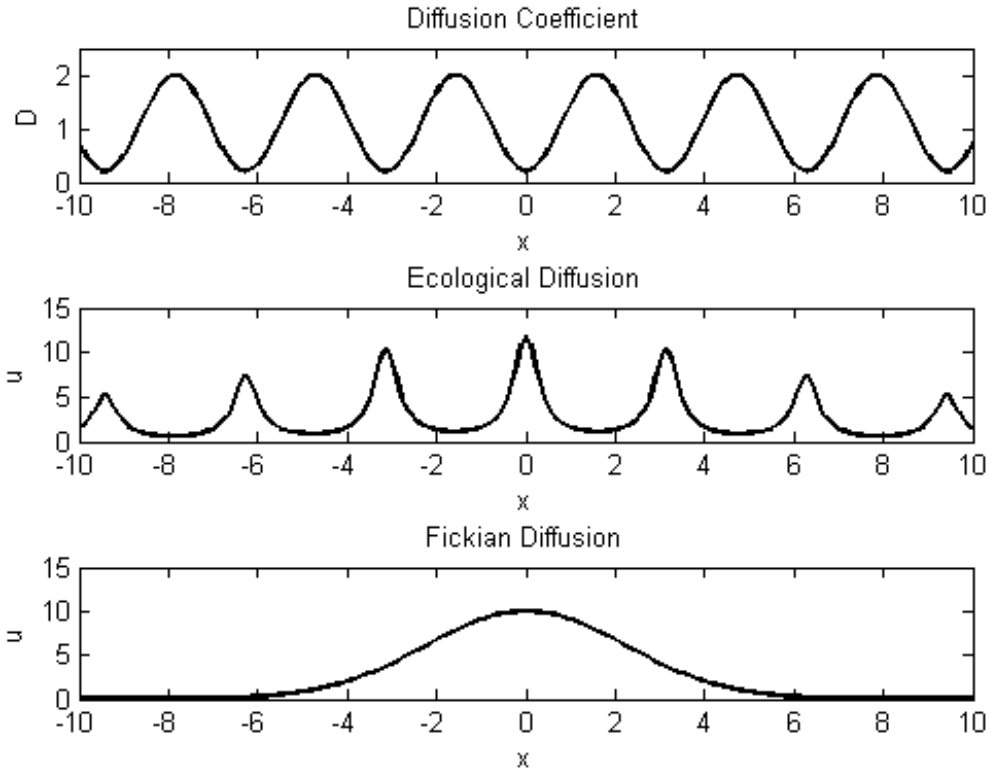

Figure 2.1: A comparison of ecological diffusion with Fickian diffusion using the same diffusion (motility) coefficient and initial condition. After the same amount of time, the distribution of animals becomes inversely proportional to the motility with ecological diffusion, while becoming smooth over the entire domain with Fickian diffusion.

[15]. The homogenization procedure, which uses the method of multiple scales [30], allows one to approximate PDEs that have rapidly-varying coefficients with similar "homogenized" PDEs having averaged coefficients. The primary advantage is that the "homogenized" PDE is framed in large scales in space and time, with the influence of the small scale variability in the averages.

Homogenized models are more efficient to solve numerically. Modeling the dispersal of organisms over a large area, such as the state of Utah, can be very computationally taxing, especially if the diffusion coefficient has variability on the scale of a meadow or stand of trees. Viewed from a suitably large spatial scale, however, many habitats have more

or less periodic structure with repetitively interspersed subpatches [21]. More generally, almost every landscape can be approximated as a section of a quasi-periodic function. This quasi-periodic structure allows us to use a homogenized PDE model to better understand a system at a large scale, while preserving the effects of fine scale variability in the diffusion coefficients. As far as we know, ecological diffusion, as defined above, has not been the subject of homogenization techniques; we will show that the homogenization technique and its effects are actually much simpler for ecological diffusion than Fickian diffusion.

Ecological diffusion and homogenization can be applied to spatial models in epidemiology. In particular, ecological diffusion is especially fitting for modeling wildlife diseases in free-ranging organisms, since the spread of a disease is linked to how hosts move and interact in a varying environment. A wildlife disease where such modeling efforts could be especially useful because of its potential impact to wildlife populations is chronic wasting disease (CWD). CWD is a contagious prion disease known to affect members of the Cervidae family which include deer (*Odocoileus* spp.), elk (*Cervus elaphus*), and moose (*Alces alces*) [4]. The disease is always fatal and in mule deer (*Odocoileus hemionus*) infected animals can live from 12-24 months before outward signs of the disease become apparent [105]. Deer-to-deer and deer-to-environment interactions are important for transmission dynamics and infectious prions can be shed into the environment from infected animals through feces, saliva and decaying carcasses where they may remain infective for many years [37, 62]. It has been suggested that over decades CWD can affect local population dynamics with possible long-term effects on ecosystems [59].

CWD was first detected in free-ranging mule deer from Utah in 2002 and is currently found in three distinct geographic areas of the state [53]. The areas found in Utah represent movement of the disease west of the Rocky Mountains and delineate the western-most boundary for distribution of CWD in the United States. To predict the impact of CWD west of the Rockies, a compartmental model would be sufficient from a disease perspective, but would not capture the spatial aspects of spread. Current spatial disease models are constrained to spread a disease or population everywhere over the domain, using Fickian

diffusion. Transmission of CWD is contingent on population densities which reflect the heterogeneity of the environment. In other words, density-dependent spatial spread is dependent on how patches of population at variable distances infect each other. This is not intuitive and requires a model incorporating ecological diffusion, to accommodate landscape variability. Here we develop a technique specifically designed to deal with spatial heterogeneity and apply it to a simple disease model. We are developing a more disease-specific CWD model with a coupled system of equations which will be the subject of a future paper. Even though the model will have increased complexity, ecological diffusion and our homogenization procedure will still apply.

To illustrate our homogenization technique we simulate the spread of CWD in mule deer in an area that includes the La Sal Mountains of Utah. Our homogenization technique introduces a way to numerically solve the model on a scale much larger (multiple kilometers) than the scale of variability (10's of meters) in the motility coefficients. Although variability in model parameters is reduced by the averaging, it turns out that homogenization of ecological diffusion returns small scale variability to the result. This preservation of small-scale population consequences, coupled with the analytic simplicity, make homogenization of ecological diffusion a very attractive technique. As we will show, the computational time is markedly reduced, while the error introduced by the homogenization procedure is asymptotically small.

2.2 Model for CWD

To illustrate the idea of homogenizing ecological diffusion, let us consider a simple spatial model for CWD in mule deer based on a general model for a disease with no recovery. What sets this model apart from other spatial epidemiology models is the use of ecological diffusion rather than diffusion with a constant coefficient as in Meade and Milner [56].

We will assume that the disease is in its initial stage, spread by direct contact of diseased individuals with healthy individuals, and always fatal. Mule deer in Utah are a managed game species, with population estimates projected using computer models. We therefore assume death from causes other than CWD is balanced by births, and we will

ignore the environmental hazard associated with CWD (which is the subject of ongoing research). Similarly, we will ignore other modeling considerations such as seasonal and sex differences in movement and age structure of the disease for purposes of developing the homogenization approach. Uninfected and infected individuals are linked as in a traditional SI model,

$$S_t = \nabla^2(\mu S) - \beta SI, \tag{2.1}$$

and

$$I_t = \nabla^2(\mu I) + \beta SI - \lambda I, \tag{2.2}$$

where S refers to the susceptible population and I refers to the infected population. The differential operator,∇^2, is the Laplacian, $\frac{\partial^2}{\partial {x_1}^2} + \frac{\partial^2}{\partial {x_2}^2}$, and the parameter, $\mu = \mu(x_1, x_2)$, is the spatially varying motility coefficient. The infection rate, β, and the rate of death from the disease, λ, may also vary spatially if behaviors are linked to habitat type. The motility, which is inversely proportional to residence time, will be low in areas where the deer linger for food and shelter, and high in the places devoid of resources [97].

In the initial stages of the spread of a disease it is appropriate to view the healthy population as predominant. When the number of infected deer is very small compared to susceptibles, $0 < I << S$, and (2.1) becomes $S_t = \nabla^2(\mu S)$, which has the steady-state solution

$$\tilde{S} = \frac{K}{\mu}, \tag{2.3}$$

where K is a constant proportional to the total number of susceptible individuals. Then the initial spread of the disease is captured by

$$I_t = \nabla^2[\mu(\boldsymbol{x})I] + \beta\tilde{S}I - \lambda I = \nabla^2[\mu(\boldsymbol{x})I] + \alpha(\boldsymbol{x})I, \tag{2.4}$$

where $\alpha(\boldsymbol{x}) = \beta\tilde{S} - \lambda = \beta\frac{K}{\mu(\boldsymbol{x})} - \lambda$ varies spatially as $\tilde{S}$ varies over the landscape. The model given in (2.4) is very general, applying to all manner of spatial invasion and dispersal situations, except using ecological diffusion.

2.3 Homogenization of a model with ecological diffusion

In order for (2.4) to reflect the connection of the spread of CWD with the movement of deer, we need to know the habitat types comprising the desired landscape and estimate a motility value for each type. The National Land Cover Database (NLCD) provided by U. S. Geological Survey Landcover Institute classifies habitat in 30×30 meter blocks [92]. If we assume those blocks form a repeating pattern over a much larger scale, say 9×9 kilometer blocks, we can regard μ as varying quickly over the small scale and much more slowly over the large scale. Viewing μ in (2.4) as varying over two different scales in this manner allows us to apply a homogenization procedure similar to the one derived for two-dimensional Fickian diffusion in Holmes [30]. However, as we will show, the result for ecological diffusion is much simpler and easier to use in computer simulations. The homogenization procedure for the one spatial dimension case is derived in Hooten et al. [32].

The easiest way to apply the homogenization procedure is to assume a quasi-periodic motility function, which allows the periodicity to vary on the large scale. We will discuss this assumption in detail in the periodicity assumption section below, showing that this assumption is much more broad then might be expected. Let the order parameter, ϵ, represent the ratio of small and large scales; for the landscape described above $\epsilon = \frac{30}{9000} = \frac{1}{300}$. Let $\boldsymbol{x}$ be the large spatial scale in two spatial dimensions, with an associated slow time scale, t. Then the small scale $\boldsymbol{y}$ is defined in relation to $\boldsymbol{x}$ by $\boldsymbol{y} = \frac{\boldsymbol{x}}{\epsilon}$. Thus $O(\epsilon)$ changes in $\boldsymbol{x}$ become $O(1)$ changes in $\boldsymbol{y}$ [80]. The fast time scale associated with $\boldsymbol{y}$ is $\tau = \frac{t}{\epsilon^2}$. The motility coefficient thus becomes a function of both spatial scales, $\mu = \mu(\boldsymbol{x}, \boldsymbol{y})$. Quasi-periodicity means there exits a vector $\boldsymbol{p(x)}$ such that

$$\mu(\boldsymbol{x}, \boldsymbol{y} + \boldsymbol{p(x)}) = \mu(\boldsymbol{x}, \boldsymbol{y}) \tag{2.5}$$

for all $\boldsymbol{x}$ and $\boldsymbol{y}$ under consideration.

2.3.1 Derivation of homogenized model

We now employ the method of multiple scales. The derivatives transform, with $\nabla \longrightarrow \nabla_x + \frac{1}{\epsilon}\nabla_y$, where the subscript indicates the variable being differentiated, and $\frac{\partial}{\partial t} \longrightarrow \frac{1}{\epsilon^2}\frac{\partial}{\partial \tau} + \frac{\partial}{\partial t} = \frac{1}{\epsilon^2}\partial_\tau + \partial_t$. Substituting the new scales and derivatives into (2.4) gives (after multiplication by ϵ^2)

$$(\partial_\tau + \epsilon^2\partial_t)I = (\nabla_y + \epsilon\nabla_x)\cdot[(\nabla_y + \epsilon\nabla_x)\mu(\boldsymbol{x},\boldsymbol{y})I] + \epsilon^2\alpha I. \tag{2.6}$$

The dependent variable, I, is now a function of t, τ, $\boldsymbol{x}$, and $\boldsymbol{y}$. We replace I in (2.6) with a power expansion in ϵ,

$$I = I_0(\boldsymbol{x},\boldsymbol{y},t,\tau) + \epsilon I_1(\boldsymbol{x},\boldsymbol{y},t,\tau) + \epsilon^2 I_2(\boldsymbol{x},\boldsymbol{y},t,\tau) + O(\epsilon^3),$$

and gather terms of common powers of ϵ.

At $O(1)$ this gives

$$\partial_\tau I_0 = {\nabla_y}^2(\mu I_0). \tag{2.7}$$

Since the term on the left hand side of (2.7) involves a derivative in the fast time scale, τ, and the equation is parabolic, the solution decays rapidly to its steady state. In fact the transient parts of the solution decay to zero as $\epsilon \to 0$ like $e^{-\frac{\mu_1 t}{L^2\epsilon^2}}$, where μ_1 is a lower bound on μ, i.e. $0 < \mu_1 < \mu$, and L^2 is the area of the largest habitat patch. Since $e^{-\frac{\mu_1 t}{L^2\epsilon^2}} << \epsilon$ for all $t > 0$, we neglect transients and solve

$${\nabla_y}^2(\mu I_0) = 0. \tag{2.8}$$

A solution for (2.8) (using periodicity in $\boldsymbol{y}$) is

$$I_0 = \frac{c(\boldsymbol{x},t)}{\mu(\boldsymbol{x},\boldsymbol{y})}, \tag{2.9}$$

with $c = c(\boldsymbol{x}, t)$ having no $\boldsymbol{y}$ dependence.

The $O(\epsilon)$ equation is

$$\partial_\tau I_1 = {\nabla_y}^2(\mu I_1) + \nabla_x \cdot [\nabla_y(\mu I_0)] + \nabla_y \cdot [\nabla_x(\mu I_0)]. \tag{2.10}$$

Substituting (2.9) into (2.10) and simplifying (noting that $\nabla_y \cdot (\mu I_0) = \nabla_y c(\boldsymbol{x}, t) = 0$), we have

$$\partial_\tau I_1 = {\nabla_y}^2(\mu I_1).$$

Considering the steady state problem as in the $O(1)$ case, the solution is of the form

$$I_1 = \frac{b(\boldsymbol{x}, t)}{\mu}.$$

Due to homogeneous boundary conditions for all orders above ϵ^0, we deduce $I_1 = 0$.

The $O(\epsilon^2)$ equation is

$$\partial_\tau I_2 + \partial_t I_0 = {\nabla_y}^2(\mu I_2) + {\nabla_x}^2(\mu I_0) + \alpha I_0. \tag{2.11}$$

Substituting (2.9) into (2.11) and considering again the steady state with respect to the fast time scale (i.e. $\partial_\tau I_2 = 0$) yields

$$\partial_t \left(\frac{c}{\mu}\right) = {\nabla_y}^2(\mu I_2) + {\nabla_x}^2 c + \alpha \frac{c}{\mu}. \tag{2.12}$$

Let $\boldsymbol{p(x)}$ in (2.5) be defined as the periodicity vector $\boldsymbol{p(x)} = [l_1(x_1), l_2(x_2)]^T$. We determine the homogenized problem by averaging each term of (2.12) over a $l_1(x_1) \times l_2(x_2)$ cell, with area $A = l_1(x_1) l_2(x_2)$, following Holmes [30]. The average of a function $v(\boldsymbol{x}, \boldsymbol{y})$ over an $l_1(x_1) \times l_2(x_2)$ cell is defined as

$$\langle v \rangle = \frac{1}{A} \int_0^{l_1(x_1)} \int_0^{l_2(x_2)} v(\boldsymbol{x}, \boldsymbol{y}) dy_1 dy_2. \tag{2.13}$$

Note that this is not the average value of the function over the entire domain. It is a local average for the current position of interest, and the region of integration depends on the (changing) local cell size.

Using the Divergence Theorem and periodicity on a cell,

$$\left\langle {\nabla_y}^2(\mu I_2)\right\rangle = \frac{1}{A}\int_{\partial\Omega_0} \boldsymbol{n}\cdot\nabla_y(\mu I_2)dS_y = 0,$$

where $\partial\Omega_0$ is the boundary of the cell, $\boldsymbol{n}$ is the outward normal vector, and dS_y is along the cell boundary. This is valid if we require $\lim_{x\uparrow x_0}(\mu_1 I) = \lim_{x\downarrow x_0}(\mu_2 I)$ and $\lim_{x\uparrow x_0}[\nabla(\mu_1 I)\cdot \boldsymbol{n}] = \lim_{x\downarrow x_0}[\nabla(\mu_2 I)\cdot\boldsymbol{n}]$ where μ_1 and μ_2 are the values of μ for two adjacent cells, x_0 is the location of their shared boundary. This means that on the boundary of cells with different motilities, the number of infected individuals that are mobile is proportional to μI. The flux of individuals over the boundary is proportional to the first derivative of μI (as opposed to μ times the derivative of I), which is a consequence of using ecological diffusion. Thus, the density of the infected population over the landscape reflects the habitat boundaries defined by the motility coefficients at the resolution of the land cover data.

Averaging the other terms in (2.12) yields

$$\left\langle \partial_t\left(\frac{c}{\mu}\right)\right\rangle = \left\langle \mu^{-1}\right\rangle \partial_t c$$

and

$$\left\langle \alpha\frac{c}{\mu}\right\rangle = \left\langle \frac{\alpha}{\mu}\right\rangle c.$$

The term ${\nabla_x}^2 c$, which has no $\boldsymbol{y}$ dependence, remains unchanged by the averaging procedure.

Equation (2.12) is now homogenized,

$$\left\langle \mu^{-1}\right\rangle \partial_t c = {\nabla_x}^2 c + \left\langle \frac{\alpha}{\mu}\right\rangle c, \tag{2.14}$$

where

$$\left\langle \mu^{-1} \right\rangle = \frac{1}{A} \int_0^{l_1(x_1)} \int_0^{l_2(x_2)} \frac{1}{\mu} dy_1 dy_2$$

and

$$\left\langle \frac{\alpha}{\mu} \right\rangle = \frac{1}{A} \int_0^{l_1(x_1)} \int_0^{l_2(x_2)} \frac{\alpha}{\mu} dy_1 dy_2.$$

Simplifying, we can write (2.14) as

$$\partial_t c = \bar{\mu} {\nabla_x}^2 c + \bar{\mu} \left\langle \frac{\alpha}{\mu} \right\rangle c, \tag{2.15}$$

where $\bar{\mu} = \frac{1}{\langle \mu^{-1} \rangle}$ is the harmonic average of $\mu(\boldsymbol{x}, \boldsymbol{y})$ over an $l_1(x_1) \times l_2(x_2)$ cell. Our homogenized equation, (2.15), is now in terms of the large spatial scale $\boldsymbol{x}$ and the slow time scale t. The small scale variability, however, still influences the leading order solution for infectives through the averages and through the definition of $c(\boldsymbol{x}, t)$. The function $c = c(\boldsymbol{x}, t)$, which is a function of the long time scale and the large spatial scale, relates to the leading order distribution of diseased animals by

$$I_0 = \frac{c(\boldsymbol{x}, t)}{\mu(\boldsymbol{x}, \boldsymbol{y})}. \tag{2.16}$$

Thus the homogenized solution reflects small scale variability (as it should), but can be solved dynamically on large time/space scales. The multiple-scale approach makes sense in the context of the spread of CWD. The spread of the disease is closely related to the movement of deer, which stabilizes rapidly on the timescale of τ, but can be viewed as stationary on the long time scale, t. Therefore, changes in the population distribution over the landscape occur on a scale of hours or days, while changes in the disease dynamics occur over years. Spatially, local movement and interaction of deer underly the large-scale spread of CWD. This homogenization technique can be applied to more complex disease or invasion models as will be illustrated in a future paper.

The result of homogenizing ecological diffusion is surprisingly simple when compared

to the homogenization of Fickian diffusion as derived in Holmes [30]. In the Fickian case the large-scale diffusion coefficient is not simply a harmonic mean but rather a matrix of averages depending on solutions to an associated elliptic PDE on a cell. The ecological diffusion result also differs from the Fickian case in that the small scale variability is still present in the solution due to its inverse proportionality to μ. This is an unexpected benefit of applying the method of multiple scales to ecological diffusion. Fickian diffusion loses ecologically realistic small-scale behavior under homogenization, but this behavior is preserved by homogenization of ecological diffusion.

Although the presence of the harmonic average of μ in the homogenized equation (2.15) is a natural result of the homogenization process, it also intuitively makes sense. As mentioned in the introduction, if μ is constant in a contiguous block, it is inversely proportional to the mean residence time in that block [97]. Given a large landscape unit containing $n_1, n_2, ..., n_k$ number of blocks with corresponding areas $A_1, A_2, ..., A_k$ and motilities $\mu_1, \mu_2, ..., \mu_k$, the projected residence time, T, for individuals in the unit would be

$$T = \frac{n_1 A_1}{\mu_1} + \frac{n_2 A_2}{\mu_2} + \cdots + \frac{n_k A_k}{\mu_k}, \tag{2.17}$$

since $\frac{A_i}{\mu_i}, i = 1, \cdots, k$, is the mean residence time of each individual block. Then the effective μ for the entire unit, which we will call $\bar{\mu}$ becomes,

$$\bar{\mu} = \frac{n_1 A_1 + n_2 A_2 + \cdots + n_k A_k}{T} = \frac{n_1 A_1 + n_2 A_2 + \cdots + n_k A_k}{\frac{n_1 A_1}{\mu_1} + \frac{n_2 A_2}{\mu_2} + \cdots + \frac{n_k A_k}{\mu_k}}, \tag{2.18}$$

where $n_1 A_1 + n_2 A_2 + \cdots + n_k A_k$ is the total area of the unit. Noting

$$\frac{n_1 A_1}{\mu_1} + \frac{n_2 A_2}{\mu_2} + \cdots + \frac{n_k A_k}{\mu_k} = (n_1 A_1 + n_2 A_2 + \cdots + n_k A_k) \left\langle \frac{1}{\mu} \right\rangle,$$

and substituting into (2.18), we see $\bar{\mu} = \frac{1}{\left\langle \frac{1}{\mu} \right\rangle}$, which is the harmonic mean of μ.

The average $\bar{\mu} \left\langle \frac{\alpha}{\mu} \right\rangle$ also has an intuitive meaning. If $\alpha_1, \alpha_2, ..., \alpha_k$ are the net rates

of change in the population density of infected deer in the corresponding blocks, $n_i A_i$, of motility μ_i, then

$$\left\langle \frac{\alpha}{\mu} \right\rangle = \frac{n_1\alpha_1\frac{A_1}{\mu_1} + n_2\alpha_2\frac{A_2}{\mu_2} + \cdots + n_k\alpha_k\frac{A_k}{\mu_k}}{n_1A_1 + n_2A_2 + \cdots + n_kA_k}.$$

Using (2.18) and simplifying,

$$\bar{\mu}\left\langle \frac{\alpha}{\mu} \right\rangle = \frac{n_1\alpha_1\frac{A_1}{\mu_1} + n_2\alpha_2\frac{A_2}{\mu_2} + \cdots + n_k\alpha_k\frac{A_k}{\mu_k}}{n_1\frac{A_1}{\mu_1} + n_2\frac{A_2}{\mu_2} + \cdots + n_k\frac{A_k}{\mu_k}} = \frac{n_1\alpha_1\frac{A_1}{\mu_1} + n_2\alpha_2\frac{A_2}{\mu_2} + \cdots + n_k\alpha_k\frac{A_k}{\mu_k}}{T}. \tag{2.19}$$

The denominator is the expected residence time, T, from (2.17). Rewriting (2.19) with $t_i = \frac{A_i}{\mu_i}$ as the mean residence time for each block, we have

$$\bar{\mu}\left\langle \frac{\alpha}{\mu} \right\rangle = \frac{n_1\alpha_1t_1 + n_2\alpha_2t_2 + \cdots + n_k\alpha_kt_k}{T}. \tag{2.20}$$

If we consider (2.15) without the diffusion term, the solution for $c_t = \bar{\mu}\left\langle \frac{\alpha}{\mu} \right\rangle c$ is the projected increase or decrease in the density of infected deer due to the time spent in the unit. It is of the form

$$\begin{aligned} c &= \underbrace{e^{\alpha_1\frac{t_1}{T}t}e^{\alpha_1\frac{t_1}{T}t}\cdots e^{\alpha_1\frac{t_1}{T}t}}_{n_1\text{times}}\underbrace{e^{\alpha_2\frac{t_2}{T}t}e^{\alpha_2\frac{t_2}{T}t}\cdots e^{\alpha_2\frac{t_2}{T}t}}_{n_2\text{times}}\cdots\underbrace{e^{\alpha_k\frac{t_k}{T}t}e^{\alpha_k\frac{t_k}{T}t}\cdots e^{\alpha_k\frac{t_k}{T}t}}_{n_k\text{times}} \\ &= (e^{n_1\alpha_1t_1}e^{n_2\alpha_2t_2}\cdots e^{n_k\alpha_kt_k})^{\frac{t}{T}} = e^{\frac{\sum_{i=1}^{k}n_i\alpha_it_i}{T}t} = e^{\bar{\mu}\left\langle \frac{\alpha}{\mu} \right\rangle t}, \end{aligned}$$

where α_i is the net rate of change in the density of infected deer and $\frac{t_i}{T}$ is the fraction of time spent in the habitat with area A_i and motility μ_i, and t is the time spent in the unit. Noting $c_t = \bar{\mu}\left\langle \frac{\alpha}{\mu} \right\rangle c$, we see that (2.20) is the projected exponential rate of change. So the average $\bar{\mu}\left\langle \frac{\alpha}{\mu} \right\rangle$ can be thought of as the net effect of the rates of contracting the disease in different habitats depending on the time spent in each habitat.

A one-dimensional example of solutions to this homogenized model is shown in Figure 2.2. The graph 2.2(c) compares the solutions for the non homogenized model (equations (2.3) and (2.4)) and the homogenized model (equations (2.15) and (2.16)) with a continuous

$\mu(x, y = \frac{x}{\epsilon})$, shown in 2.2(a). The solution illustrates the idea that the population density of diseased animals will be greater in areas of low motility and less in areas of high motility.

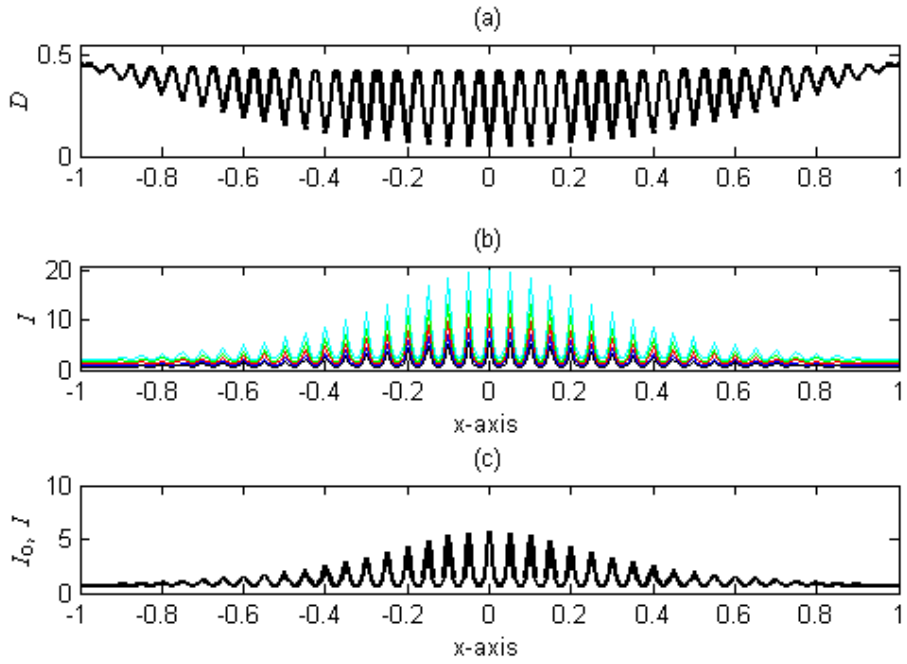

Figure 2.2: Graph(a) shows a one-dimensional example of a continuous $\mu(x, y = \frac{x}{\epsilon})$ with an obvious relationship between the large and small scales. $\mu(x, y) = 0.45 - 0.2(1 - x^2)(1 + \cos(2\pi y))$, with $\epsilon = 0.05$. The time evolution of solution is shown in graph(b). The lightest shade is the initial condition, with subsequent times becoming darker. The solutions, I for the non-homogenized model and I_0 for the leading order distribution of sick animals, are plotted on top of each other in graph(c). The difference between I and I_0 is not visually apparent with the maximum error, $max(|I - I_0|) = 0.027$.

2.3.2 Periodicity assumption

The homogenization procedure we have just described is facilitated by a quasi-periodicity assumption on the motility coefficient. We want to apply this procedure to natural landscapes that are not periodic in the strict sense, but also not completely random. Here we wish to argue that the assumption of quasi-periodicity applies broadly, and in particular to natural landscapes. When viewed at large scales there are repeating elements such as

mountains and valleys or subpatches of different habitat types. We apply this procedure to landscapes by allowing the periodicity to vary with the slow variable $\boldsymbol{x}$ [30], as in (2.5).

To illustrate this idea in one dimension, consider functions, $f(x)$, which have Fourier transforms of the form

$$\hat{f} = \frac{1}{\epsilon}\hat{g}\left(\frac{k-k_0}{\epsilon}\right) + \text{ c.c.},$$

where c.c. denotes the complex conjugate. The graph of $|\hat{f}|^2$ has a peak at k_0, indicating repeating elements at a scale of $\frac{2\pi}{k_0}$.

The inverse Fourier transform for $f(x)$ is

$$2\pi f(x) = \int_{-\infty}^{\infty} \frac{1}{\epsilon}\hat{g}\left(\frac{k-k_0}{\epsilon}\right) e^{ikx} dk + \text{ c.c.} \tag{2.21}$$

Let $l = \frac{k-k_0}{\epsilon}$. Then $k = k_0 + \epsilon l$, $dk = \epsilon\ dl$, and (2.21) becomes

$$2\pi f(x) = \int_{-\infty}^{\infty} \frac{1}{\epsilon}\hat{g}(l) e^{i(k_0+\epsilon l)y}\epsilon\ dl + \text{ c.c.} = e^{ik_0 y}\int_{-\infty}^{\infty} \hat{g}(l) e^{il(\epsilon y)} dl + \text{ c.c.}$$

Noting $x = \epsilon y$ gives

$$f(x) = e^{ik_0 y} g(x = \epsilon y) + \text{ c.c.},$$

where $e^{ik_0 y}$ is the carrier wave and $g(x)$ is a slowly-varying envelope function.

Writing $g(x)$ in polar coordinates, $g(x) = h(x)e^{im(x)x}$, where m and h are both real. Then

$$f(x) = h(x)e^{i(k_0 y + m(x)x)} + \text{ c.c.} = h(x)e^{iy(k_0+\epsilon m(x))} + \text{ c.c.},$$

using $x = \epsilon y$. Therefore $f(x)$ is periodic with the period $p(x) = \frac{2\pi}{k_0+\epsilon m(x)}$ which varies in the slow variable x.

Thus, functions with clear, narrow peaks in their spectrum can naturally be viewed as quasi-periodic. While this is no guarantee that a given motility distribution will be quasi-periodic, all of the landscape that we have classified using deer motilities in Utah had precisely this Fourier structure, possibly due to interactions between the 30×30 meter

landscape classification and natural periodicities of the landscape. In any event we now assume that the landscape of interest can be viewed as periodic in the fast scale with slowly varying periodic function, $\boldsymbol{p(x)}$. Now the challenge is that we do not know $\boldsymbol{p(x)}$ precisely, and the homogenization procedure outlined above requires exact knowledge of $\boldsymbol{p} = [l_1(x_1), l_2(x_2)]$. We now address this difficulty.

If we divide the landscape into rectangular regions for the averaging procedure, we can view each region as a multiple of the quasi-periodicity function $\boldsymbol{p(x)} = [l_1(x_1), l_2(x_2)]^T$ plus a small remainder. Let R^* be the chosen rectangular region with area A_{R^*} that contains a region R with area $A_R = Nl_1(x_1)Ml_2(x_2)$, where NM is the largest multiple of an $l_1(x_1)l_2(x_2)$ cell that fits into R^*. Then the region $R^* - R$ is the small remainder with area A_{R^*-R} (See Figure 2.3). Let f be a motility function with periodicity as defined in (2.5). Then using the average defined in (2.13)

$$\begin{aligned}\langle f\rangle &= \frac{1}{Nl_1Ml_2}\int_0^{Nl_1(x_1)}\int_0^{Ml_2(x_2)} f(\boldsymbol{x},\boldsymbol{y})dy_1dy_2 = \frac{1}{A_R}\int_R fdA \\ &= \frac{1}{A_R}\left[\int_R fdA + \int_{R^*-R} fdA - \int_{R^*-R} fdA\right] \\ &= \frac{A_{R^*}}{A_R}\langle f\rangle_{R^*} - \frac{1}{A_R}\int_{R^*-R} fdA.\end{aligned}$$

So,

$$\langle f\rangle_{R^*} = \frac{A_R}{A_{R^*}}\langle f\rangle + \frac{1}{A_{R^*}}\int_{R^*-R} fdA. \tag{2.22}$$

Since R is a smaller region than R^*, $\frac{A_R}{A_{R^*}} < 1$ and the second term in (2.22) can be bounded by

$$\left|\frac{1}{A_{R^*}}\int_{R^*-R} fdA\right| < \frac{[2l_1l_2(N+1) + 2l_1l_2(M+1)]|f|_{\max}}{l_1l_2NM} = \frac{2(M+N+2)|f|_{\max}}{NM},$$

resulting in

$$\langle f\rangle_{R^*} < \langle f\rangle + \frac{2(M+N+2)|f|_{\max}}{NM}.$$

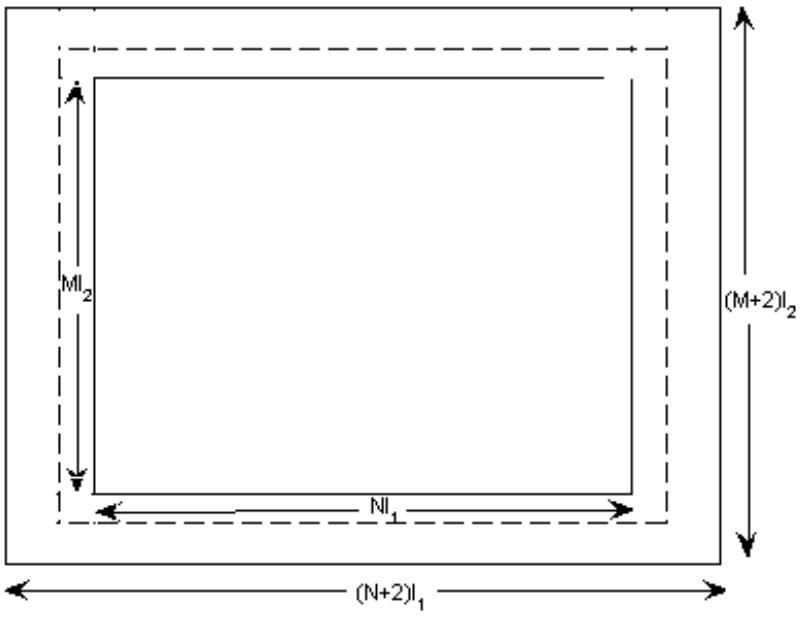

Figure 2.3: An illustration of choosing a rectangle to average over without knowing $\boldsymbol{p(x)}$ explicitly. The region enclosed in the dashed line is R^*. The smallest rectangle is the region R with area Nl_1Ml_2.

If we choose N and a corresponding M such that

$$\frac{2(M+N+2)|f|_{\max}}{NM} < \epsilon,$$

then

$$\langle f \rangle_{R^*} = \langle f \rangle + O(\epsilon).$$

Thus, the lack of explicit knowledge concerning $\boldsymbol{p(x)}$ does not influence the homogenization at leading order if we replace $\langle \mu \rangle$ with $\langle \mu \rangle_{R^*}$, since the introduced error is $O(\epsilon)$.

2.4 A two-dimensional example

To illustrate our homogenization result, we apply the simple model, (2.3) and (2.4), and the homogenized model, (2.15) and (2.16), to the spread of CWD in a 26.1×33.36 kilometer piece of mule deer habitat in the La Sal mountains of Utah. Land cover types comprising the area were determined using the National Land Cover Database [31]. Motility coefficients (μ) were estimated from GPS movement data for collared deer collected by the Utah Division of Wildlife Resources [53]. This was done by parsing the movement data by habitat type, then estimating the mean-squared displacement per time for all movements within each habitat [97]; these efforts will be discussed in more detail in a future paper. Motility values for the different habitat types in the area are illustrated in Figure 2.4 and given in Table 2.1. The habitat types for the inset in Figure 2.4 are shown in detail in Figure 2.5. We used an initial population of 7400 deer for the entire area and a small distribution of infected deer (equivalent to approximately 38 deer) in the eastern part of the mountains where the disease was first found [100]. We used the infection rate, $\beta = 0.0326$ yr^{-1} density^{-1}, and the death rate from CWD, $\lambda = 0.481$ yr^{-1}, found in Miller et al. [58] and converted to units of days^{-1}.

Table 2.1: The estimated motility values (μ) for the land cover types used in the two dimensional example.

Land cover type	**Estimated** μ $\left(\frac{\mathbf{km^2}}{\mathbf{day}}\right)$
rock	2.01
scrub	0.97
conifer forest	0.66
deciduous forest	0.65
mixed forest	0.52
pasture	0.85
cultivated crops	0.86
grassland	0.51
developed (low intensity)	0.29
developed (medium intensity)	0.30
developed (open space)	0.70
woody wetlands	0.55
open water	3.02

An alternating direction implicit (ADI) numerical method with no-flux boundaries was used to compute the population density of infected deer over time for both the homogenized

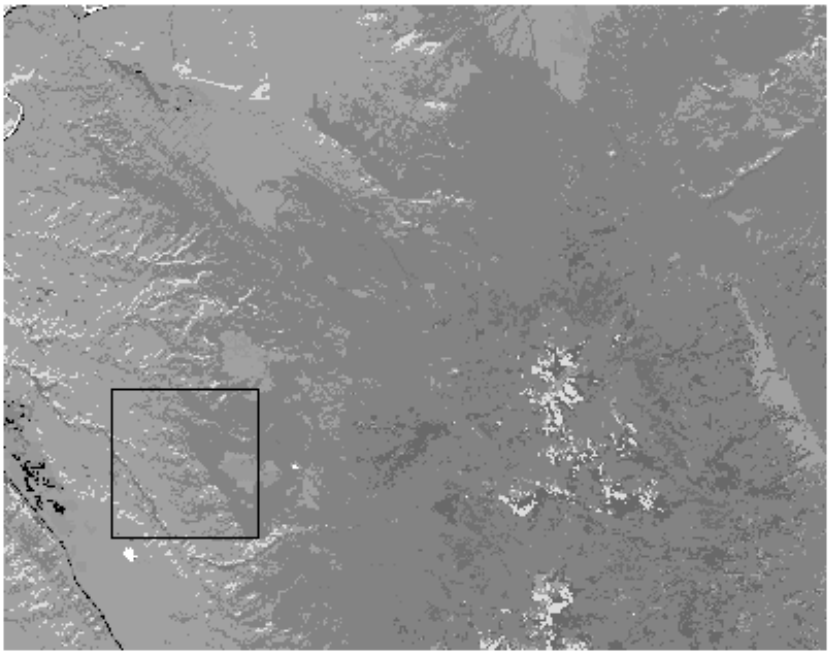

Figure 2.4: The assigned motility values for the habitat types of mule deer habitat in the La Sal mountains of Utah. Light shades indicate areas of high motility and darker shades indicate areas of low motility. A closer view of the outlined portion is shown in figure 2.5.

and non-homogenized models. ADI is an implicit finite difference method which splits each time step into two stages, a discretization in the x_1 direction, followed by a discretization in the x_2 direction [64]. This is equivalent to solving two tridiagonal systems for each time step. The details of this method are included in the Appendix. We chose an ADI method for its ease in accommodating the variable motility coefficient, as well as its efficiency and stability.

For the non-homogenized model (2.4) we chose a computational grid that aligned with the 30×30 meter land cover type blocks. For the homogenized model (2.15) and (2.16), we chose $\epsilon = 0.01$ which corresponds to averaging over 3000×3000 meter blocks. The technique is also valid for other choices of $\epsilon << 1$. We used a computational grid of 600×600 meter blocks for the numerical solution of the homogenized model, with each computational grid

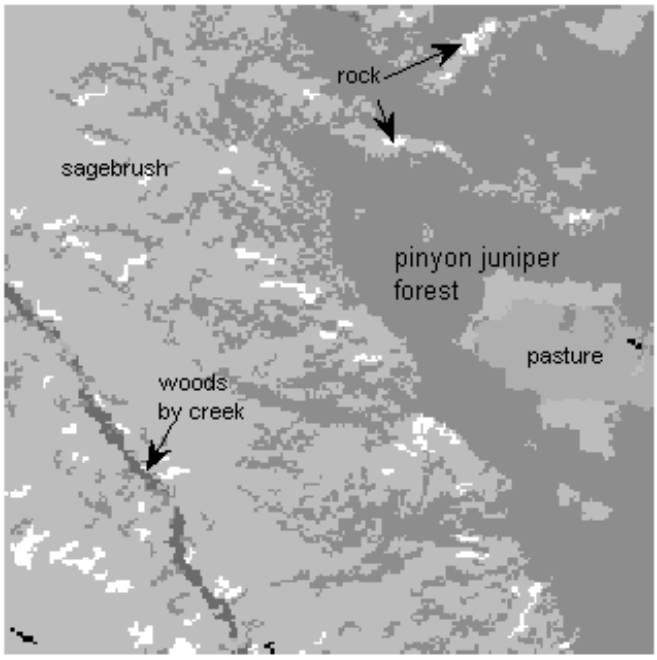

Figure 2.5: The assigned motility values for the habitat types in the outlined portion of Figure 2.4. The high motilities represent areas such as barren rock formations (where deer are absent) and sagebrush areas where deer spend a great amount of time moving (light shades). The low motilities represent areas where the residence time is high such as in pinyon juniper, deciduous, or mixed forest habitats where they bed and ruminate during daylight hours (dark shades).

point being the center of a 3000×3000 meter block used for averaging. The periodicity assumption was used to provide μ values for a grid larger than the study area for computing averages at grid points on the boundary. This choice resulted in a significant reduction in the number of needed operations as compared with solutions for the non-homogenization model. The non-homogenized model with n spatial steps in each direction and m time steps takes $O(mn^2)$ operations. If δ is the ratio of the large scale spatial steps to small scale spatial steps ($\delta = 0.05$ in our example), then the homogenized model with δn spatial steps in each direction with δm time steps takes $O(\delta^3 mn^2)$ operations. In terms of time saved for this example, the non-homogenized model took 45 hours, 6 minutes and 11.51 seconds

to run for 365 days, compared to 3.85 seconds for the homogenized model. That is $\frac{1}{42000}$ of the time, a substantial computational savings.

The results of the two-dimensional example are shown in Figures 2.6 and 2.7. Figure 2.6 shows the population densities for infected deer after 1 year for the homogenized model. Solving (2.15) for the intermediate variable c resulted in the infection being spread over the landscape at the diffusion rate of the averaged motilities $\bar{\mu}$. The density of infected deer is then prorated by division by μ in (2.16). This places disease hotspots in the habitat types where deer naturally gather, such as forests and riparian areas. As expected the model predicts low densities of infected animals in areas of high motility, such as rocky, barren areas and developed open space. A comparison of the homogenized and non-homogenized models is shown in Figure 2.7. The maximum error between the homogenized and non-homogenized models is consistently $O(\epsilon)$. The surfaces in this figure are not smooth, but reflect the effect of motility on the density of infected deer.

2.5 Discussion

When modeling population densities of animals over a heterogeneous environment, ecological diffusion, $\nabla^2[\mu(x_1, x_2)u]$, allows for the accumulation of animals in habitats where they linger and not in areas they naturally avoid. Fickian diffusion, $\nabla[D(x_1, x_2)\nabla u]$, gives a smooth distribution of animals over the landscape, disregarding the underlying motility.

The model used in this paper is a general model for the spread of a disease, using ecological diffusion. It is meant to illustrate the appropriateness of ecological diffusion in the context of heterogeneous landscapes and to demonstrate our homogenization procedure. We are developing a more disease specific CWD model, which will be the subject of a future paper. Contact with disease agents in the environment as well as contact between susceptible and infected individuals will be considered. The behavioral differences of male and female deer during the seasons of the year will be incorporated to more effectively model disease dynamics. Female deer form matrilineal groups with fidelity to summer and winter ranges while male deer wander between groups, especially during breeding season

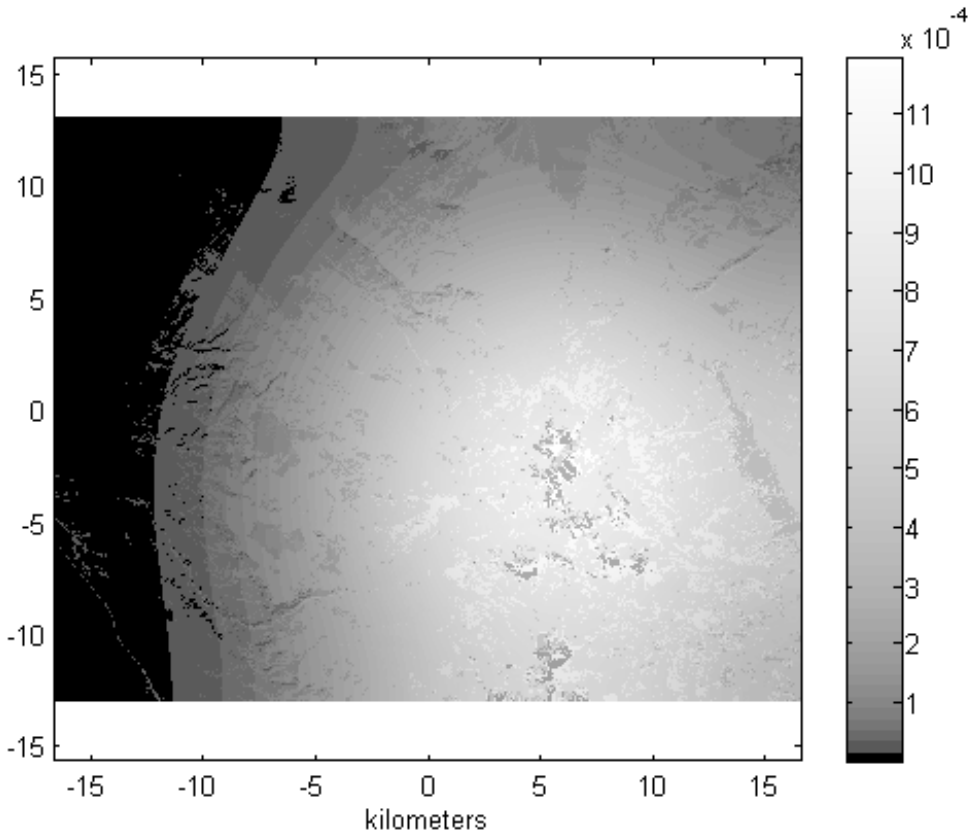

Figure 2.6: A view of the values for the population densities for infected deer for the homogenized model. The idea that animals collect in areas with low motility and leave areas of high motility is illustrated when compared with the motility values in Figure 2.4.

[53]. The estimation of motility values for male and female deer from GPS movement data using Bayesian methods will be explored. Harvesting and culling practices for the study area will be modeled as well.

This will result in a system consisting of separate equations for males and females in both susceptible and infected classes and an equation for environmental hazard. How behavioral differences between males and females affect disease spread can be explored through various infection rates. The environmental impact of diseased females vs males can also be explored.

Another management application of this model is determining a critical population of deer for which the wave speed of the spread of CWD is zero, that is, is the wavefront speed

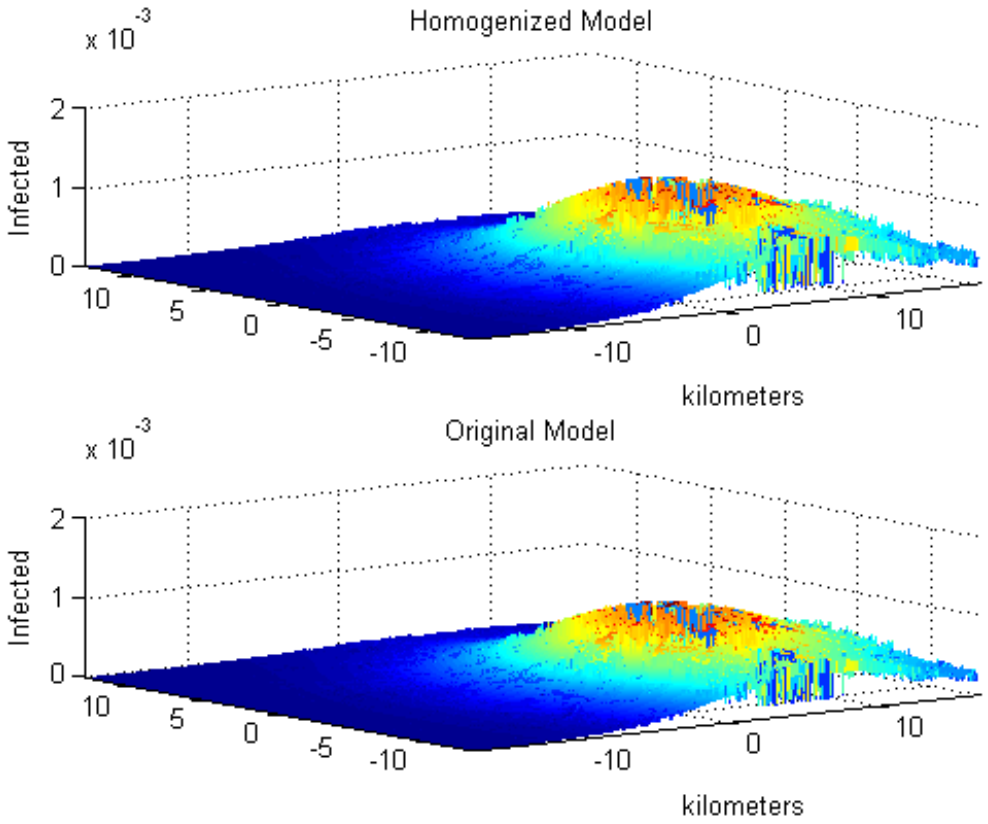

Figure 2.7: This figure shows results from running the homogenized model with $\epsilon = 0.01$ and the original model. The maximum error between the two models was 1.86×10^{-4}. An initial condition representing a small density of diseased deer in the eastern part of the region was used. This graph represents the spread of the disease over a year in the 26.1×33.36 kilometer study area.

in this area sufficient to allow the disease to propagate? The wave speed, v, for solutions to the homogenized PDE, can be determined for an area of interest by $v \approx 2\sqrt{\bar{\mu}\bar{\alpha}}$ [88], where $\bar{\alpha} = \bar{\mu}\left\langle \frac{\alpha}{\mu} \right\rangle$ and $\alpha = \beta\tilde{S} - \lambda$. The number, N, of deer for a steady state population with density $\tilde{S} = \frac{K}{\mu}$, is given by

$$N = \iint_A \frac{K}{\mu} dA = K \iint_A \frac{1}{\mu} dA = KA\left\langle \frac{1}{\mu} \right\rangle,$$

where A is the area of the region of interest. Then $K = \frac{\bar{\mu}N}{A}$ and the wave speed becomes

$$v \approx 2\sqrt{\bar{\mu}^2 \left\langle \frac{\frac{\beta\bar{\mu}N}{A\mu} - \lambda}{\mu} \right\rangle} = 2\bar{\mu}\sqrt{\left\langle \frac{\beta\bar{\mu}N}{A\mu^2} - \frac{\lambda}{\mu} \right\rangle}.$$

The value of N for which

$$\left\langle \frac{\beta\bar{\mu}N}{A\mu^2} - \frac{\lambda}{\mu} \right\rangle = \frac{\beta N\bar{\mu}}{A} \left\langle \frac{1}{\mu^2} \right\rangle - \lambda \left\langle \frac{1}{\mu} \right\rangle = 0$$

is

$$N = \frac{\lambda A}{\beta} \left\langle \frac{1}{\mu} \right\rangle^2 \left\langle \frac{1}{\mu^2} \right\rangle^{-1}.$$

For our study area, using the values for β, λ, and μ given in Section 2.4, the critical population would be $N = 12,447$. The current population is estimated at $7,400$ deer with a goal of $13,000$ [100]. If the infection rate, $\beta = 0.0326$, is appropriate for CWD in the La Sal mountains, the current deer population is less than the critical population suggesting that the disease will not spread out of the area. If the number of deer approaches the goal of 13,000 animals, however, the critical population would be exceeded and the wave speed would no longer be zero. It is important to note that this critical population was determined with an infection rate calculated from data for disease spread in a captive herd, scaled down a factor of 10 for the larger ranges of wild deer [58]. If for example, the infection rate is 10 times larger ($\beta = 0.326$, as fitted by Miller et al.), the critical population would be 1,245 deer, far below the present population, indicating that the disease can spread through the study area. We will revisit this idea with the more disease-specific model.

The homogenization procedure we have described will be invaluable in simulations of more complex models over large areas. In fact, the homogenization of ecological diffusion can be applied to many spatial invasion and dispersal models as well as spatial epidemiology models, when the effect of heterogeneous landscapes on spread is desired. Homogenization preserves small scale variability while allowing computation on a large scale.

CHAPTER 3

A SPATIAL MODEL FOR CHRONIC WASTING DISEASE IN MULE DEER [1]

3.1 Introduction

Chronic wasting disease (CWD) is an infectious prion disease that affects mule deer (*Odocoileus hemionus*), as well as other members of the Cervidae family, namely white-tailed deer (*Odocoileus virginianus*), elk (*Cervus elaphus*), and moose (*Alces alces shirasi*) [4]. It is a rare, slowly-developing disease that is always fatal, and infected mule deer may live 12-24 months before showing visible signs of the disease [105]. The disease may be contracted by direct contact with infected deer [61], as well as by contact with contaminated environments [37]. Prions shed into the environment through the feces, saliva, and decaying carcasses of infected deer may remain infective for many years [62]. The existence of both horizontal and environmental transmission pathways sets CWD apart from other infectious wildlife diseases.

Miller et al. [59] have suggested that over decades, CWD has the potential to affect local population dynamics with possible long-term effects on ecosystems. Mathematical models are critical tools in assessing the impact of CWD on deer populations and analyzing different management strategies [86]. CWD has been modeled in many different ways which include discrete-time deterministic models [63], individual-based models [26], difference equation models [36], and SI epidemic models [58, 104].

Even though these models have made important inroads to understanding disease dynamics, they ignore the spatial aspect of disease spread. An understanding of the spatial variation in the distribution of susceptible hosts is critical in predicting the emergence or spread of an infectious disease to new geographic regions [91], particularly considering the lingering environmental hazard of CWD. A spatial picture of where the disease has been is critical to management. Transmission of CWD is contingent on population densities which

[1] Coauthored by Martha Garlick, James Powell, and Mevin Hooten, anticipated submission to Bulletin of Mathematical Biology, August 2012

reflect the heterogeneity of the environment. In fact, environments can act as the principal organizers for spatial processes, such as disease spread [5, 82]. In other words, density-dependent spatial spread is dependent on how patches of population at variable distances infect each other [23].

For the most part, spatial models for CWD have been statistical. Conner and Miller [13] use cluster analysis and Farnsworth et al. [18] use a Bayesian hierarchical model to study spatial spread in free-ranging mule deer populations in Colorado, while Joly et al. [41] use spatial analysis to study the spread of CWD in white-tailed deer in Wisconsin. All of these approaches require a large body of data, which is not available in areas where the disease is in its initial stages, such as Utah.

A deterministic, process-based model does not need the same amount of data to be useful. Rates of movement can be inferred from measurements of healthy deer, and transmission parameters estimated for other populations used in an appropriately constructed mechanistic model. One mechanism to introduce spread as a spatial process involves diffusion. Diffusion was first applied to epidemiology by Kendall in 1965 [45] and has been used to model the spatial spread of diseases in wildlife populations for many years, such as rabies in fox [42, 68], foot and mouth disease in feral pigs [77], and conjunctivitis in house finches [34]. These models use constant diffusion coefficients, which imply that disease spreads at the same rate through all parts of the host's range.

Hosseini et al. [34] recognized that a key aspect of the spatial spread of a directly transmitted disease is how the hosts carrying the pathogen move over the landscape. In order for dispersal to reflect heterogeneous landscapes, diffusion rates need to vary with habitat type [43]. Fickian diffusion, of the form $\frac{\partial u}{\partial t} = \nabla[D(x_1, x_2)\nabla u]$, models the distribution of organisms from high densities to low densities at a rate proportional to the density gradient [29]. In this type of diffusion, the environment affects the rate at which populations respond to gradients through the diffusion coefficient, D. Since the diffusion equation seeks to minimize population gradients, it eventually distributes organisms equally in habitats that provide food and shelter as those which do not.

On the other hand, ecological diffusion, represented by $\frac{\partial u}{\partial t} = \nabla^2[(\mu(x_1, x_2)u]$, allows for distinct population differences at habitat boundaries [74], reflecting the aggregation of organisms in desirable habitats and their dispersal from undesirable ones. The variable motility coefficient $\mu(x_1, x_2)$ represents the rate at which organisms choose to leave a habitat patch, irrespective of density gradients [97]. Ecological diffusion can be applied to spatial models in epidemiology to make the connection between how hosts move and how diseases spread. Population density in an area increases as motility decreases, increasing the probability of disease transmission, potentially affecting disease dynamics.

Even though diffusion models with variable coefficients have been recognized as necessary to model dispersal over heterogeneous landscapes [71], variable coefficients are often abandoned in practice. This is chiefly for two reasons: added mathematical complication and lack of data to derive motility coefficients for all landcover types in a study area. Increased computing power and homogenization techniques can aid in dealing with mathematical complication for numerical solutions [23] and advances in telemetry have enhanced data collection over diverse habitats [72]. Homogenization of partial differential equations (PDEs) is a technique for facilely accommodating small scale variability in diffusion coefficients for large scale simulation [15]. It uses the method of multiple scales [30] to approximate PDEs that have rapidly-varying coefficients with similar, "homogenized" PDEs having averaged coefficients, operating on much broader scales. Homogenized models are more efficient to solve numerically. In epidemiology homogenization has been used with Fickian diffusion to model the spread of feline leukemia [21] and with ecological diffusion in an unstructured CWD model [23].

In this paper we present a spatial, sex-structured model for the spread of CWD in mule deer, accounting for disease-specific behaviors of male and female deer separately through motility parameters and infection rates. Both direct deer-to-deer transmission as well as indirect environment-to-deer transmission are included. We apply a homogenization procedure for ecological diffusion [23] to the system of equations to facilitate a numerical solution over a large domain, simulating the spread of CWD in Southeast Utah. This homogeniza-

tion procedure is strikingly simple when compared to similar techniques for Fickian diffusion equations. The homogenized system not only provides a multi-scale approach to disease spread, it also provides averaged coefficients that can be applied to predict invasion speed and critical population size from epidemic spread. This can give insight into the receptivity of invasion of certain landscape features, which can aid managers in decision-making.

3.2 Model for Disease Transmission and Population Movement

Deer behavior is dependent upon the season of the year. Female deer form matrilinear groups that show strong fidelity to winter and summer ranges. Male deer wander more, especially during breeding season when they cover a wide area searching for receptive females [69]. Males interact with each other in competition for females and males test females for receptiveness through extensive licking [49]. Thus, male breeding behavior may contribute to higher infection rates for males [53]. Farnsworth et al. [19] found CWD prevalence in males to be much higher than in females. To incorporate the behavioral differences between male and female deer, we develop a sex-structured model following the SI framework of Anderson and May [1], with the addition of environmental hazard and ecological diffusion. We do not include latency, since the existence and duration of a latency period is not known [58] and evidence suggests agent shedding occurs long before clinical signs of CWD appear [60].

The equations for susceptible deer are:

$$\begin{aligned}
\frac{\partial S_F}{\partial t} &= \nabla^2(\mu_F S_F) - \beta_{FF} S_F I_F - \beta_{MF} S_F I_M - \gamma_F S_F H + \Phi_F(S_F) \\
\frac{\partial S_M}{\partial t} &= \nabla^2(\mu_M S_M) - \beta_{FM} S_M I_F - \beta_{MM} S_M I_M - \gamma_M S_M H + \Phi_M(S_M),
\end{aligned}$$

where S refers to the susceptible population density, I to the infected population density, and H to the amount of infectious material in the environment. The subscripts F and M refer to female and male deer respectively. The differential operator,∇^2, is the Laplacian, $\frac{\partial^2}{\partial {x_1}^2} + \frac{\partial^2}{\partial {x_2}^2}$. The motility coefficients μ_F and μ_M vary over space, reflecting differences

in movement patterns between males and females. We allow for an infection rate for each of four types of interactions, females infecting other females, β_{FF}, males infecting females, β_{MF}, males infecting other males, β_{MM}, and females infecting males, β_{FM}. The parameters γ_F and γ_M are the rates at which susceptible females and males contract the disease from the environment. The functions Φ_F and Φ_M contain appropriate birth and death terms for susceptibles which are not needed in detail for our modeling approach, which will use steady-state approximations for susceptible populations.

The equations for infected deer are:

$$\frac{\partial I_F}{\partial t} = \nabla^2(\mu_F I_F) + \beta_{FF} S_F I_F + \beta_{MF} S_F I_M + \gamma_F S_F H - \omega I_F - \phi I_F \tag{3.1}$$

$$\frac{\partial I_M}{\partial t} = \nabla^2(\mu_M I_M) + \beta_{FM} S_M I_F + \beta_{MM} S_M I_M + \gamma_M S_M H - \omega I_M - \phi I_M. \tag{3.2}$$

The death rate for infectives, ω, includes death due to CWD. It may also be influenced by the increased number of deaths of infected deer from predation [104] and vehicle collisions [48] over that of healthy deer. One preventative measure in Utah is that visibly sick deer are shot on sight and their carcasses removed. The parameter ϕ is the rate of this culling. The total number of susceptible and infected deer is given by $N = S_F + S_M + I_F + I_M$.

The change over time of the amount of prions in the environment is modeled by a DE for environmental hazard, H,

$$\frac{\partial H}{\partial t} = \alpha_F I_F + \alpha_M I_M + \alpha_{DF} \omega I_F + \alpha_{DM} \omega I_M - \delta H. \tag{3.3}$$

Male mule deer can weigh 50 to 100 kilograms more than female mule deer, so we assume their contribution to prion pollution in the environment may differ significantly from that of females. The parameters α_F and α_M are rates that feces and urine pollute the environment, while α_{DF} and α_{DM} are rates that decaying carcasses pollute. The parameter δ is the rate at which hazardous material leaves the environment, whether via deactivation (unknown means) or being washed away or covered up by soil deposition. The parameters for this

model and the subsequent simulations are given in Table 3.1.

Table 3.1: The parameters for the CWD model and values used in the simulations.

Parameter	Description	Value	Source
μ_F, μ_M	Motility coefficients	See Table 2	Estimated
β_{FF}, β_{MF}, β_{FM}, β_{MM}	Direct transmission rates	8.767×10^{-5}- 9.315×10^{-5} density^{-1} day^{-1}	Miller et al., 2006
γ_F, γ_M	Transmission rates from contaminated environments	0.0022 mass^{-1} day^{-1}	Miller et al., 2006
ω	Death rate from CWD	0.0013 day^{-1}	Miller et al., 2006,
ϕ	Cull rate	0 day^{-1}	Assigned
α_F, α_M	Rates at which prions are excreted	0.00030411 mass density^{-1} day^{-1}	Miller et al., 2006
α_{DF}, α_{DM}	Rates at which infected carcasses pollute the environment	0.1 mass density^{-1}	Assigned
δ	Rate at which infectious material leaves the environment	0.007 day^{-1}	Miller et al., 2006

3.2.1 Rescaling to Reduce Number of Free Parameters

In Utah the number of infected deer is much smaller than the number of susceptible deer, i.e. $0 < I_F << S_F$ and $0 < I_M << S_M$, because the disease is rare [100]. Therefore, considering the initial density of susceptible deer to be close to the density at carrying capacity ($S_F(0) + S_M(0) = K$) and the initial density of infected deer to be much smaller ($I_F(0) + I_M(0) = \eta K$, $0 < \eta << 1$) leads to the following scales: $\bar{S}_F = \frac{S_F}{K}$, $\bar{S}_M = \frac{S_M}{K}$, $\bar{I}_F = \frac{I_F}{\eta K}$, $\bar{I}_M = \frac{I_M}{\eta K}$, and $\bar{H} = \frac{H}{\alpha_{DM}\eta K}$. Rescaling time with $\bar{t} = \omega t$ leads to a non-dimensional system if we assume the spatial coordinates, x_1 and x_2 are such that $\left|\nabla^2(\mu_F \bar{S}_F)\right| \sim 1$. Rescaling the equations for susceptibles in this manner yields:

$$\frac{\partial \bar{S}_F}{\partial \bar{t}} = \frac{1}{\omega}\left[\nabla^2(\mu_F \bar{S}_F) + \Phi_F(\bar{S}_F) - \eta K \bar{S}_F\left(\beta_{FF}\bar{I}_F - \beta_{MF}\bar{I}_M - \gamma_F \alpha_{DM}\bar{H}\right)\right] \tag{3.4}$$

$$\frac{\partial \bar{S}_M}{\partial \bar{t}} = \frac{1}{\omega}\left[\nabla^2(\mu_M \bar{S}_M) + \Phi_M(\bar{S}_M) - \eta K \bar{S}_M\left(\beta_{FM}\bar{I}_F - \beta_{MM}\bar{I}_M - \gamma_M \alpha_{DM}\bar{H}\right)\right]. \tag{3.5}$$

Hunting and habitat management practices in Utah are aimed at reaching and maintaining a population objective for mule deer, determined by wildlife managers [100] and

given as a number of deer. Assuming the functions Φ_F and Φ_M contain birth, death, and hunting rates such that a population level is maintained (i.e. $\frac{K\beta}{\omega} \sim 1$) and neglecting the terms multiplied by the small parameter η, (3.4) and (3.5) become:

$$\frac{\partial \bar{S}_F}{\partial \bar{t}} = \frac{1}{\omega}\nabla^2(\mu_F \bar{S}_F) \quad \text{and} \quad \frac{\partial \bar{S}_M}{\partial \bar{t}} = \frac{1}{\omega}\nabla^2(\mu_M \bar{S}_M),$$

which have steady-state solutions $\hat{S}_F = \frac{C_F}{\mu_F}$ and $\hat{S}_M = \frac{C_M}{\mu_M}$, respectively. The constants C_F and C_M are proportional to the density at carrying capacity, K. The Utah Division of Wildlife Resources (UDWR) expresses the population of deer at carrying capacity as a target population in numbers of individuals, N. For our modeling purposes, we need the carrying capacity expressed as a density of the number of individuals per kilometer at carrying capacity, K, chosen such that $\iint_A \left(\hat{S}_F + \hat{S}_M\right) dA = KA \approx N$. Rescaling (3.1)-(3.3) and using $\hat{S}_F$ and $\hat{S}_M$ for the susceptible populations, our system becomes:

$$\frac{\partial \bar{I}_F}{\partial \bar{t}} = \frac{1}{\omega}\left[\nabla^2(\mu_F \bar{I}_F) + \left(\beta_{FF}\hat{S}_F - \omega - \phi\right)\bar{I}_F + \beta_{MF}\hat{S}_F\bar{I}_M + \gamma_F\alpha_{DM}\hat{S}_F\bar{H}\right], \tag{3.6}$$

$$\frac{\partial \bar{I}_M}{\partial \bar{t}} = \frac{1}{\omega}\left[\nabla^2(\mu_M \bar{I}_M) + \left(\beta_{MM}\hat{S}_M - \omega_I - \phi\right)\bar{I}_M + \beta_{FM}\hat{S}_M\bar{I}_F + +\gamma_M\alpha_{DM}\hat{S}_M\bar{H}\right], \tag{3.7}$$

and

$$\frac{\partial \bar{H}}{\partial \bar{t}} = \frac{\alpha_F}{\alpha_{DM}\omega}\bar{I}_F + \frac{\alpha_M}{\alpha_{DM}\omega}\bar{I}_M + \frac{\alpha_{DF}}{\alpha_{DM}}\bar{I}_F + \bar{I}_M - \frac{\delta}{\omega}\bar{H}. \tag{3.8}$$

Thus, the spread of CWD in the male and female populations is connected through the environmental hazard, as well as the gender-specific steady-state population sizes and infection rates. In fact, the steady-state population size of an area is inversely proportional to the motility ($\hat{S}_F \sim \frac{1}{\mu_F}$), so the density of infectives increases when the motility decreases. In other words, the environment plays a key role in how disease spreads through both density-dependent transmission and dispersal of infectives.

3.2.2 Homogenization

The system (3.6)-(3.8) must be solved numerically and in order to do so over a large area, we employ a homogenization procedure. To illustrate this procedure, we assume that habitat structure is locally quasi-periodic, as when the landscape is composed of repetitively dispersed subpatches [21, 23], i.e., natural landscapes are not periodic in the strict sense, but are also not completely random. As shown in Garlick et al. [23], we do not need an explicit knowledge of this periodicity in order for this homogenization procedure to work. Landscape classification data is available at various resolutions. The LANDFIRE data base, from the Landscape Fire and Resource Management Planning Tools sponsored by the US Department of the Interior and the US Department of Agriculture Forest Service, classifies habitat in 30×30 meter blocks [93]. This provides the needed separation of scales, as we can regard the motilities μ_F and μ_M as varying quickly over the small scale and much more slowly over the large scale.

Let ϵ ($0 < \epsilon << 1$) be an order parameter representing the ratio of small and large scales [80]; for example, a small scale of 30 meters and a large scale of 3 kilometers would yield $\epsilon = \frac{30}{3000} = \frac{1}{100}$ (as in Garlick et al. [23]). Let $\boldsymbol{x}$ be coordinates of the large spatial scale, with an associated slow time scale, t. Then the small spatial scale $\boldsymbol{y}$ is defined by the relation, $\boldsymbol{y} = \frac{\boldsymbol{x}}{\epsilon}$, and the fast time scale corresponding to the small spatial scale becomes $\tau = \frac{t}{\epsilon^2}$. The motility coefficients become functions of both spatial scales, $\mu_F = \mu_F(\boldsymbol{x}, \boldsymbol{y})$ and $\mu_M = \mu_M(\boldsymbol{x}, \boldsymbol{y})$. Quasi-periodicity means that there exists a vector, $\boldsymbol{p}(\boldsymbol{x})$, such that

$$\mu_F(\boldsymbol{x}, \boldsymbol{y} + \boldsymbol{p}(\boldsymbol{x})) = \mu_F(\boldsymbol{x}, \boldsymbol{y}) \quad \text{and} \quad \mu_M(\boldsymbol{x}, \boldsymbol{y} + \boldsymbol{p}(\boldsymbol{x})) = \mu_M(\boldsymbol{x}, \boldsymbol{y}), \tag{3.9}$$

for all $\boldsymbol{x}$ and $\boldsymbol{y}$ in the domain. Quasi-periodicity facilitates the homogenization procedure, but is not strictly necessary for it.

With the introduction of these two scales, the derivatives become: $\nabla \longrightarrow \nabla_x + \frac{1}{\epsilon}\nabla_y$, where the subscript indicates whether the long scale ($\boldsymbol{x}$) or short scale ($\boldsymbol{y}$) variable is differentiated, and $\frac{\partial}{\partial t} \longrightarrow \frac{1}{\epsilon^2}\frac{\partial}{\partial \tau} + \frac{\partial}{\partial t} = \frac{1}{\epsilon^2}\partial_\tau + \partial_t$. Substituting the new scales and derivatives

into (3.6)-(3.8), after multiplication by ϵ^2, gives:

$$\begin{aligned}(\partial_\tau + \epsilon^2\partial_t)I_F &= \frac{1}{\omega}(\nabla_y + \epsilon\nabla_x)\cdot[(\nabla_y + \epsilon\nabla_x)\mu_F I_F] \\ &\quad + \frac{\epsilon^2}{\omega}\left[\left(\beta_{FF}\hat{S}_F - \omega - \phi\right)I_F + \beta_{MF}\hat{S}_F I_M + \gamma_F\alpha_{DM}\hat{S}_F H\right], \\ (\partial_\tau + \epsilon^2\partial_t)I_M &= \frac{1}{\omega}(\nabla_y + \epsilon\nabla_x)\cdot[(\nabla_y + \epsilon\nabla_x)\mu_M I_M] \\ &\quad + \frac{\epsilon^2}{\omega}\left[\left(\beta_{MM}\hat{S}_M - \omega - \phi\right)I_M + \beta_{FM}\hat{S}_M I_F + \gamma_M\alpha_{DM}\hat{S}_M H\right],\end{aligned}$$

and

$$(\partial_\tau + \epsilon^2\partial_t)H = \epsilon^2\left[\frac{\alpha_F + \alpha_{DF}\omega}{\alpha_{DM}\omega}I_F + \left(\frac{\alpha_M}{\alpha_{DM}\omega} + 1\right)I_M - \frac{\delta}{\omega}H\right],$$

where we have dropped the bar notation on the rescaled variables for convenience.

We replace I_F with a series expansion in ϵ:

$$I_F = I_{F_0} + \epsilon I_{F_1} + \epsilon^2 I_{F_2} + O(\epsilon^3),$$

and use similar expansions for I_M and H. Collecting terms at common powers of ϵ, the $O(1)$ equations are:

$$\partial_\tau I_{F_0} = \frac{1}{\omega}\nabla_y^2(\mu_F I_{F_0}), \tag{3.10}$$

$$\partial_\tau I_{M_0} = \frac{1}{\omega}\nabla_y^2(\mu_M I_{M_0}), \tag{3.11}$$

and

$$\partial_\tau H_0 = 0.$$

Since (3.10) and (3.11) are parabolic, the solutions decay exponentially to their steady state in fast time scales [23]. The steady-state solutions for I_{F_0} and I_{M_0} are:

$$I_{F_0} = \frac{c_{IF}(\boldsymbol{x}, t)}{\mu_F(\boldsymbol{x}, \boldsymbol{y})} \quad \text{and} \quad I_{M_0} = \frac{c_{IM}(\boldsymbol{x}, t)}{\mu_M(\boldsymbol{x}, \boldsymbol{y})}, \tag{3.12}$$

where c_{IF} and c_{IM} are functions without any $\boldsymbol{y}$ or τ dependence. The leading order solution for environmental hazard, $H_0 = H_0(\boldsymbol{x}, \boldsymbol{y}, t)$, however, depends on both spatial scales.

The $O(\epsilon)$ equations are:

$$\partial_\tau I_{F_1} = \frac{1}{\omega}\left[\nabla_y^2(\mu_F I_{F_1}) + \nabla_y \cdot [\nabla_x (\mu_F I_{F_0})] + \nabla_x \cdot [\nabla_y (\mu_F I_{F_0})]\right], \tag{3.13}$$

$$\partial_\tau I_{M_1} = \frac{1}{\omega}\left[\nabla_y^2(\mu_M I_{M_1}) + \nabla_y \cdot [\nabla_x (\mu_M I_{M_0})] + \nabla_x \cdot [\nabla_y (\mu_M I_{M_0})]\right], \tag{3.14}$$

and

$$\partial_\tau H_1 = 0. \tag{3.15}$$

Substituting (3.12) into (3.13) and (3.14) and simplifying (noting that $\nabla_y(\mu_F I_{F_0}) = \nabla_y c_{IF}(\boldsymbol{x}, t) = 0$ and $\nabla_y(\mu_M I_{M_0}) = \nabla_y c_{IM}(\boldsymbol{x}, t) = 0$), we obtain

$$\partial_\tau I_{F_1} = \nabla_y^2(\mu_F I_{F_I}) \quad \text{and} \quad \partial_\tau I_{M_1} = \nabla_y^2(\mu_M I_{M_I}).$$

Considering the steady-state problems for I_{F_1} and I_{M_1} as in the $O(1)$ case and solving (3.15), yields solutions:

$$I_{F_1} = \frac{b_{IF}(\boldsymbol{x}, t)}{\mu_F(\boldsymbol{x}, \boldsymbol{y})}, \quad I_{M_1} = \frac{b_{IM}(\boldsymbol{x}, t)}{\mu_M(\boldsymbol{x}, \boldsymbol{y})}, \quad \text{and} \quad H_1 = b_H(\boldsymbol{x}, \boldsymbol{y}, t). \tag{3.16}$$

The solutions in (3.16) are precisely the same form as the solutions in (3.12), therefore any boundary condition satisfied by (3.12) leaves homogeneous boundary conditions for (3.16), giving $I_{F_1} = I_{M_1} = H_1 = 0$.

The $O(\epsilon^2)$ equations are:

$$\partial_\tau I_{F_2} + \partial_t I_{F_0} = \frac{1}{\omega}\Bigg[\nabla_y^2(\mu_F I_{F_2}) + \nabla_x^2(\mu_F I_{F_0}) + \gamma_F \alpha_{DM} \hat{S}_F H_0 + \left(\beta_{FF}\hat{S}_F - \omega - \phi\right) I_{F_0} + \beta_{MF}\hat{S}_F I_{M_0}\Bigg],$$

$$\partial_\tau I_{M_2} + \partial_t I_{M_0} = \frac{1}{\omega}\Bigg[\nabla_y^2(\mu_M I_{M_2}) + \nabla_x^2(\mu_M I_{M_0}) + \gamma_M \alpha_{DM}\hat{S}_M H_0 + \left(\beta_{MM}\hat{S}_M - \omega - \phi\right) I_{M_0} + \beta_{FM}\hat{S}_M I_{F_0}\Bigg],$$

and

$$\partial_\tau H_2 + \partial_t H_0 = \frac{\alpha_F}{\alpha_{DM}\omega} I_{F_0} + \frac{\alpha_M}{\alpha_{DM}\omega} I_{M_0} + \frac{\alpha_{DF}}{\alpha_{DM}} I_{F_0} + I_{M_0} - \frac{\delta}{\omega} H_0,$$

where the mixed derivative terms containing I_{F_1} or I_{M_1} have vanished since $I_{F_1} = I_{M_1} = 0$.

In the fast time scale, τ, I_{F_2} and I_{M_2} tend to steady-state solutions rapidly, so relevant equations in the slower time scale are

$$\partial_t \frac{c_{IF}}{\mu_F} = \frac{1}{\omega}\Bigg[\nabla_y^2(\mu_F I_{F_2}) + \nabla_x^2 c_{IF} + \gamma_F \alpha_{DM}\hat{S}_F H_0 + \left(\beta_{FF}\hat{S}_F - \omega - \phi\right)\frac{c_{IF}}{\mu_F} + \beta_{MF}\hat{S}_F \frac{c_{IM}}{\mu_M}\Bigg], \tag{3.17}$$

$$\partial_t \frac{c_{IM}}{\mu_M} = \frac{1}{\omega}\Bigg[\nabla_y^2(\mu_M I_{M_2}) + \nabla_x^2 c_{IM} + \gamma_M \alpha_{DM}\hat{S}_M H_0 + \left(\beta_{MM}\hat{S}_M - \omega - \phi\right)\frac{c_{IM}}{\mu_M} + \beta_{FM}\hat{S}_M \frac{c_{IF}}{\mu_F}\Bigg], \tag{3.18}$$

and

$$\partial_t H_0 = \frac{\alpha_F}{\alpha_{DM}\omega}\frac{c_{IF}}{\mu_F} + \frac{\alpha_M}{\alpha_{DM}\omega}\frac{c_{IM}}{\mu_M} + \frac{\alpha_{DF}}{\alpha_{DM}}\frac{c_{IF}}{\mu_F} + \frac{c_{IM}}{\mu_M} - \frac{\delta}{\omega} H_0, \tag{3.19}$$

where the values for I_{F_0} and I_{M_0} in (3.12) have been used to write equations in terms of dependent variables on slower scales, $c_{IF}(\boldsymbol{x}, t)$ and $c_{IM}(\boldsymbol{x}, t)$. Note that dependence on the small scale, $\boldsymbol{y}$, is retained through coefficients containing $\hat{S}_F$ or $\hat{S}_M$.

We now explain the averaging procedure associated with homogenization in two spatial dimensions in terms of infected females. The procedure is the same for infected males. Let $\boldsymbol{p}(\boldsymbol{x})$ in (3.9) be defined as the periodicity vector $\boldsymbol{p}(\boldsymbol{x}) = [l_1(x_1), l_2(x_2)]^T$. We determine the

homogenized problem by averaging each term of the system (3.17)-(3.19) over a $l_1(x_1) \times l_2(x_2)$ cell, with area $A_{\text{cell}} = l_1(x_1)l_2(x_2)$. The average of a function $v(\boldsymbol{x}, \boldsymbol{y})$ over an $l_1(x_1) \times l_2(x_2)$ cell is defined as

$$\langle v \rangle = \frac{1}{A_{\text{cell}}} \int_0^{l_1(x_1)} \int_0^{l_2(x_2)} v(\boldsymbol{x}, \boldsymbol{y}) dy_1 dy_2, \tag{3.20}$$

a local average for the current position of interest [30].

Using periodicity on a cell and the Divergence Theorem,

$$\left\langle {\nabla_y}^2 (\mu_F I_{F_2}) \right\rangle = \frac{1}{A_{\text{cell}}} \int_{\partial\Omega_0} \boldsymbol{n} \cdot \nabla_y (\mu_F I_{F_2}) dS_y = 0,$$

where $\partial\Omega_0$ is the boundary of the cell, $\boldsymbol{n}$ is the outward normal vector, and dS_y is along the cell boundary. The periodicity on the small scale also gives that the flux of individuals on either side of the cell boundary is the same. The number of infected individuals that are mobile (i.e. leaving the area) is proportional to $\mu_F I_F$, and continuity conditions therefore apply to this quantity, i.e., $\mu_F I_F$ (the number of individuals) and $\nabla(\mu_{F_1} I_F)$ (the flux) are continuous across boundaries. The net flux of individuals over the boundary is proportional to the first derivative of $\mu_F I_F$ (as opposed to μ_F times the derivative of I_F), which is a consequence of the ecological diffusion model for movement. Similarly, $\langle \nabla_y^2 (\mu_M I_{M_2}) \rangle = 0$.

We apply averaging to all terms in (3.17). This means the parameters that depend on small-scale variability $\boldsymbol{y}$ stay inside of averages of the form (3.20), while parameters and variables without $\boldsymbol{y}$ dependence can be moved outside of the averages, i.e.,

$$\begin{aligned}
\left\langle \partial_t \frac{c_{IF}}{\mu_F} \right\rangle &= \left\langle \frac{1}{\mu_F} \right\rangle \partial_t c_{IF}, \\
\left\langle \nabla_x^2 c_{IF} \right\rangle &= \nabla_x^2 c_{IF}, \\
\left\langle \frac{1}{\omega} \left(\beta_{FF} \hat{S}_F - \omega - \phi \right) \frac{c_{IF}}{\mu_F} \right\rangle &= \left\langle \frac{1}{\omega} \left(\beta_{FF} \hat{S}_F - \omega - \phi \right) \frac{1}{\mu_F} \right\rangle c_{IF}, \\
\left\langle \frac{\beta_{MF} \hat{S}_F}{\omega} \frac{c_{IM}}{\mu_M} \right\rangle &= \frac{\beta_{MF}}{\omega} \left\langle \frac{\hat{S}_F}{\mu_M} \right\rangle c_{IM},
\end{aligned}$$

and

$$\left\langle \frac{\gamma_F \alpha_{DM} \hat{S}_F}{\omega} H_0 \right\rangle = \frac{\gamma_F \alpha_{DM}}{\omega} \left\langle \hat{S}_F H_0 \right\rangle.$$

The averages are similar for the equation for I_M and H_0, except that the environmental hazard H_0 depends upon both spatial scales, so it must remain inside of the averages.

We obtain our homogenized system after averaging (3.17)-(3.19) and simplifying. The homogenized equations are differential equations in the large spatial and slow time scales, with small-scale variability expressed through the averages:

$$\begin{aligned} \partial_t c_{IF} = {} & \frac{\bar{\mu}_F}{\omega} \nabla_x^2 c_{IF} + \bar{\mu}_F \left\langle \frac{1}{\omega} \left(\beta_{FF} \hat{S}_F - \omega - \phi \right) \frac{1}{\mu_F} \right\rangle c_{IF} \\ & + \bar{\mu}_F \frac{\beta_{MF}}{\omega} \left\langle \frac{\hat{S}_F}{\mu_M} \right\rangle c_{IM} + \bar{\mu}_F \frac{\gamma_F \alpha_{DM}}{\omega} \left\langle \hat{S}_F H_0 \right\rangle, \end{aligned} \tag{3.21}$$

$$\begin{aligned} \partial_t c_{IM} = {} & \frac{\bar{\mu}_M}{\omega} \nabla_x^2 c_{IM} + \bar{\mu}_M \left\langle \frac{1}{\omega} \left(\beta_{MM} \hat{S}_M - \omega - \phi \right) \frac{1}{\mu_M} \right\rangle c_{IM} \\ & + \bar{\mu}_M \frac{\beta_{FM}}{\omega} \left\langle \frac{\hat{S}_M}{\mu_F} \right\rangle c_{IF} + \bar{\mu}_M \frac{\gamma_M \alpha_{DM}}{\omega} \left\langle \hat{S}_M H_0 \right\rangle, \end{aligned} \tag{3.22}$$

and

$$\partial_t \langle H_0 \rangle = \bar{\mu}_F^{-1} \left(\frac{\alpha_F}{\alpha_{DM} \omega} + \frac{\alpha_{DF}}{\alpha_{DM}} \right) c_{IF} + \bar{\mu}_M^{-1} \left(\frac{\alpha_M}{\alpha_{DM} \omega} + 1 \right) c_{IM} - \frac{\delta}{\omega} \langle H_0 \rangle, \tag{3.23}$$

where $\bar{\mu}_F = \frac{1}{\left\langle \frac{1}{\mu_F} \right\rangle}$ and $\bar{\mu}_M = \frac{1}{\left\langle \frac{1}{\mu_M} \right\rangle}$. In fact, $\bar{\mu}_F$ and $\bar{\mu}_M$ are harmonic averages of the motilities, a natural product of this form of homogenization [23].

Note that (3.23) is in terms of the averaged environmental hazard, $\langle H_0 \rangle$, the hazard terms in (3.21) and (3.22) are averages of steady state populations multiplying the hazard, $\left\langle \hat{S}_F H_0 \right\rangle = C_F \left\langle \frac{H_0}{\mu_F} \right\rangle$ and $\left\langle \hat{S}_M H_0 \right\rangle = C_M \left\langle \frac{H_0}{\mu_M} \right\rangle$. It is a reasonable assumption that there is a correlation between the deer aggregation and prion contamination. Therefore, in the following simulations, we used $\left\langle \frac{H_0}{\mu_F} \right\rangle = \sigma_F \left\langle \frac{1}{\mu_F} \right\rangle \langle H_0 \rangle$ and $\left\langle \frac{H_0}{\mu_M} \right\rangle = \sigma_M \left\langle \frac{1}{\mu_M} \right\rangle \langle H_0 \rangle$ for constants σ_F and σ_M. The constants can be calculated by returning to the small scale to compute the difference between $\left\langle \frac{H_0}{\mu_F} \right\rangle$ and $\left\langle \frac{1}{\mu_F} \right\rangle \langle H_0 \rangle$ after each time step. This is a time

consuming process and we found that over a sufficient time period (≥ 1 year), $\sigma_F = \sigma_M = 1$ gives very similar results, as shown in the next section.

Our homogenized model is much easier to solve numerically than (3.6)-(3.8), yet retains the small scale variability through division by the motility coefficient (3.12). This allows us to run simulations over a large domain, exploring several different spread scenarios.

3.3 Simulating Spread of CWD

CWD was first detected in the free-ranging mule deer population in the La Sal Mountains of Utah in 2002. Since then 54 positive cases have been identified in the state out of 19,000 deer tested. The area with the highest prevalence is the La Sal Mountains in Southeast Utah with 38 of the positive cases [100]. During the 2011 hunting season the first positive CWD case was found in the vicinity of the Abajos Mountains [54]. Exploring the spread of CWD from the La Sal Mountains southwest to the Abajo Mountains is the objective for our simulations. A map of Southeast Utah with these mountain ranges circled is found in Figure 3.1. In this section, we define the area for the simulations, including boundary and initial conditions. We explain our method for estimating motilities from GPS collar data and outline sources for the other model parameters. Then we describe the assumptions for the different simulations and compare the results.

3.3.1 Study Area

Our study area is the trapezoidal region east of the Colorado River in Southeast Utah, shown in Figure 3.1. The Colorado River acts as a barrier to deer movement [27], so we approximate it by a line and reflect values across it to simulate a no-flux boundary. (See Figure 3.2.) No-flux boundary conditions are used for the other boundaries of the region as well, assuming no deer enter or leave.

Characteristic of the Colorado Plateau ecoregion [101], our study area is comprised of high mountains, the La Sal Mountains and the Abajo Mountains, surrounded by valleys, canyons, shrubland, deserts, and farmland. Most deer migrate, sometimes for more

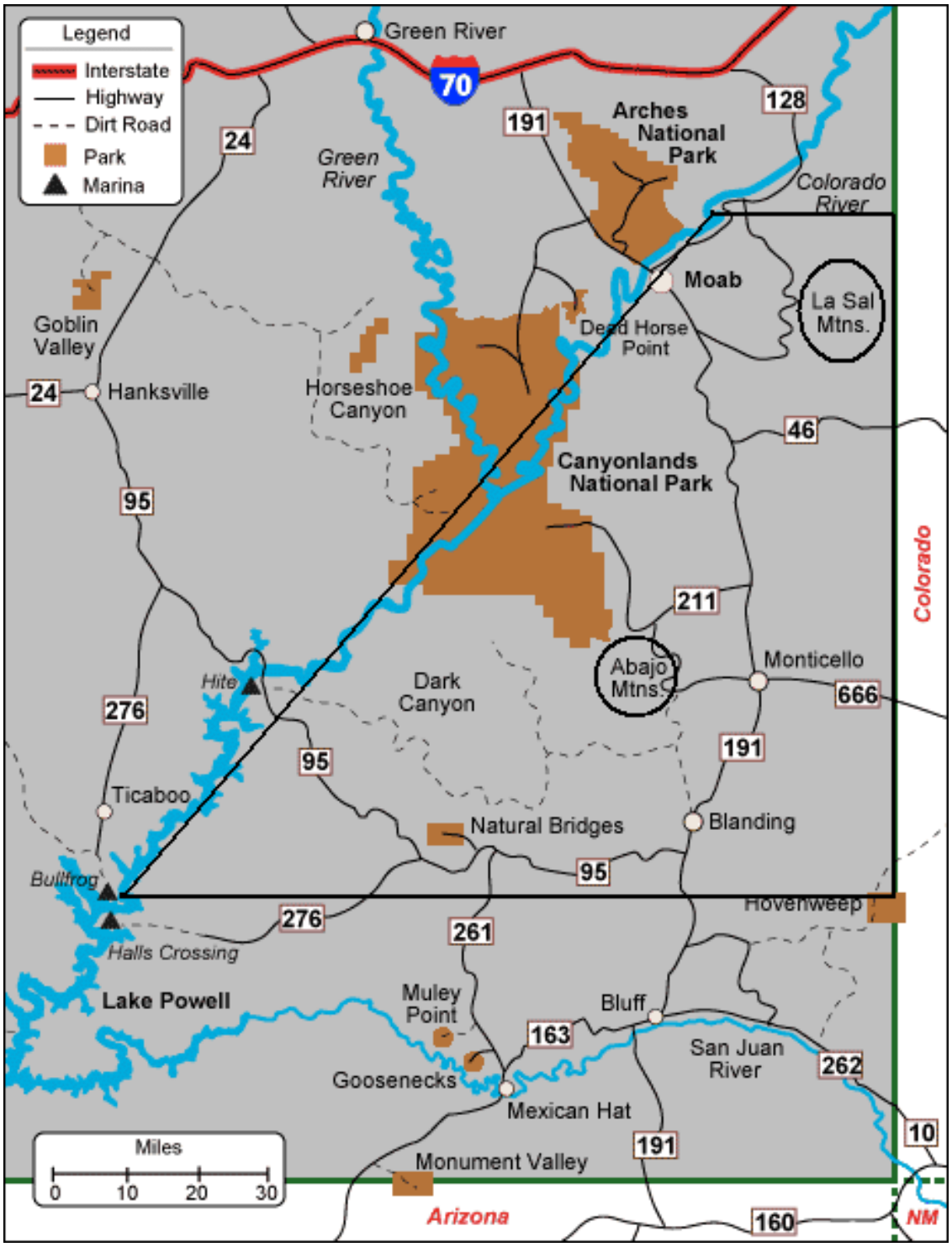

Figure 3.1: A map of Southeast Utah which includes the La Sal Mountains and the Abajo Mountains (circled) [81]. Our study area is enclosed by the trapezoid. The Colorado River acts as a barrier to deer movement.

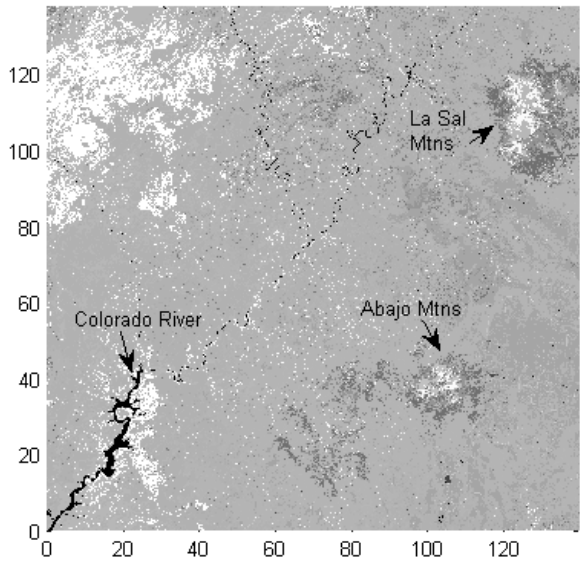

(a) Breeding season motilities for male deer

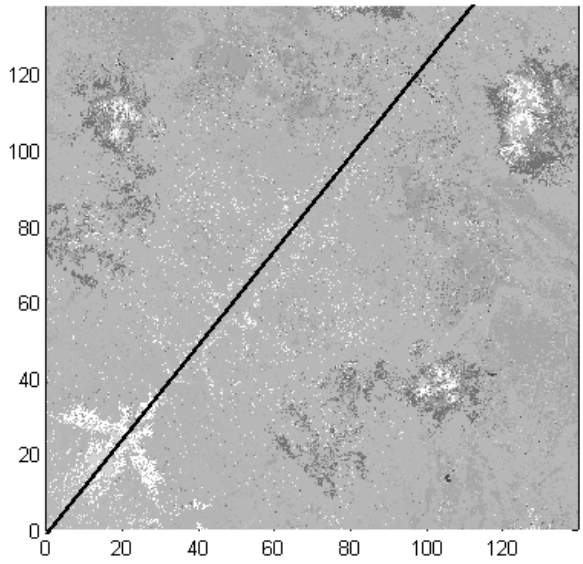

(b) Reflection about the Colorado River

Figure 3.2: Motilities for male deer during breeding season. Dark shades indicate small motility values, while light shades indicate large values. The area for our simulation is the trapezoidal region east of the Colorado River shown in (a). The Colorado River is approximated by a line and values are reflected across that line, to create no-flux condition at the boundary, as shown in (b).

than 80 kilometers, between lower elevation winter ranges and higher elevation summer ranges. Important winter range habitats include sagebrush-steppe, pinyon-juniper woodlands, salt desert shrub, and ponderosa pine forests below 7,500 feet. Also, many deer winter in irrigated agricultural areas. Summer habitats include aspen forests, mountain shrub communities, Gambel oak forests, montane sagebrush-steppe, spruce-fir and mixed conifer forests, and montane parks and meadows [79].

Since the La Sal and Abajo Mountains are approximately 100 kilometers apart (see Figure 3.1), separated by critical winter range habitat, a management concern has been the spread of CWD from the La Sals to the Abajos. In fact the first CWD positive deer was found near the Abajos during the 2011 hunting season. We chose our study area to include these two mountain ranges so we can explore this spread.

The Utah Division of Wildlife Resources (UDWR) divides the state into Wildlife Management Units. Our study area is contained in two of those units, La Sal (#13) and San Juan (#14). A 15 buck/100 doe ratio is the goal of harvesting practices in these units. Steady-state populations for our simulations were taken from post-hunting season estimates from computer models used by the UDWR [100]. There is a 2% CWD prevalence in bucks in the La Sal Mountains, while prevalence is believed to be less than 1% in the doe population [100]. Samples are drawn from hunter-harvested deer for testing and since female deer are not routinely hunted in Utah, there is little known about CWD prevalence in females.

3.3.2 Model Parameters

In 2005-06, the UDWR collared 50 deer, a mix of adult males, young males, and adult females, in the La Sal Mountains. GPS data was collected on their movement, with an emphasis on deer locations during breeding season, to explore the connection between breeding behaviors and movement [53]. The time intervals for collecting location data depended on the time of year: 12 hour intervals in late winter/early spring, 6 hour intervals during spring migration/early summer, 12 hour intervals during summer/early fall, and 30 minute intervals during fall migration/breeding season.

Mule deer exhibit high site fidelity to traditional summer and winter ranges with seasonal migration occurring during specific times of the year. Females form matrilinear groups which remain cohesive particularly during the breeding season when males begin wandering between groups looking for receptive females [53]. This somewhat complicates the idea of a motility being assigned to a land cover type, because the use of various habitats by deer varies widely by sex and season. Partitioning the GPS movement data by sex and by season allowed us to estimate motilities for males and females during winter, summer, and breeding season. We did not compute motilities specifically for spring or fall migration, since migration occurs during a relatively short period of time and represents the change of motility between seasons, i.e. spring migration is the population response to the change in motility between winter and summer.

To obtain motility coefficients, we used movement data from 11 female deer and 11 male deer, selected for having the most complete data (approximately a year long). The method of Johnson et al. [39] and the R contributed package CRAWL were used to fit a continuous time correlated random walk model to the location data and predict locations at one minute time intervals, as outlined in Chapter 4 . This method considers movement as a continuous process, so irregular time intervals were not an issue. A sample of 50 possible paths were drawn from the predictive posterior distribution for possible paths for each deer. We used the LANDFIRE data set [93] to classify each predicted location by land cover type. We counted the minutes spent in each of 38 land cover types and calculated the mean time spent (residence times) in units of minutes per block. The motility coefficients were obtained from the residence times by taking the multiplicative inverse and converting to units of square kilometers per day. These values are found in Table 3.2. The summer, breeding season, and winter motilities for male and female deer are compared in Figure 3.3 for the area containing the La Sal Mountains.

The other parameters used in the simulations are found in Table 3.1, many from Miller et al. [58]. Since Miller et al. fit their ordinary differential equation models with data from captive mule deer, they adjusted the infection rate downward by a factor of ten for free-

Table 3.2: Mule deer motility coefficients in square kilometers per day. Small numbers indicate habitats where deer linger, while large numbers highlight areas they quickly leave.

LANDFIRE	**Winter**		**Summer**		**Breeding**	
Classification, EVT	**male**	**female**	**male**	**female**	**male**	**female**
11 open water	0.10	0.22	0.29	0.40	0.27	0.99
21 dev. open space	0.57	0.44	0.16	0.12	0.25	0.05
22 dev. low intensity	0.54	0.38	0.07	0.08	0.03	0.02
23 dev. med. Intensity	0.42	0.41	0.40	1.30	0.41	0.96
31 barren	0.44	0.37	0.12	0.06	0.20	0.43
81 pasture/hay	0.51	0.31	0.08	0.36	0.17	0.03
82 irrigated crops	1.43	0.62	0.14	0.05	0.19	0.52
2001 sparse veg.	0.41	0.51	0.29	0.14	0.53	1.30
2006 alpine sparse veg.	0.82	1.56	0.09	0.08	0.21	12.96
2011 aspen	0.29	0.23	0.05	0.03	0.12	0.04
2016 pinyon-juniper	0.27	0.19	0.11	0.05	0.19	0.07
2051 dry mixed conifer	0.23	0.20	0.15	0.04	0.10	0.06
2052 mixed conifer	0.53	0.64	0.11	0.07	0.56	0.06
2054 ponderosa pine woodland	0.23	0.23	0.15	0.04	0.19	0.04
2055 dry spruce-fir	1.73	0.97	0.08	0.03	0.56	12.96
2057 subalpine limber pine	12.96	0.18	0.12	0.08	0.95	12.96
2061 aspen/mixed conifer	0.66	0.40	0.08	0.05	0.23	0.02
2062 mtn. mahogany	0.44	0.28	0.16	0.02	0.11	0.04
2064 low sagebrush	0.29	0.23	0.10	0.04	0.17	0.07
2066 saltbrush scrub	0.73	0.31	1.10	3.33	0.88	0.51
2080 big sagebrush	0.20	0.15	0.15	0.04	0.15	0.06
2081 salt desert scrub	0.32	0.21	0.12	0.46	0.19	0.25
2086 foothill scrub	0.47	0.36	0.19	0.08	0.11	0.34
2093 sand shrubland	0.72	0.64	0.10	5.83	0.70	0.22
2103 semi-desert chaparral	0.13	0.31	0.15	0.02	0.18	0.05
2107 Gambel oak	0.81	0.31	0.09	0.13	12.96	0.08
2117 ponderosa pine savanna	0.28	0.33	0.18	0.02	0.23	0.05
2126 sagebrush steppe	0.27	0.12	0.08	0.11	0.31	0.03
2135 semi-desert grassland	0.28	0.32	0.36	0.61	0.08	0.38
2153 greasewood flat	0.33	0.20	0.10	0.65	0.33	0.08
2159 riparian	0.29	0.18	0.14	0.04	0.20	0.08
2160 subalpine riparian	0.52	0.12	0.07	0.03	0.57	0.08
2180 intro. riparian	0.34	0.22	0.19	0.04	0.18	0.12
2181 annual grass	0.27	0.17	0.18	0.24	0.13	0.06
2210 shrubland-blackbrush	0.26	0.20	0.20	0.11	0.19	0.13
2214 shrubland-manzanita	0.28	0.22	0.07	0.05	0.15	0.06
2217 shrubland-Gambel oak	0.21	0.20	0.08	0.03	0.08	0.05
2220 shrubland-big sagebrush	0.22	0.14	0.20	0.10	0.38	0.03

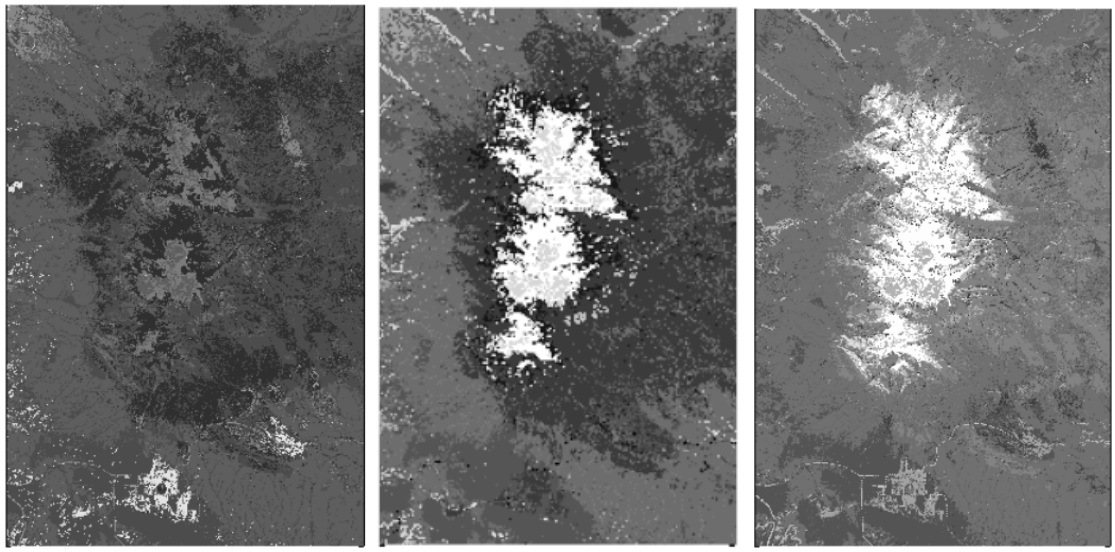

(a) Female Summer (b) Female Breeding (c) Female Winter

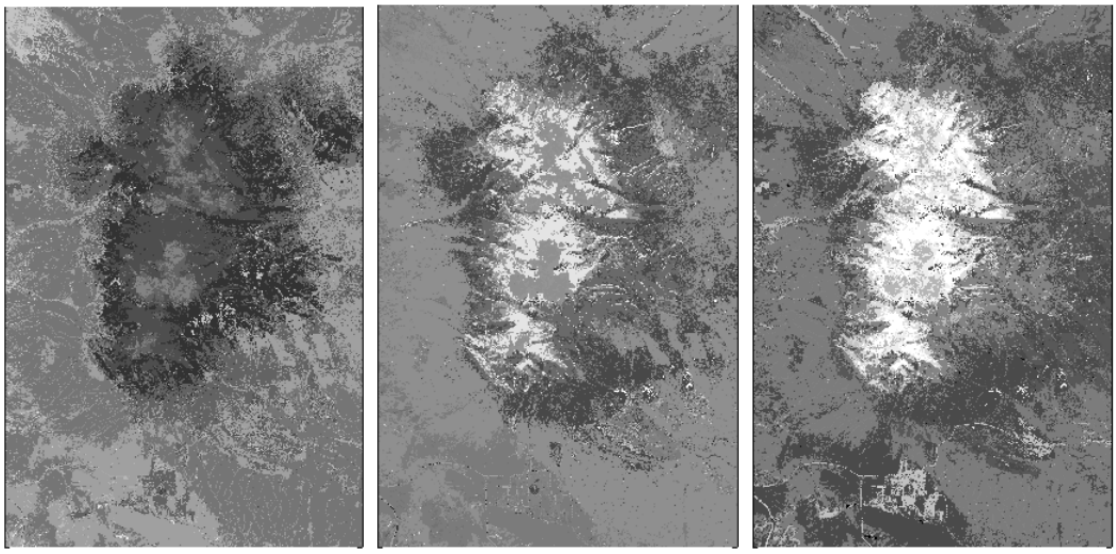

(d) Male Summer (e) Male Breeding (f) Male Winter

Figure 3.3: Comparison of motilities for female and male during summer, breeding season, and winter in an area including the La Sal Mountains. Dark shades represent low motility, i.e., areas where the deer aggregate and spend time, while the lighter regions represent high motility i.e., areas that they avoid or move through quickly. In summer the deer are in the mountains and then move to lower elevations for winter.

ranging mule deer, assuming that natural populations would exhibit one tenth the density. Our model uses motilities to reflect the spatial spread of the disease, which means that where motility is low, the deer are congregating, occasionally as tightly as the captive herd in Miller et al. [58]. It is therefore unclear what infectivity parameters to use. We explore infection rates between the scaled and unscaled values in the simulations.

Our model assumes a steady-state population in the study area. This means that even though the seasonal change in motilities redistributes the deer at the beginning of each season, the total number of deer, N, in the domain needs to remain the same. The constants, C_F and C_M for the steady-state population densities, $\hat{S}_F = \frac{C_F}{\mu_F}$ and $\hat{S}_M = \frac{C_M}{\mu_M}$, were computed separately for each season to maintain this constant number of deer.

3.3.3 Simulations

We conducted several simulations of the spread of CWD from the La Sal Mountains to the Abajo Mountains, exploring different infection rates. The use of variable motility was compared to a constant motility and the model with environment hazard was compared to one without. Other simulations explored the spread during different seasons and a comparison of two ways to average the environmental hazard, $\left\langle \frac{H_0}{\mu_F} \right\rangle$ (the average that is the consequence of homogenization) or $\left\langle \frac{1}{\mu_F} \right\rangle \langle H_0 \rangle$ (an approximation based on the assumption that deer aggregation and prion contamination are correlated), as discussed at the end of Section 3.2.2.

An alternating direction implicit (ADI) numerical method was adapted for the system of homogenized equations (3.21)-(3.23) [64] (see Appendix). We chose a spatial computational step of 600 meters in both directions and a time step of 5 days although other step sizes work as well. The averaging was done over 3000 meter blocks ($\epsilon = 0.01$). We started with an initial number of infected deer (which depends on the simulation) in the La Sal Mountains and simulated the spread over ten years. Table 3.3 displays the results of simulations exploring different infection rates. The number of infected deer were computed from densities (number of infectives per square kilometer) by $N_{IF} = \iint\limits_A I_F dA$ and

$N_{IM} = \iint_A I_M dA$, where N_{IF} is the number of infected females and N_{IM} is the number of infected males.

Table 3.3: Simulations exploring different infection rates for the CWD model over 10 years. Steady state-state populations are from estimations made by the UDWR with computer models [100]. Numbers of females are indicated by f and numbers of males by m. The results are in terms of numbers of infected males and females. The simulation numbers (1, 2, ..., 10) are to aid in referring to particular simulations in the text.

Simulation	**1**	**2**	**3**	**4**	**5**
Steady-state pop.	22,430 f	22,430 f	22,430 f	22,430 f	22,430 f
	4070 m	4070 m	4070 m	4070 m	4070 m
Initial inf.	47 f	47 f	47 f	130 f	47 f
	32 m	32 m	32 m	32 m	32 m
β_{FF}, β_{MF}	8.9315×10^{-5}	5.39×10^{-4}	6.25×10^{-4}	6.25×10^{-4}	6.25×10^{-4}
β_{MM}, β_{FM}	8.9315×10^{-5}	5.39×10^{-4}	6.25×10^{-4}	0.00125	0.00125
Notes	2007 pop.	$\times 6$	$\times 7$	1% prev. in f	$\beta_{MM} = \beta_{FF} \times 2$
Results					
No. of inf. f	0 f	44 f	199 f	539 f	205 f
No. of inf. m	0 m	1 m	4 m	18 m	7 m

Simulation	**6**	**7**	**8**	**9**	**10**
Steady-state pop.	22,430 f	22,430 f	22,430 f	16,957	33,565
	4070 m	4070 m	4070 m	2543	5035
Initial inf.	47 f	47 f	47 f	29 f	79 f
	32 m	32 m	32 m	11 m	54 m
β_{FF}, β_{MF}	6.25×10^{-4}	6.25×10^{-4}	7.15×10^{-4}	6.25×10^{-4}	6.25×10^{-4}
β_{MM}, β_{FM}	0.0019	0.0019	0.00212	0.0019	0.0019
Notes	$\beta_{MM} = \beta_{FF} \times 3$	No hazard	$\times 8$	2010 pop.	Obj. pop.
Results					
No. of inf. f	214 f	112 f	1058 f	7 f	all
No. of inf. m	13 m	5 m	55 m	0 m	all

The first eight simulations use the 2007 estimated populations (the peak population estimate for the last ten years) for the study area of 22,430 females and 4070 males, using an 18:100 buck to doe ratio (from post hunting season population counts). Initial conditions of 2% prevalence in males (32 infectives) and 0.5% prevalence in females (47 infectives) were used for Simulations 1-3 and 5-8. The infection rate from Miller et al. [58] of 8.9315×10^{-5} (Table 3.3) resulted in the disease dying out in ten years (Simulation 1). This has not been the case since new cases of CWD have been detected in the La Sal Mountains every year since 2002. Increasing this rate by a factor of ten for a simulation resulted in all deer becoming infected.

An infection rate of 5.39×10^{-4} ($8.9315 \times 10^{-5} \times 6$) yields one infected male and 44

infected females at the end of ten years (Simulation 2). Increasing the rate to 6.35×10^{-4} yields 199 infected females and 4 infected males (Simulation 3). Changing the number of initial infected females from 47 to 130 (1% prevalence) resulted in 539 infected females and 18 infected males (Simulation 4). Returning to 0.5% prevalence in females and setting the infection rate for males ($\beta_{MM} = \beta_{FM} = 0.00125$) to be twice that of females ($\beta_{FF} = \beta_{MF} = 6.23 \times 10^{-4}$) increases the number of infectives to 205 females and 7 males (Simulation 5). Tripling the infection rate for males gives 214 infected females and 13 infected males (Simulation 6). The result of this simulation is shown in Figure 3.4.

Keeping the same initial conditions and infection rates, we ran the model without prions collecting in the environment (Simulation 7). After 10 years the number of infected females was 112 compared to 214 for the model with environmental hazard. The number of infected males was 5 compared to 13. Simulation 8 resulted in an increase in infected males (from 32 to 55 over 10 years) by using infection rates $\beta_{FF} = \beta_{MF} = 7.15 \times 10^{-4}$ and $\beta_{MM} = \beta_{FM} = 0.00212$. It is interesting to note that this was the only one of the first eight simulations that resulted in an increase in infected male deer from the initial amount of infectives. The number of infective females, however, increased for lower infection rates. This could be due to the fact that the estimated motilities for males are consistently larger than those for females (see Table 3.2) in key mule deer habitats, such as sagebrush steppe, pinyon-juniper forest, and ponderosa pine woodland. This means that female deer congregate more, while male deer wander more. This connection between motility and disease spread is a basic feature of the CWD model.

Next we returned to $\beta_{FF} = \beta_{MF} = 6.23 \times 10^{-4}$and $\beta_{MM} = \beta_{FM} = 0.0019$ and varied the steady-state population of susceptibles. The estimated population for the study area for 2010 with 15 bucks to 100 does (from post hunting season population counts) is 16,957 females and 2543 males. Using these numbers resulted in 7 infected females and 0 infected males (Simulation 9). The goal of the UDWR for the two management units in our study area is to have an objective population of 38,600 mule deer [100]. Using this population with the goal of 15 bucks to 100 does, all the deer become infected by the end of 10 years

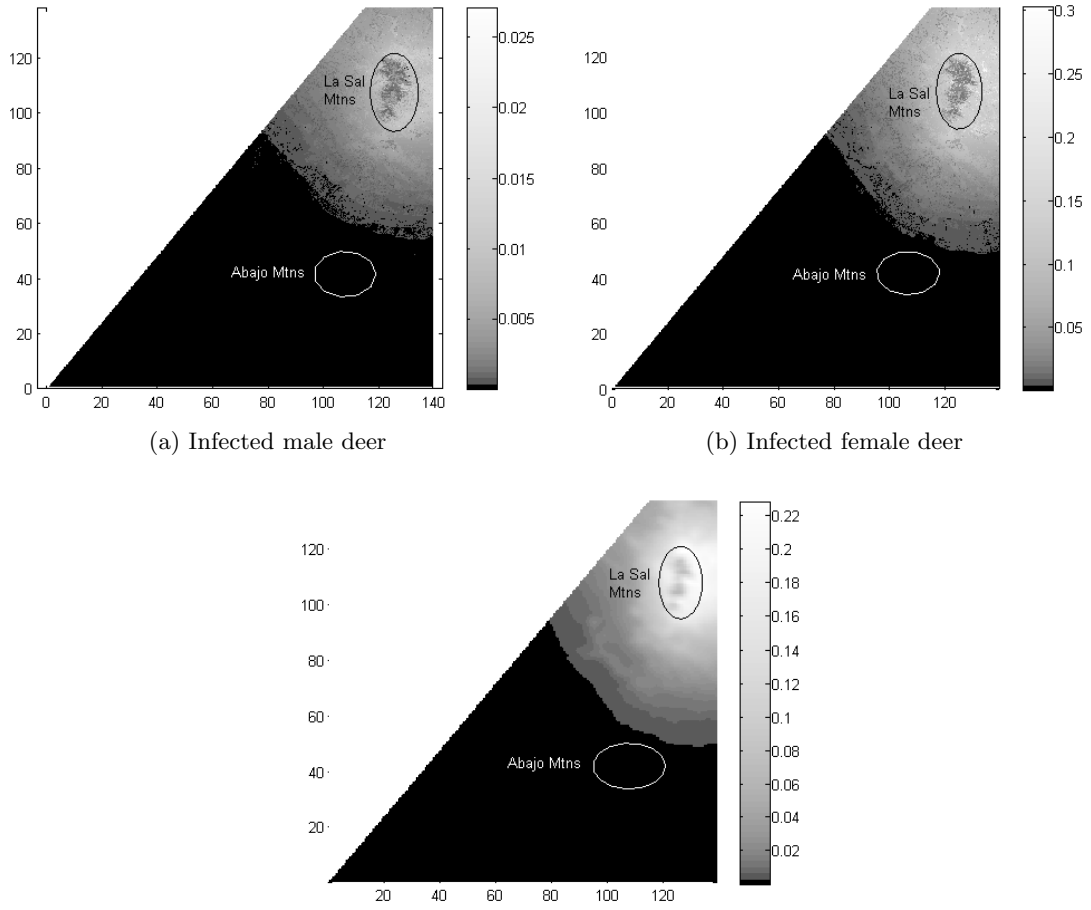

(a) Infected male deer

(b) Infected female deer

(c) Environmental hazard

Figure 3.4: The results of running the simulation for ten years using $\beta_{FF} = \beta_{MF} = 6.5 \times 10^{-4}$ and $\beta_{MM} = \beta_{FM} = 0.0019$. The initial conditions are shown in Table 3.3, Simulation 6. The lighter the shade the higher the density (in number per square kilometer) of infected deer in (a) and (b) and the higher the concentration of prions in the environment in (c). The densities of infected male and female deer were returned to the small scale at the end of the simulations by using interpolation. Environmental hazard, however, remains in terms of the homogenization scale, which accounts for the smooth appearance. The amount of environmental hazard is in units of mass per square kilometer.

(Simulation 10).

We compared our model with variable motilities to one using a constant motility, computed as a weighted average (Simulations 11 and 12 in Table 3.4). Beginning with 214 infected females and 64 infected males and a susceptible population of 21,348 females and 3202 males, the model with variable motilities resulted in 890 infected females and 40 infective males after 10 years, compared to 48 infected females and 2 infected males for the mode with constant motility. The spread was much wider for the constant motility model as expected (see Figure 3.5). This is a substantial difference, illustrating that low motilities in the variable motility model aggregate deer causing an increase in the number of infectives while slowing the spread into new areas, an effect absent in the constant motility model.

Table 3.4: The results of simulations comparing variable motilities with a constant motility (Simulations 11 and 12) and a comparison of two ways of averaging the environmental hazard (Simulations 13 and 14).

Simulation	**11**	**12**	**13**	**14**
Steady-state pop.	21,348 f	21,348 f	22,430 f	22,430 f
	3202 m	3202 m	4070 m	4070 m
Initial inf.	214 f	214 f	47 f	47 f
	64 m	64 m	32 m	32 m
β_{FF}, β_{MF}	0.0005562	0.0005562	0.000625	0.000625
β_{MM}, β_{FM}	0.0007843	0.0007843	0.0019	0.0019
Notes	2002 pop.	Constant motility	$\left\langle \frac{H}{\mu} \right\rangle$	$\left\langle \frac{1}{\mu} \right\rangle \langle H \rangle$
Results				
No. of inf. f	890 f	48 f	94 f	105 f
No. of inf. m	40 m	2 m	5 m	6 m

As mentioned at the end of Section 3.2.2, we save computational time by using $\left\langle \frac{H_0}{\mu_F} \right\rangle = \sigma_F \left\langle \frac{1}{\mu_F} \right\rangle \langle H_0 \rangle$ (similar for male motilities). In simulations 13 and 14 (See Table 3.4.) we test this using $\sigma_F = \sigma_M = 1$. The average $\left\langle \frac{H_0}{\mu_F} \right\rangle$ is computed by returning to the small scale every time step. In order to make this computationally feasible, we subsampled the motility matrix for our study area, using every third value. This resulted in 94 infected females and 5 infected males at the end of 10 years. Subsampling in this same manner for the simulation using $\sigma_F \left\langle \frac{1}{\mu_F} \right\rangle \langle H_0 \rangle$, we obtained similar results, 105 infected females and 6 infected males. This indicates that the approximation is worth the computational savings and makes it possible to numerically solve the equations for a large domain.

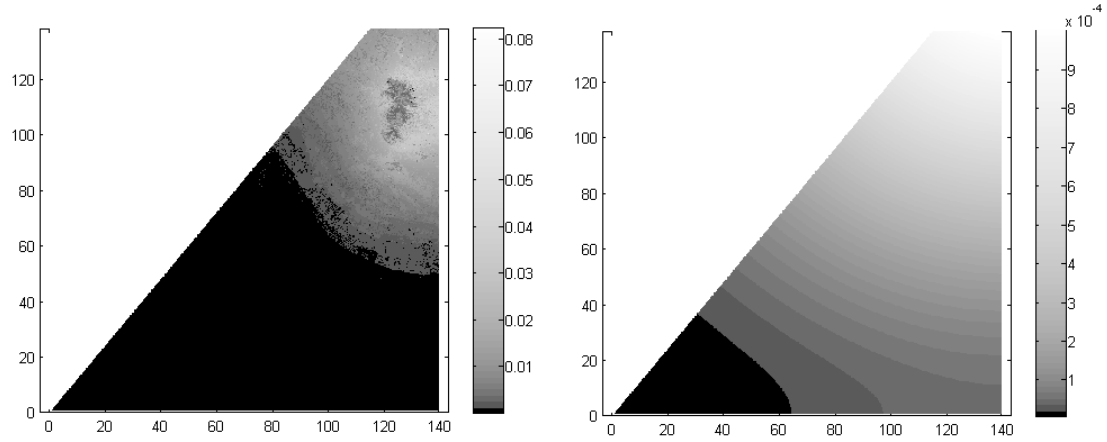

(a) Variable motility coefficient (b) Constant motility coefficient

Figure 3.5: The density of male infectives simulated with variable motilities (a) and with a constant motility (b) computed as a weighted average of the male motilities. For the initial vales and infection rates used see Table 3.4, Simulations 11 and 13. The simulation with variable motilities predicted a total of 930 infected deer after 10 years, while the constant motility simulation predicted a total of 50 infected deer.

The motilities for males and females vary with season, so we ran a simulation to compare the spread of CWD over a single season to see if time of year influences spread. The same steady-state susceptible population and number of infectives were used at the beginning of each season. The length of each season is defined by how the GPS movement data was collected (153 days for summer, 61 days for breeding season, and 151 days for winter). The results are found in Table 3.5 and shown in Figure 3.6 for male deer. Even though breeding season is much shorter than winter, the increase in infectives was very similar. However, the spread of infectives during winter was much wider than during breeding season. Breeding season had a net increase of 0.23 infected females per day and 0.1 infected males per day, much higher that 0.1 infected females per day and 0.05 infected males per day during winter. This reflects that breeding behaviors can increase the number of new infectives this time of year.

3.4 Stability and asymptotic speed of spread

The application of homogenization to our CWD model facilitated the simulations over

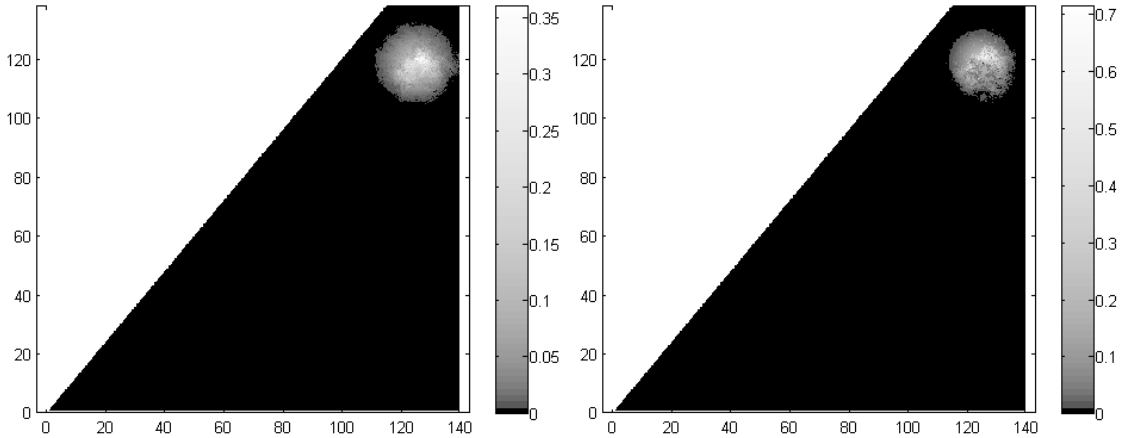

(a) Summer

(b) Breeding season

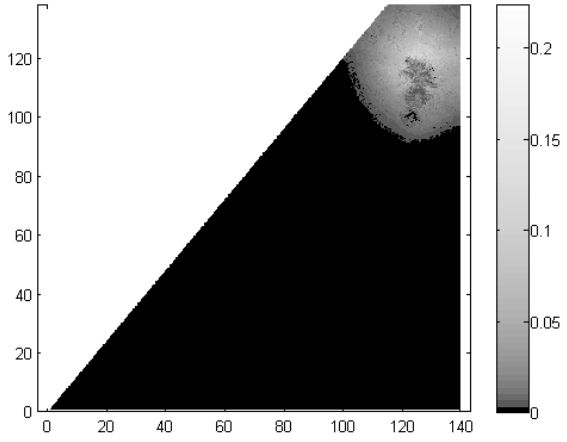

(c) Winter

Figure 3.6: A comparison of CWD spread for one season for male mule deer. The same initial values were used at the beginning of each season, as found in Table 3.5. The resulting numbers of infectives were quite similar (31 for summer, 38 for breeding season, and 40 for winter). However, spread occurred over a much larger area during winter than during breeding season and summer.

Table 3.5: Comparison of CWD spread over one season. The length of each season is defined by how the GPS movement data was collected (153 days for summer, 61 days for breeding season, and 151 days for winter). The number of infectives per day is the net increase or decrease in the number of infectives divided by the length of the season.

Simulation	**15**	**16**	**17**
Steady-state pop.	22,430 f	22,430 f	22,430 f
	4070 m	4070 m	4070 m
Initial inf.	47 f	47 f	47 f
	32 m	32 m	32 m
β_{FF}, β_{MF}	0.000625	0.000625	0.000625
β_{MM}, β_{FM}	0.0019	0.0019	0.0019
Notes	1 summer	1 breeding season	1 winter
Results			
No. of inf. f	59 f	61 f	62 f
No. of inf. m	31 m	38 m	40 m
f inf. per day	0.08	0.23	0.1
m inf. per day	-0.007	0.1	0.05

a large area of Utah. The small-scale variability is preserved in the averaged coefficients. Those coefficients are also important in examining the asymptotic invasive speed of disease spread. Skellam [90] introduced this idea for constant coefficient reaction-diffusion equations by estimating the speed of the spread of muskrats across Europe. Shigesada and Kawasaki [88] extended it to ecological diffusion over an environment composed of two types of patches. In this section we further develop this concept for ecological diffusion over a heterogeneous landscape composed of many different habitat types, with the goal of using the averaged coefficients from the homogenized equations to explore invasion speeds and critical population levels for specific areas.

The spatially-structured "invasibility" of large-scale landscapes can be examined via the homogenized equations (3.21)-(3.23). If we consider the system without the environmental hazard, assuming horizontal transmission occurs on a faster time scale than accumulation of prions in the environment, the system becomes:

$$\partial_t u = D_1 \nabla_x^2 u + A_1 u + A_2 v \tag{3.24}$$

$$\partial_t v = D_2 \nabla_x^2 v + B_1 v + B_2 u., \tag{3.25}$$

where $u = c_{IF}$ and $v = c_{IM}$ for notational simplicity. The coefficients, after multiplication by ω to return to the original time scale, are defined as follows:

$$D_1 = \bar{\mu}_F, \quad D_2 = \bar{\mu}_M \tag{3.26}$$

$$A_1 = \bar{\mu}_F \left\langle \left(\beta_{FF}\hat{S}_F - \omega - \phi\right)\frac{1}{\mu_F}\right\rangle, \quad B_1 = \bar{\mu}_M \left\langle \left(\beta_{MM}\hat{S}_M - \omega - \phi\right)\frac{1}{\mu_M}\right\rangle, \tag{3.27}$$

$$A_2 = \bar{\mu}_F\beta_{MF}\left\langle \frac{\hat{S}_F}{\mu_M}\right\rangle, \quad \text{and} \quad B_2 = \bar{\mu}_M\beta_{FM}\left\langle \frac{\hat{S}_M}{\mu_F}\right\rangle. \tag{3.28}$$

At the leading edge of the spread of the disease, we assume a traveling solution of the form

$$\begin{pmatrix} u \\ v \end{pmatrix} = \begin{pmatrix} u_0 \\ v_0 \end{pmatrix} e^{\sigma t + \lambda(x-ct)}, \tag{3.29}$$

where u_0 and v_0 are arbitrary constants, σ is the growth rate, λ is the shape of the front, and c is the asymptotic speed. Substituting (3.29) into (3.24) and (3.25) and rearranging gives the dispersion relation,

$$\begin{pmatrix} -\sigma + c\lambda + A_1 + D_1\lambda^2 & A_2 \\ B_2 & -\sigma + c\lambda + B_1 + D_2\lambda^2 \end{pmatrix}\begin{pmatrix} u_0 \\ v_0 \end{pmatrix} = \begin{pmatrix} 0 \\ 0 \end{pmatrix}. \tag{3.30}$$

Setting the determinant of the matrix in (3.30) to zero, with $\sigma = 0$ (no growth in the traveling frame of reference) and $\frac{d\sigma}{d\lambda} = 0$ (maximum growth) results in the system of equations,

$$f(c, \lambda, \boldsymbol{\theta}) = (c\lambda + A_1 + D_1\lambda^2)(c\lambda + B_1 + D_2\lambda^2) - A_2B_2 = 0 \tag{3.31}$$

$$\frac{df}{d\lambda} = (c + 2D_1\lambda)(c\lambda + B_1 + D_2\lambda^2) + (c + 2D_2\lambda)(c\lambda + A_1 + D_1\lambda^2) = 0, \tag{3.32}$$

where $\boldsymbol{\theta}$ is a vector containing the parameters.

We can obtain an expression for the wave speed, c, by multiplying (3.31) by -2 and (3.32) by λ and adding the resulting equations together.

$$c = g(\lambda, \boldsymbol{\theta}) = \frac{-2(D_1 D_2 \lambda^4 + A_2 B_2 - A_1 B_1)}{\lambda(D_1 \lambda^2 + D_2 \lambda^2 - A_1 - B_1)}. \tag{3.33}$$

We substitute (3.33) into (3.31) to obtain a polynomial in λ, $F(\lambda, \boldsymbol{\theta}) = 0$. For a given set of parameters, $\boldsymbol{\theta}$, we can numerically find a point ($\lambda < 0$, c) that satisfies $F(\lambda, \boldsymbol{\theta}) = 0$ and $c = g(\lambda, \boldsymbol{\theta})$. We desire $\lambda < 0$ to be consistent with the exponentially decreasing shape of the wavefront.

The parameters, defined in (3.26)-(3.28), are dependent on the motilities, μ_F and μ_M, and steady-state population densities, $\hat{S}_F$ and $\hat{S}_M$. The number, N_F, of female deer is given by

$$N_F = \iint_A \hat{S}_F dA = \iint_A \frac{C_F}{\mu_F} dA = C_F A \left\langle \frac{1}{\mu_F} \right\rangle,$$

where A is the area of a region of interest. Likewise, the number of males is given by $N_M = C_M A \left\langle \frac{1}{\mu_M} \right\rangle$. Then $C_F = \frac{\mu_F N_F}{A}$ and $C_M = \frac{\mu_M N_M}{A}$ and (3.27)-(3.28) become:

$$A_1 = \frac{\bar{\mu}_F^2}{A} \left\langle \frac{1}{\mu_F^2} \right\rangle \beta_{FF} N_F - \bar{\mu}_F \left\langle \frac{1}{\mu_F} \right\rangle (\omega + \phi), \tag{3.34}$$

$$B_1 = \frac{\bar{\mu}_M^2}{A} \left\langle \frac{1}{\mu_M^2} \right\rangle \beta_{MM} N_M - \bar{\mu}_M \left\langle \frac{1}{\mu_M} \right\rangle (\omega + \phi), \tag{3.35}$$

$$A_2 = \frac{\bar{\mu}_F^2}{A} \left\langle \frac{1}{\mu_F \mu_M} \right\rangle \beta_{MF} N_F, \quad \text{and} \quad B_2 = \frac{\bar{\mu}_M^2}{A} \left\langle \frac{1}{\mu_F \mu_M} \right\rangle \beta_{FM} N_M. \tag{3.36}$$

Now our exploration of c values can be framed in terms of N_F and N_M, for an area of interest and given motilities, infection rates, death rate, and cull rate.

To illustrate this, we used two rectangular regions in our study area, shown in Figure 3.7. Area A includes the La Sal Mountains and contains critical summer range habitats. It is where CWD was first discovered in Utah in 2002. Area B is critical winter range between the La Sal and Abajo Mountains, and the area through which a wave of infection

would have to travel to reach the Abajo Mountains.

Using population estimates for 2007 and 2010, and the population goal of the UDWR (objective), we calculated the female and male population for each area separately for summer and winter, subject to the respective motilities. Those populations in Area A and Area B for winter are shown as points on the graphs in Figure 3.8. For infection rates $\beta_{FF} = \beta_{MF} = 6.23 \times 10^{-4}$and $\beta_{MM} = \beta_{FM} = 0.0019$, the areas where the invasive speed, c, is greater or lesser than zero are indicated. For these infection rates all of the population points fall in the region of positive invasive speed, although for Area A the 2010 winter population estimate (193 males and 1233 females) is close to the $c = 0$ curve, indicating a much slower rate of spread.

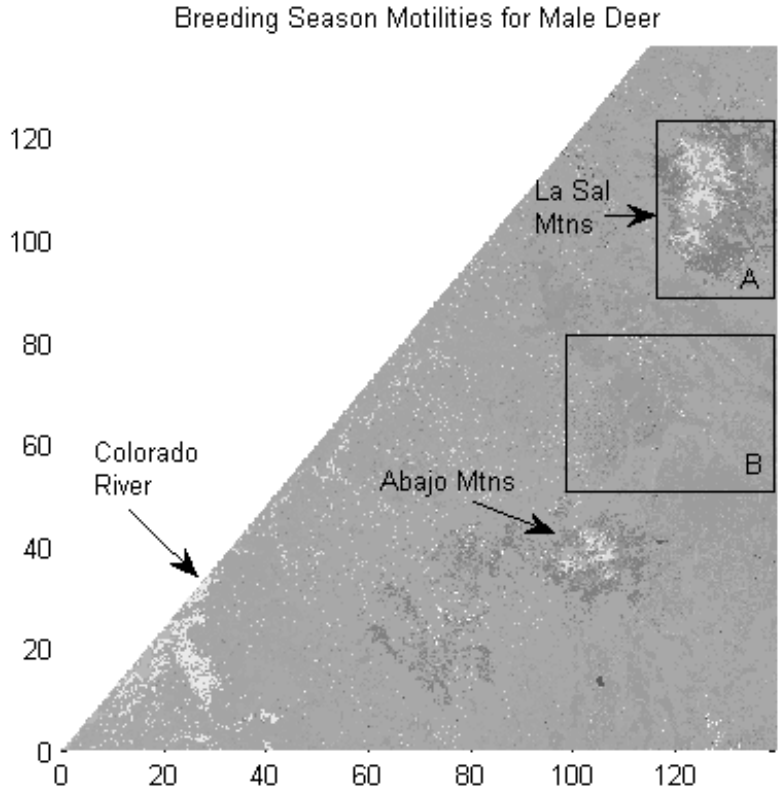

Figure 3.7: Areas averaged across for critical population examples. Area A includes the La Sal Mountains and is critical summer range for mule deer. It is where CWD was first discovered in Utah (2002). Area B is an area between the La Sal and Abajo mountain ranges and is critical winter range.

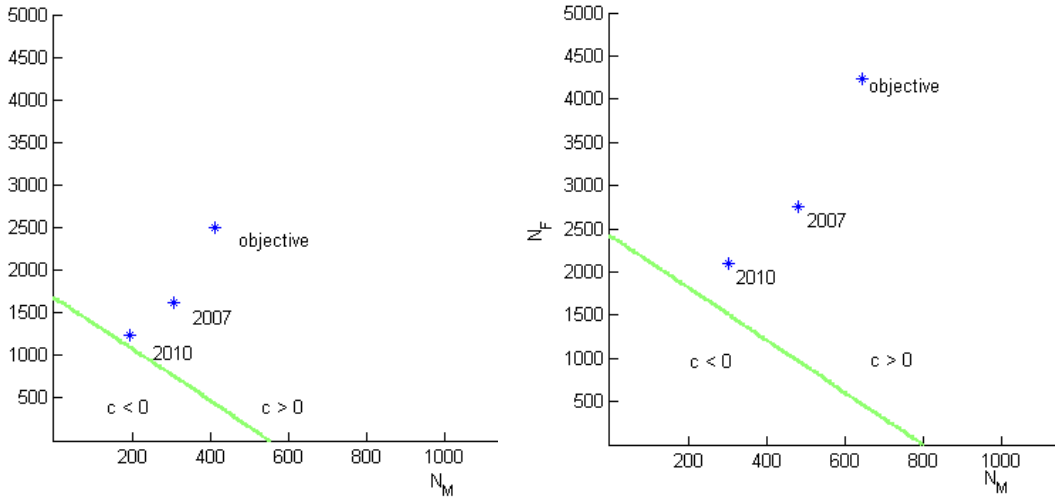

(a) La Sals (Area A)

(b) Area between the mountains (Area B)

Figure 3.8: The asterisks show populations for these areas subject to winter motilities for male (N_M) and female (N_F) deer using the population estimates for 2007and 2010, and the objective goal. The green curves indicated where the asymptotic invasive speed is zero using infection rates $\beta_{FF} = \beta_{MF} = 6.23 \times 10^{-4}$and $\beta_{MM} = \beta_{FM} = 0.0019$. In Area A the 2010 estimated population is close to the $c = 0$ line.

Figure 3.9 compares the $c = 0$ curves for a variety of infection rates for Area A with summer motilities. The scaled infection rate from Miller et al. [58], 8.93×10^{-5}, produces the longest curve. This rate would mean that the disease for all the population estimates would not diffuse from the La Sals. The discovery of CWD in the Abajos indicates that the disease has spread from the La Sals [54]. An infection rate of greater than 3.57×10^{-4} is needed for spread from a population the size of the 2007 estimate. This increases to 5.36×10^{-4} for a population at the 2010 level.

Figure 3.10 includes contours of speed, c, for Area A, comparing summer and winter results, using $\beta_{FF} = \beta_{MF} = 6.23 \times 10^{-4}$and $\beta_{MM} = \beta_{FM} = 0.0019$. The units of c are kilometers per day. Converting them to kilometers per year helps put population size into the context of the speed needed for CWD to spread the 100 kilometers from the La Sal Mountains to the Abajo Mountains. For summer (Figure 3.10a) $9.125 < c < 10.95$ km yr^{-1} at the objective population level, while $c < 5.475$ km yr^{-1} at the 2010 population level. For winter the 2007 population level c is between 7.3 km yr^{-1} and 10.95 km yr^{-1}. This

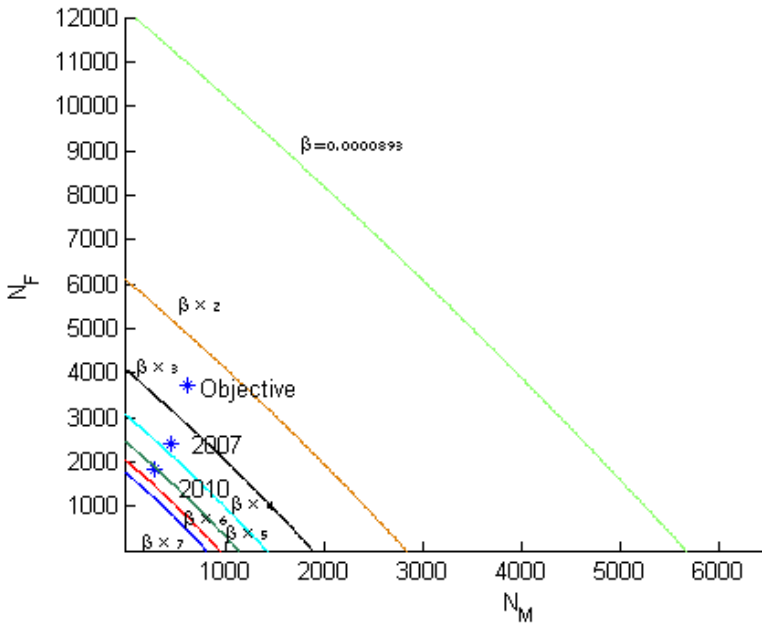

Figure 3.9: A comparison of $c = 0$ lines for many different infection rates for the La Sals (Area A) with summer motilities. The longest curve is for an infection rate of $\beta = 8.93\times10^{-5}$ as in Miller et al. [58]. This rate is multiplied by 2, then 3, etc., until the curve closest to the origin, which is $\beta = 8.93 \times 10^{-5} = 6.23 \times 10^{-4}$ (the rate used in Figure 3.8).

would be a rate fast enough for the disease to spread 100 kilometers from the La Sals to the Abajos in approximately 10 years.

3.5 Discussion and Conclusion

In this paper we have presented a spatial model for the spread of CWD in Utah, incorporating ecological diffusion as a way to connect disease spread to animal movement. Motility coefficients were estimated separately for each season for both male and female deer. Our modeling efforts show that ecological diffusion is an effective way to connect large-scale disease spread to small-scale animal movement. Our homogenization technique allows us to model spread of CWD over a large area with computational ease and provides us with coefficients for analyzing asymptotic rates of spread.

CWD in Utah is rare and in its initial stages, so there are many things we do not know about it, including infection rates, amounts of prions in the environment and how long they

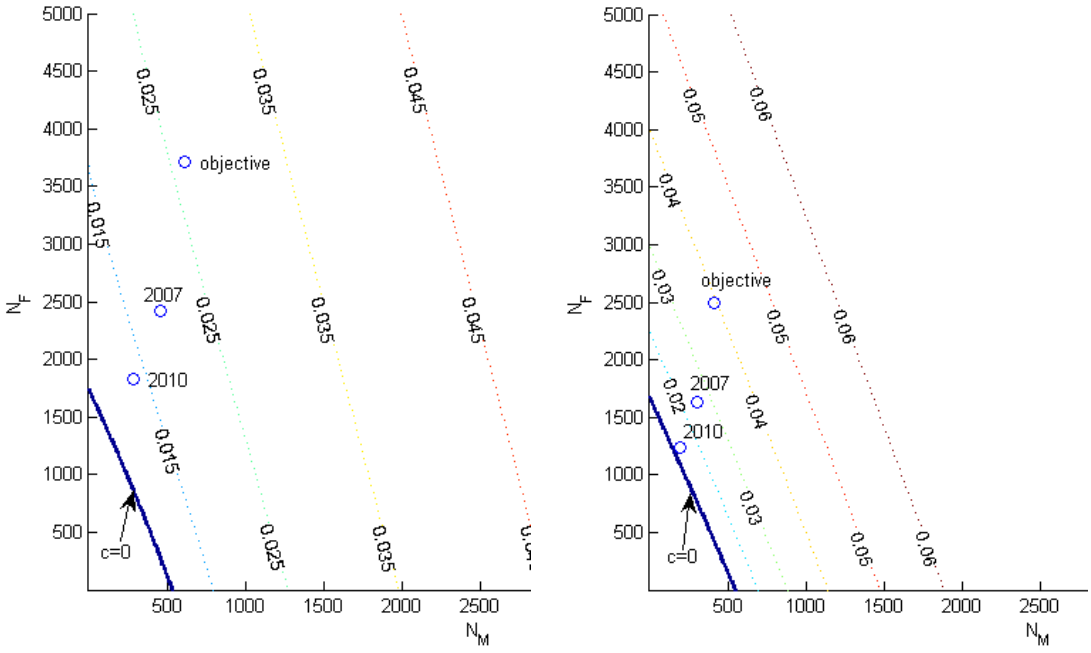

(a) La Sals (Area A) Summer

(b) La Sals (Area A) Winter

Figure 3.10: A look at the contours for speeds, c, Area A. With summer motilities the estimated population for 2010 is between $c = 0.01$ and $c = 0.015$ kilometers per day, which is between 3.7 and 5.5 kilometers per year. Using winter motilities, the estimated population for 2010 falls between $c = 0$ and $c = 0.01$, making the speed of invasion for that population less than 3.7 kilometers per year. The infection rates $\beta_{FF} = \beta_{MF} = 6.23 \times 10^{-4}$and $\beta_{MM} = \beta_{FM} = 0.0019$ were used.

stay infective, and the prevalence of CWD in the female population. Because of this lack of knowledge, there are many ways to explore spread with the CWD model, varying initial conditions, infection rates, and influence of the environment.

However, CWD has been present in the La Sal Mountains for 10 years and has just recently been detected in the Abajos. Our simulations showed that this time line is plausible for our model with very reasonable infection rates. The rates and initial conditions in Simulation 6 (see Table 3.2) would result in 1 infected deer in the Abajos after 10 years and 2 infected deer after 12 years. The increased infection rates in Simulation 8 gives 3 infected deer in the Abajos after 10 years.

Connecting the landscape with speed of invasion and critical population levels can

be important from a management perspective. The permeability of key portions of the landscape for different population levels and infectivities can be analyzed using the methods of Section 3.4. These methods allow spread to be analyzed separately for areas of high prevalence. Current populations increase spread, but lower target populations in selected areas could potentially stop spread from those areas.

In the future this model could be applied to other areas in the Western U.S. where CWD is a concern to wildlife managers. Also, the techniques outlined can be extended to many ecological applications. Not only can they be used to model other wildlife diseases, but they can be applied to insect infestations, invasive species, and escaped genetically modified organisms. Tying the spatial structure of the environment to how organisms move is key to understanding spread and invasive speed of organisms and diseases.

CHAPTER 4
ESTIMATING RESIDENCE TIMES FROM GPS MOVEMENT DATA FOR ECOLOGICAL DIFFUSION MODELS [1]

4.1 Introduction

Ecological studies have been widely impacted by the onslaught of GPS collar data and the availability of several land classification data sets. Meaningfully incorporating information from this data into ecological models is a challenge. One piece of information that can be very useful is a measure of how much time an organism spends in a particular habitat (residence time or residence index [97]). Residence time can be incorporated into spatiotemporal models over heterogeneous environments dealing with invasive spread, spread of disease, habitat use or population dynamics.

In diffusion models, residence time can be considered as inversely proportional to the diffusion coefficient under the assumption that individuals move via a random walk [80]. Thus, residence time provides a connection between an individual's movement and the redistribution of a population [97]. The classic reaction-diffusion equation, $\frac{\partial u}{\partial t} = D\nabla^2 u + f(u)$, assumes a constant diffusion rate, modeling the spread of organisms over a homogeneous landscape [90].

Both Fickian and ecological diffusion provide a way to incorporate variable diffusion coefficients into spatial models to accommodate heterogeneous environments. Fickian diffusion, of the form $\frac{\partial u}{\partial t} = \nabla[D(x_1, x_2)\nabla u]$, models the random redistribution of organisms from high densities to low densities at a rate proportional to the population density gradient. In terms of a random walk, organisms leave different habitats at the same rate until there is no longer a population gradient. This eventually distributes organisms uniformly in habitats that provide food and shelter as well as those which do not, and does not connect population distribution with residence time [23]. On the other hand, ecological diffusion,

[1] Coauthored by Martha Garlick, James Powell, Mevin Hooten, and Leslie McFarlane

represented by $\frac{\partial u}{\partial t} = \nabla^2[D(x_1, x_2)u]$, allows for distinct population differences at habitat boundaries, reflecting the aggregation of organisms in desirable habitats and their dispersal from undesirable ones. For ecological diffusion the variable diffusion coefficient, $D(x_1, x_2)$, represents the rate of movement of organisms (motility), which is the multiplicative inverse of residence time. In fact residence time is proportional to the equilibrium population density (the population density as $t \to \infty$). In other words, the faster organisms move through an environment (the less time they spend), the smaller we expect the population density at equilibrium in that environment to be [97].

The effect of heterogeneous landscapes on the dispersal of populations and the spread of diseases has been the subject of many studies [103]. Dunning et al. [35] stressed the need to link population models to landscape features in order to examine possible population response to local and global change. Such models have been applied to the movement of hispid cotton rats [9], the abundance of scarab beetles [3], and the spread of feline leukemia virus [21]. Fragmented landscapes, where favorable habitat for a species is surrounded by less favorable habitat, are examined by Cantrell and Cosner [10]. They use diffusion models that consider population growth rate to differ between regions of different habitat types and apply them to refuge design. Ovaskainen and Cornell [75] also explore the need for diffusion processes to be discontinuous at habitat boundaries. This necessitates classifying landscapes in order to determine habitat-specific diffusion and mortality coefficients [73]. McRae et al. [55] use a circuit theory approach to equate the connectivity of landscapes to the flow of electrical current. Brooks et al. [8] use spatially explicit network models to study how heterogeneous structure can promote the persistence of species in landscapes.

Statistical approaches that tie species preference to habitat include using resource selection functions (RSFs). A RSF is a function that is proportional to the density of locations used by a population given the resources present at all locations on a desired domain [22]. For most applications, the value of RSF models is how well they predict the location of organisms on a landscape [7]. This approach describes probabilities based on data and requires enough observations relative to the chosen classification scheme to have confidence.

Because of this, RSF's are often limited to populations at equilibrium [6], but see Johnson et al. [40] and Forester et al. [22]. Here we present a different way to relate habitat and population. A PDE model provides a mechanism for movement, so we can look at the dynamics of spread and the effects of transients, not just the steady state.

Even though diffusion models with variable coefficients have been recognized as necessary to model dispersal over heterogeneous landscapes [70], variable coefficients are often abandoned in practice. This is chiefly for two reasons: added mathematical complication and lack of data to derive diffusion coefficients (motilities) for all landcover types in a study area. Increased computing power and homogenization techniques can aid in dealing with the mathematical complication for numerical solutions [23] and advances in telemetry have enhanced data collection over diverse habitats.

Land classification data is available in blocks as small as 30×30 meters. Ideally for modeling purposes, one would like to associate each 30×30 pixel with a residence time for a population. However, by necessity GPS data from collared animals are collected at discrete time intervals and are often nonuniform temporally. Due to battery-life, length of study, and other considerations, data points may be hours or even days apart. Thus the land cover data can be at a much finer resolution than the GPS location data. This means that there may be very little or no data collected in habitat types of low residence time.

Traditional methods of analyzing animal movement to determine motilities involve approximating mean-squared displacement over time by connecting data points with straight lines [44]. When data are collected at irregular time intervals, this means dividing moves into smaller segments or combining moves [96], which can obscure the underlying movement process [95]. Since telemetry removes the observer from data collection, it is difficult to make a connection between movelength and habitat preference [97].

Other methods of extracting measures of residency out of movement data exist in the literature. Ovaskainen and Cornell solve for occupancy times from problems that are adjoint to the original ecological diffusion problem [73, 74, 75]. They apply this technique to mark/recapture data from butterfly movement studies. Pedersen et al. [78] use

a process-based statistical approach to estimating residency and behavior from movement data collected with electronic tags. A hidden Markov model on a spatial grid in continuous time is used to compute the joint posterior probability distribution of location and behavior at each point in time. They demonstrate this method by analyzing southern bluefish tuna (*Thunnus maccoyii*) telemetry data.

Johnson et al. [39] use a continuous-time correlated random walk (CTCRW) model which makes the assumption that successive moves are related to each other, i.e. animals have inertia that keeps them moving for a period of time at a nearly constant rate [97]. The moves in a random walk (the basis of an ecological diffusion model) are not correlated. However, habitat types in natural landscapes *are* correlated, i.e. nearby locations are more likely to be of similar land cover type than distant locations. An animal in a preferred habitat is likely to remain there, rather than move to an undesirable one. A random walk over a heterogeneous environment reflects this. The probability that an organism stays in a desirable patch is greater than the probability of leaving it for a less desirable patch. Thus a random walk inherits structure from the environment.

In this paper we discuss how to use the methods of Johnson et al. [38, 39] to fit a CTCRW model to GPS collar data from mule deer (*Odocoileus hemionus*) in the La Sal Mountains of Utah and obtain the posterior predictive distribution (PPD) of animal paths between data points at a desired uniform time interval. The PPD for the path is classified according to a land cover data set and residence times for each land cover type are inferred. This allows inference to be made in finer detail than given by the collected data, including the ability to estimate time in very infrequently visited landscape types. Motilities can then be calculated for use as ecological diffusion coefficients, such as the model for the spread of chronic wasting disease (CWD) in mule deer in Chapter 3. Lastly, we conduct a simulation study to examine if we can recover our results using simulated data over landscapes with differing correlation structures to test how motility estimates are affected.

4.2 Methods

To estimate residence time, we follow the methods of Johnson et al. [39], which we briefly describe. The data are fit to a CTCRW model, considering movement as a change in location. If $\boldsymbol{\mu}(t)$ is a continuous, smooth path of locations, then the instantaneous rate of change in location is velocity, $\boldsymbol{v}(t)$. An Ornstien-Uhlenbeck process can be used to model velocity, defined by

$$\boldsymbol{v}(t+\Delta) = \boldsymbol{\gamma} + e^{-\beta\Delta}[\boldsymbol{v}(t) - \boldsymbol{\gamma}] + \boldsymbol{\zeta}(\Delta), \tag{4.1}$$

where Δ is the change in time, $\boldsymbol{\gamma}$ is mean velocity, β is an autocorrelation parameter, and $\boldsymbol{\zeta}$ is a two-dimensional Gaussian random variable,

$$\boldsymbol{\zeta} \sim N(0, \sigma^2[1 - \exp(-2\beta\Delta)]/2\beta). \tag{4.2}$$

The correlation parameter, β, controls how rapidly the influence of past speed decays; large β implies more rapid decay. The parameter σ controls the overall variability in velocity through the time step Δ. When Δ is close to zero there is almost no change in velocity. However, when $\Delta \to \infty$ the next velocity is completely random with variance σ^2. Equations (4.1) and (4.2) are therefore defining the velocity at time $t+\Delta$ as a random variable whose variance grows with Δ plus an adjustment related to the velocity at time t. Then $\boldsymbol{\mu}(t)$ is a continuous-time location process obtained by

$$\boldsymbol{\mu}(t) = \boldsymbol{\mu}(0) + \int_0^t \boldsymbol{v}(s)ds. \tag{4.3}$$

This equation essentially says that the location at time t is the initial location plus the "sum" of all the steps taken between the initial time and time t. Thus a model for animal location is obtained by modeling velocity. The CTCRW model is defined by (4.1) and (4.3).

The velocity and location of an animal at any time t along its continuous path can be represented by this model. However, this continuous process can only be observed at a finite number of sampled times, subject to measurement error. To account for error and to

expedite likelihood calculation, the CTCRW model is placed into a Gaussian state-space model (SSM) formulation which uses the Kalman filter [17]. The SSM is given by two equations, the observation equation,

$$\boldsymbol{y}_i = \boldsymbol{Z}_i\boldsymbol{\alpha}_i + \boldsymbol{\epsilon}_i, \tag{4.4}$$

and the state equation,

$$\boldsymbol{\alpha}_{i+1} = \boldsymbol{T}_i\boldsymbol{\alpha}_i + \boldsymbol{\eta}_i, \tag{4.5}$$

where $\boldsymbol{y}_i$ is the observed location at time t_i, $\boldsymbol{\epsilon}_i$ is a normal measurement error with variance H_i, $\boldsymbol{\alpha}_i = [\boldsymbol{\mu}(t_i), \boldsymbol{v}(t_i)]'$ is the current state vector, $\boldsymbol{Z}_i$ and $\boldsymbol{T}_i$ are transformation matrices and the vectors $\boldsymbol{\eta}_i$ are normal error vectors with covariance matrix $\boldsymbol{Q}_i$. The matrices $\boldsymbol{T}_i$, and $\boldsymbol{Q}_i$ depend on a vector $\boldsymbol{\theta}$ of the movement parameters, β and σ from (4.1) and (4.2). Even though the CTCRW is not Markovian (meaning the current location is dependent upon all the past locations, not just the previous one), the SSM combines the velocity and location processes in such a way that a Markovian process results for $\boldsymbol{\alpha}_i$ [39].

We use the Bayesian methods of Johnson et al. [38] to predict locations at a uniform time interval between the observed locations. The posterior predictive distribution of the actual movement path is the conditional distribution of the unknown states, $\boldsymbol{\alpha}$, given the observed locations, $\boldsymbol{y}$, and is denoted by $[\boldsymbol{\alpha}|\boldsymbol{y}]$, where the notation $[\cdot|\cdot]$ refers to a conditional distribution $f(\cdot|\cdot)$. Figure 4.1 shows possible paths drawn from a posterior predictive distribution for the movement of a male mule deer during breeding season. We use $[\boldsymbol{\alpha}|\boldsymbol{y}]$ to find the posterior predictive distribution of residence times, $[g(\boldsymbol{\alpha})|\boldsymbol{y}]$, by landcover type, where $g(\boldsymbol{\alpha})$ is a function relating movement to landscape. In the following application, the function $g(\boldsymbol{\alpha})$ is the number of minutes spent in each land cover type. The posterior predictive mean can be used for a point-estimate of $g(\boldsymbol{\alpha})$ [11]. Therefore, we seek to find the posterior expectation

$$E(g(\boldsymbol{\alpha})|y) = \int g(\boldsymbol{\alpha})[\boldsymbol{\alpha}|\boldsymbol{y}]d\alpha.$$

This integral is analytically intractable, but can be approximated using Monte Carlo integration of the form:

$$E(g(\boldsymbol{\alpha}|\boldsymbol{y})) \approx \frac{\sum_{k=1}^{K} g(\boldsymbol{\alpha}^k)}{K},$$

where $\boldsymbol{\alpha}^k$, $k = 1, ..., K$, represents a sample drawn from $[\boldsymbol{\alpha}|\boldsymbol{y}]$. By the Strong Law of Large Numbers, the accuracy of this approximation increases as the sample size increases [84]. Techniques for drawing this sample are outlined in Johnson et al. [38].

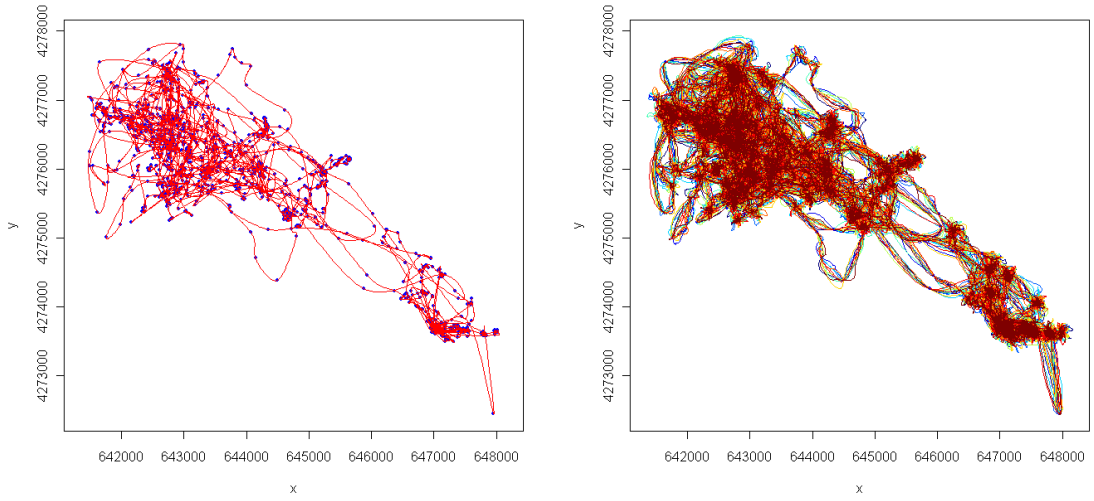

(a) A CTCRW model fit to GPS data.

(b) Ten predicted paths.

Figure 4.1: The path of one male deer during breeding season when locations were recorded every 30 minutes. A CTCRW model is fit to the GPS data (in UTM coordinates) as shown in (a). The posterior predictive distribution of animal paths between data points at one minute intervals is obtained. Ten paths drawn from this distribution are shown in (b).

4.2.1 Estimating mule deer residence times for a chronic wasting disease model

Chronic wasting disease (CWD) is a contagious prion disease that affects members of the Cervidae family, including mule deer (*Odocoileus hemionus*) [4]. It is a rare, slowly developing disease that is always fatal. Infected mule deer may live 12-24 months before showing visible signs of the disease [105]. The disease may be contracted by direct contact with infected deer as well as indirectly via contact with prions in the environment. Prions

shed into the environment through the feces and decaying carcasses of infected deer remain infective for many years [62]. The spread of CWD is connected to the movement of deer through the environment and where they congregate; obviously rates of infection will increase in habitats where deer spend more time. We also desire residence times to calculate motilities for an ecological diffusion model of CWD spread [23].

CWD was first detected in the free-ranging mule deer population of Utah in 2002 and is currently found in three distinct areas in the state [53]. In 2005-6 the Utah Department of Wildlife Resources collared 50 deer, a mix of adult males, young males, and adult females, in the La Sal Mountains of southeastern Utah, one of the areas with known cases of CWD. Movement data was collected at different intervals, depending on the time of year: 12 hour intervals in late winter/early spring (December 15th to April 14th), 6 hour intervals during spring migration (April 15th to May 14th), 12 hour intervals during the summer/early fall (May 15th to October 14th), and 30 minute intervals during fall migration and breeding season (October 15th to December 15th). This choice of irregular data was to save the GPS collar's battery life for the main focus of their research, the behavior of deer during breeding season and how it might relate to CWD [53]. This makes the CTCRW model very attractive in obtaining predictions for unobserved times.

Mule deer exhibit high site fidelity to traditional summer and winter ranges with seasonal migration occurring during specific times of the year. Females form matrilinear groups which remain cohesive particularly during the breeding season when males begin wandering among groups looking for receptive females [53]. This somewhat complicates the idea of residence time, because the use of various habitats varies widely depending on sex and season. Partitioning the GPS movement data by sex and then by season allowed us to estimate residence times for males and females during winter, summer and breeding season. We did not compute residence times specifically for spring or fall migration, since migration occurs during a relatively short period of time and represents the change of motility between seasons, i.e. spring migration in a diffusion model is the population response to change in motility between winter and summer.

For this example, we chose the movement data from 11 female deer and 11 male deer, selected for having the most complete data (approximately a year). The methods described in the previous section were used to fit a CTCRW model to the location data and predict locations at one minute time intervals. A sample of 50 possible paths were drawn from the predictive posterior distribution of paths for each deer. A CTCRW model fit to the GPS data for one male deer during breeding season in shown in Figure 4.1a. Ten predicted paths for that deer are shown in Figure 4.1b.

The LANDFIRE data set from the Landscape Fire and Resource Management Planning Tools sponsored by the U.S. Department of the Interior and the U.S. Department of Agriculture Forest Service was used to classify each predicted location by land cover type [93]. The residence time was estimated for each of the 38 land cover types in the area by dividing the number of minutes spent in each type by the number of cells of that type. The LANDFIRE grid cells are 30x30 meters, so the residence times are in units of minutes per 900 square meters. The motility for each land cover type was obtained by taking the multiplicative inverse of the mean residence time and converting to units of square kilometers per day. We use these motilities as the coefficients for the CWD model in Chapter 3.

4.2.2 Simulation study to check accuracy of residence time estimations

We conducted a simulation study to test the accuracy of using a CTCRW model to estimate motilities for an ecological diffusion model. This involved generating animal movement data by simulating a random walk over landscapes composed of the land cover types with our estimated motilities for male deer during breeding season. We used the techniques described in this paper to estimate residence times for the simulated data and compared them to our estimates for the GPS data.

We did this for four different landscapes: the La Sal Mountains study area, another piece of Utah encompassing the Abajo Mountains, and two artificial landscapes comprised of land cover types in the same proportions as the study area, one with a high degree of spatial correlation called “Rockies” and the other with no spatial correlation called “Random” (see

Figure 4.2). Our expectation was that the more correlated the landscape, the better we would recover our original estimates (from the CTCRW model), i. e., residence times from the Rockies simulation would best reflect our estimates and the values obtained from the Random simulation would be the farthest from our estimates. We expected results from the La Sal and Abajo simulations to fall somewhere in between Rockies and Random simulations.

The Abajo Mountain area contains the same land cover types as the La Sal study area, but in different proportions (see Table 4.1). They are both dominated by pinyon-juniper forests and big sagebrush steppe. The La Sal area has more blackbrush shrubland, Gambel oak shrubland and ponderosa pine woodlands, while the Abajo area has more riparian habitat, irrigated cropland, and developed open space. They contain similar amounts of aspen forests, mixed conifer forests, and salt desert scrub, as well as many of the land covers comprising less than one percent of the study area.

The Rockies landscape was generated using Fourier transforms, where the power law was chosen, but the phase was generated randomly. This resulted in a mountains and valleys landscape shown in Figure 4.2c. We parsed the land cover types according to elevation and assigned them to similar "elevation" on the Rockies landscape in the same proportion as they occur in the study area. This put high elevation habitat such as alpine vegetation and spruce-fir forest types at the "peaks" and lower elevation habitats such as shrublands and sagebrush steppe in the "valleys." This created a spatially correlated environment with similar land covers following contours around the mountains. The higher elevation types are more mixed.

The other artificial landscape was populated with the land cover types in a random fashion to purposely avoid spatial correlation. A matrix with uniformly distributed random numbers between zero and one was assigned landcover types by value in the same proportion as the study area (Figure 4.2d).

For the simulations we associated the land cover types on our landscapes with the motilities, $D(x_1, x_2)$, calculated from our estimated residence times. For convenience, we

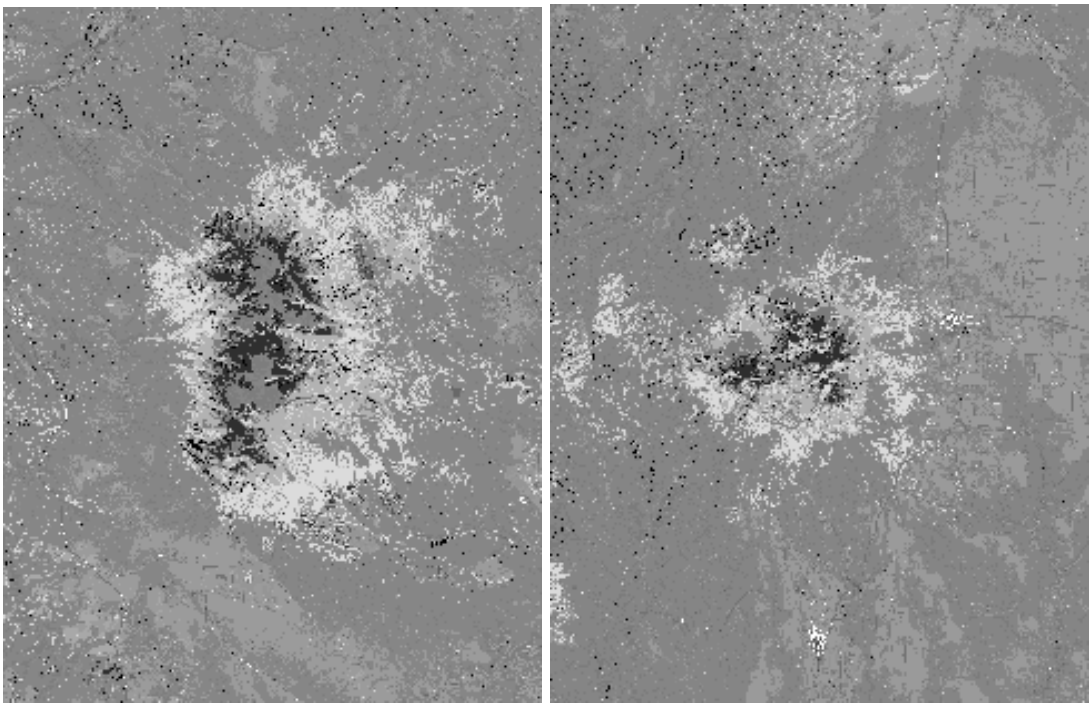

(a) La Sal Mountains (b) Abajo Mountains

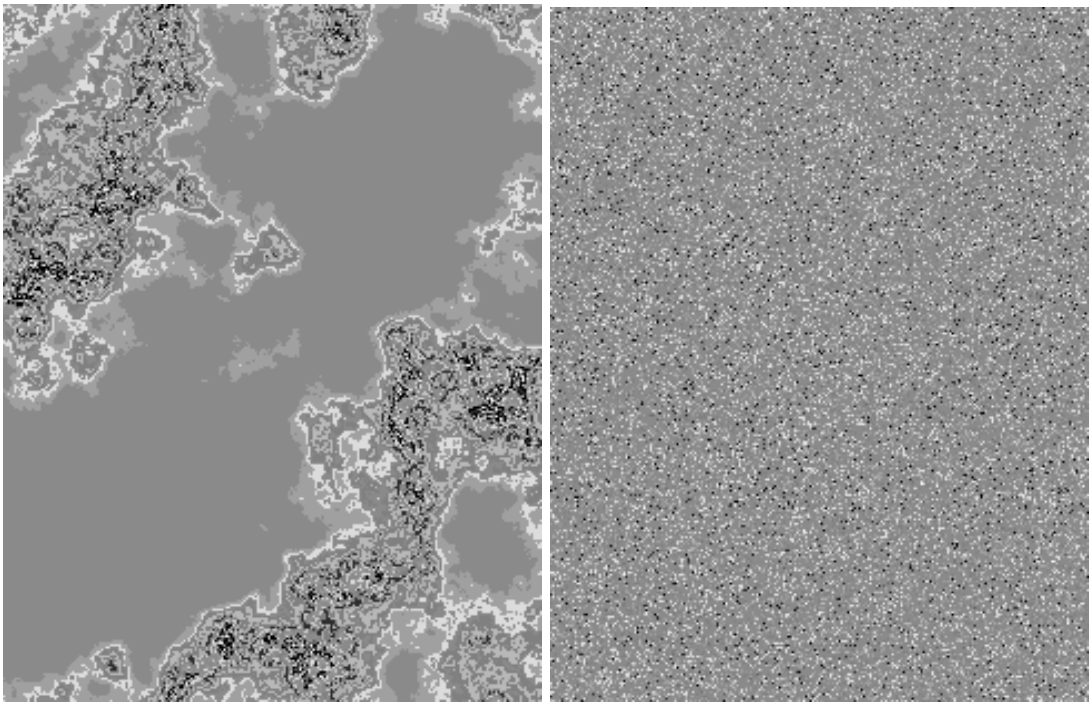

(c) Rockies (d) Random

Figure 4.2: Male breeding season residence times for the La Sal study area (a) and three other landscapes used for simulating data (b)-(d). The lighter the color, the larger the residence time

Table 4.1: Comparative composition of the La Sal Mountains and the Abajo Mountains with respect to the LANDFIRE classification in percentage of area comprised of the 38 landcover types. Both are dominated by pinyon-juniper forests and big sagebrush steppe. The La Sal area has more blackbrush shrubland, Gambel oak shrubland, and ponderosa pine woodlands, while the Abajo area has more riparian habitat, irrigated cropland, and developed open space.

LANDFIRE class, EVT	**La Sals**	**Abajos**
2016 pinyon-juniper	33.96	45.88
2210 shrubland-blackbrush	14.33	3.68
2080 big sagebrush	12.82	22.20
2217 shrubland-Gambel oak	6.10	3.61
2054 ponderosa pine woodland	5.48	2.98
31 barren	4.97	4.09
2011 aspen	4.75	2.24
2159 riparian	2.97	4.98
2181 annual grass	2.19	0.29
2055 dry spruce-fir	1.82	0.56
2061 aspen/mixed conifer	1.65	1.51
2051 dry mixed conifer	1.19	1.03
2081 salt desert scrub	1.12	0.92
2006 alpine sparse veg.	0.87	0.08
2180 into. riparian	0.81	0.72
81 pasture/hay	0.78	0.42
2135 semi-desert grassland	0.56	0.59
2064 low sagebrush	0.54	0.21
21 dev. open space	0.37	1.28
2126 sagebrush steppe	0.33	0.03
2160 subalpine riparian	0.31	0.11
2001 sparse veg.	0.27	0.53
2086 foothill scrub	0.27	0.06
2153 greasewood flat	0.26	0.14
2062 mtn. mahogany	0.22	0.06
2052 mixed conifer	0.21	0.06
2220 shrubland-big sagebrush	0.21	0.02
11 open water	0.14	0.05
22 dev. low intensity	0.11	0.14
2214 shrubland-manzanita	0.11	0.09
2057 subalpine limber pine	0.06	0.08
2093 sand shrubland	0.06	0.02
2107 Gambel oak/mixed shrubland	0.05	0.01
2117 ponderosa pine savanna	0.05	0.01
2066 saltbrush scrub	0.04	0.03
82 irrigated crops	0.03	1.25
2103 semi-desert chaparral	0.03	0.06
23 dev. med. intensity	0.01	0.02

chose a move length of $\lambda = 30$ meters, the same length as the resolution of the land cover data. Moves could occur in one of four directions: to the left, to the right, to the back, or to the front of a cell. The probability of a "deer" leaving a cell with the highest motility, $D_{\max}$, was assigned to be one and the time step, τ, was given by $\tau = \frac{\lambda^2}{4D_{\max}}$. Thus the probabilities, $p_i(x_1, x_2)$, associated with the other motilities, $D_i(x_1, x_2)$, were computed by $p_i(x_1, x_2) = \frac{4D_i(x_1,x_2)\tau}{\lambda^2}$.

Movement data were simulated by randomly placing a "deer" on a landscape in a pixel with probability of leaving determined by the motility value of that pixel. A random probability was generated and compared to the assigned probability to determine if the "deer" moved to one of the neighboring cells or if it stayed at its present location [33]. This process was repeated to generate data over a time period equivalent to the GPS data for one hundred "deer" on each landscape. We used the CTCRW method described above to find the mean residence times for each land cover type for the simulated deer movement data. Figure 4.3 shows an example of a randomly generated deer path. The resulting mean residence times are found in Table 4.2.

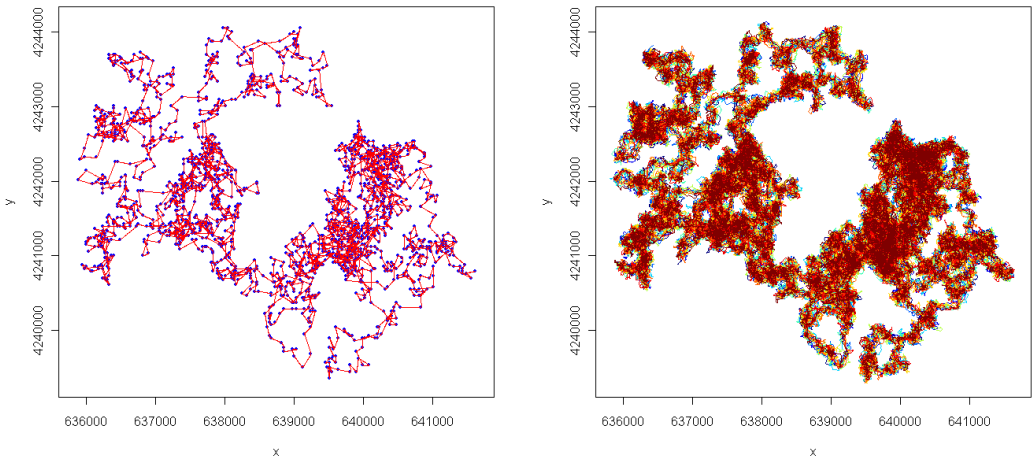

(a) A CTCRW model fit to simulated data.

(b) Ten predicted paths.

Figure 4.3: The path of one "deer" from simulated data generated from a random walk on the Rockies landscape using male breeding season motilities. The result of fitting a CTCRW model to the simulated data is shown in (a). Ten paths drawn from the posterior predictive distribution of possible paths are shown in (b).

Table 4.2: The estimated mean residence times (in minutes per 900 square meters) for male deer in breeding season along with the results of the simulation study. The % column contains the percent of the study area comprised of the LANDFIRE classification

LANDFIRE class, EVT	**%**	**Estimates**	**La Sals**	**Abajos**	**Rockies**	**Random**
2016 pinyon-juniper	33.96	6.1284	5.5396	5.6153	5.1256	6.1409
2210 shrubland-blackbrush	14.33	6.1988	5.1553	5.1881	4.9690	6.1500
2080 big sagebrush	12.83	7.9882	6.0249	6.3503	6.2434	6.3979
2217 shrubland-Gambel oak	6.10	17.2963	8.1951	8.5378	10.5163	7.7320
2054 ponderosa pine woodland	5.48	6.1460	5.4697	5.5044	5.3005	6.1666
31 barren	4.97	5.8287	5.1422	5.1583	5.0195	6.1289
2011 aspen	4.75	10.4703	7.4592	6.5389	7.2476	6.7374
2159 riparian	2.97	5.7012	5.3716	5.4342	5.1601	6.0686
2181 annual grass	2.19	9.3082	6.6501	6.3365	6.1507	6.5629
2055 dry spruce-fir	1.82	2.5780	4.0319	3.9751	3.7102	5.6930
2061 aspen/mixed conifer	1.65	5.3677	5.2024	5.7521	4.5089	6.0364
2051 dry mixed conifer	1.19	12.9073	6.8212	6.9238	6.7621	7.2030
2081 salt desert scrub	1.12	6.2901	5.0093	5.5245	5.4434	6.0573
2006 alpine sparse veg.	0.87	6.3097	4.2381	7.0273	4.9201	6.1493
2180 intro. Riparian	0.81	6.7048	5.6766	5.6933	5.3216	6.3304
81 pasture/hay	0.78	7.4735	6.1251	5.7295	6.2712	6.3169
2135 semi-desert grassland	0.56	16.8702	7.1224	7.4385	8.4597	7.6052
2064 low sagebrush	0.54	7.1320	6.5440	6.2279	6.0251	6.3635
21 dev. open space	0.37	4.8107	5.6594	5.2826	5.1800	6.0976
2126 sagebrush steppe	0.33	4.0139	5.9668	5.9298	3.9437	5.9550
2160 subalpine riparian	0.31	1.9653	4.8881	5.6183	3.4173	5.5280
2001 sparse veg.	0.27	1.7176	4.8877	4.7694	3.6360	5.4629
2086 foothill scrub	0.27	10.9961	6.3732	6.2591	5.2638	6.8808
2153 greasewood flat	0.26	4.0367	4.7750	5.2311	4.4725	6.0037
2062 mtn. mahogany	0.22	11.6190	5.9221	6.2949	5.4936	6.9027
2052 mixed conifer	0.21	1.7614	4.4341	3.7039	4.4660	5.4484
2220 shrubland-big sagebrush	0.21	2.7432	5.5883	6.8648	4.1794	5.8685
11 open water	0.14	4.1000	5.8648	4.1516	6.0864	5.8683
22 dev. low intensity	0.11	41.3987	10.0692	10.1730	10.6117	10.8746
2214 shrubland-manzanita	0.11	7.8721	6.9641	7.1103	6.9690	6.2530
2057 subalpine limber pine	0.06	1.5378	4.8033	4.4024	4.5231	5.4974
2093 sand shrubland	0.06	2.5885	4.4541	4.7153	5.9698	5.9064
2107 Gambel oak	0.05	2.3265	4.6019	7.5572	3.6945	5.5422
2117 ponderosa pine savanna	0.05	6.7272	5.7592	5.6381	3.9705	6.0573
2066 saltbrush scrub	0.04	1.5907	4.2600	4.5788	3.3309	5.9263
82 irrigated crops	0.03	7.9258	12.4117	5.0358	4.3445	6.3766
2103 semi-desert grassland	0.03	7.3856	7.5975	5.6886	3.6767	5.7342
23 dev. med. intensity	0.01	2.8090	6.7414	8.8104	3.6416	5.4073
Weighted R			0.4206	0.4868	0.6115	0.3941

4.3 Results

Two types of results are reported below, the residence times estimations and the simulation results. Residence times were estimated from GPS data collected from the La Sal study area for both male and female mule deer for winter, summer, and breeding season. The simulations were conducted using breeding season residence times for male mule deer. Data were simulated and residence times were estimated, using the same methods as used for the GPS data.

4.3.1 Residence time estimates for La Sal study area

Estimated residence times, as shown in Table 4.3, appear to reflect seasonal mule deer behavior. Pinyon-juniper woodlands, sage brush steppe, and low elevation ponderosa pine forests are important winter (December 15th to April 14th) habitats for both female and male deer, as well as semi-desert grassland and salt desert scrub [101]. Winter residence times for these land cover types range from 4.5 to 11 minutes/900 meters^2 for both sexes. Riparian, mountain mahogany, and pasture/hay were used more by females, while males had a higher residence time in semi-desert chaparral.

Residence times in relatively inaccessible habitat (alpine vegetation, dry spruce-fir forest, and mixed conifer forest for both sexes; limber pin, subalpine riparian , and aspen/mixed conifer for males) were small (< 3 min/900m^2), indicating that deer migrate to lower elevations this time of year. However, values for aspen forests, and mixed conifer forests for both males and females and limber pine and subalpine riparian areas for females were in the range of known winter habitats (5-10.5 min/900m^2). Deer may be able to access these areas during part of the season depending on local snow accumulation. Also the methods of Johnson et al. [38, 39] predict paths between data points without knowledge of seasonal deer behavior, so paths may cross areas not used by deer this time of year.

During summer months (April 15 to October 14) females, who actively raise young, spend large amounts of time in areas rich in cover and desirable food resources [79]. This is reflected in the high female residence times (40-65 min/900m^2) for Gambel oak, ponderosa

Table 4.3: Estimated residence times in minutes per 900 sq. meters. Male and female mule deer residence times were calculated separately for winter, summer and breeding season. Generally, residence times for high elevation habitats are much lower in winter than in summer.

LANDFIRE	**Winter**		**Summer**		**Breeding**	
Classification, EVT	**male**	**female**	**male**	**female**	**male**	**female**
11 open water	12.78	5.90	4.52	3.20	4.10	1.31
21 dev. open space	2.29	2.92	7.89	10.46	4.81	26.77
22 dev. low intensity	2.40	3.44	17.59	16.24	41.40	84.80
23 dev. med. intensity	3.10	3.14	3.29	1.00	2.81	1.36
31 barren	2.93	3.50	11.00	21.11	5.83	3.00
81 pasture/hay	2.56	4.19	15.68	3.65	7.47	39.34
82 irrigated crops	0.91	2.11	9.09	24.14	7.93	2.49
2001 sparse veg.	3.15	2.55	4.49	9.25	1.72	1.00
2006 alpine sparse veg.	1.58	0.83	14.19	16.22	6.31	0.00
2011 aspen	4.45	5.72	26.79	41.18	10.47	29.67
2016 pinyon-juniper	4.79	6.79	12.40	27.61	6.13	19.45
2051 dry mixed conifer	5.75	6.42	8.69	35.48	12.91	21.90
2052 mixed conifer	2.44	2.03	12.31	19.23	1.76	22.54
2054 ponderosa pine woodland	5.66	5.56	8.62	34.53	6.15	30.28
2055 dry spruce-fir	0.75	1.33	17.09	43.81	2.58	0.00
2057 subalpine limber pine	0.00	7.29	10.78	16.88	1.54	0.00
2061 aspen/mixed conifer	1.95	3.24	16.84	26.57	5.37	56.10
2062 mtn. mahogany	2.96	4.56	8.27	63.06	11.62	31.35
2064 low sagebrush	4.43	5.77	12.88	35.90	7.13	17.84
2066 saltbrush scrub	1.78	4.15	1.18	0.39	1.59	2.56
2080 big sagebrush	6.34	8.81	8.82	32.57	7.99	21.98
2081 salt desert scrub	4.02	6.30	10.95	2.82	6.29	5.16
2086 foothill scrub	2.75	3.63	6.81	17.20	11.00	3.79
2093 sand shrubland	1.81	2.03	13.68	0.22	2.59	5.84
2103 semi-desert grassland	9.87	4.18	8.69	58.01	7.39	24.44
2107 Gambel oak	1.60	4.23	14.06	10.18	2.33	16.43
2117 ponderosa pine savanna	4.58	3.95	7.42	65.22	6.73	26.49
2126 sagebrush steppe	4.80	11.27	16.75	12.05	4.01	39.58
2135 semi-desert grassland	4.60	4.07	3.61	2.13	16.87	3.37
2153 greasewood flat	3.97	6.65	12.45	2.00	4.04	15.75
2159 riparian	4.52	7.31	9.26	33.15	5.70	16.53
2160 subalpine riparian	2.50	10.42	18.16	44.85	1.97	16.62
2180 intro. Riparian	3.87	5.88	6.68	37.35	6.70	10.79
2181 annual grass	4.83	7.65	7.30	5.40	9.31	21.84
2210 shrubland-blackbrush	4.99	6.56	6.60	12.20	6.20	10.01
2214 shrubland-manzanita	4.57	5.96	18.10	25.90	7.87	21.27
2217 shrubland-Gambel oak	6.05	6.43	16.52	42.03	17.30	28.32
2220 shrubland-big sagebrush	5.85	9.57	6.65	13.14	2.74	45.36

pine, spruce-fir, and aspen forests and semi-desert chaparral, riparian habitat, and mountain mahogany shrubland. Some land cover types such as saltbrush scrub, sparse vegetation, salt desert scrub, sand shrubland, semi-desert grassland, and greasewood flats have little to no use during this time of the year for females, as shown by low residence times (0.22-3 min/900m^2). Male mule deer spend time in high mountain aspen, spruce, and fir forests and subalpine riparian areas (12-27 min/900m^2) at lower levels than females. They spend more time than females in lower elevation land cover types such as sagebrush steppe, shrublands, and low-intensity developed areas (14-18 min/900m^2).

Breeding season (October 15 to December 14) residence times for females are consistent with seasonal migration from high elevations to lower elevations. The female residence times for alpine sparse vegetation, spruce-fir forests, and subalpine limber pine are zero. With fawns older and mobile, females can use more open areas such as low-intensity developed land, pasture, hay fields, and sagebrush steppe, as shown by the high residence times (30-84 min/900m^2). Males also move to lower elevation open areas during breeding season. The highest residence times for males (10-42 min/900m^2) are for land cover types such as low-intensity developed land, aspen and dry mixed conifer forests, foothill scrub and shrubland, and semi-desert grassland.

Generally the residence times are consistence with seasonal behavior, especially the use of distinct summer and winter ranges. The behavioral differences are reflected as well. Females tend to spend time in habitats with cover when raising young, while males wander, using many types of land cover.

4.3.2 Simulation study results

Residence times estimated from the simulated data are compared for the four different landscapes (see Figure 4.2) in Table 4.2. The second column of Table 4.2 shows the percentage of the La Sal Mountains study area comprised of each land cover classification. Using these percentages as weights, the correlation coefficients, R, were calculated for each simulation. The random landscape simulation had the lowest value, $R = 0.3941$, while

the Rockies landscape simulation had the highest, $R = 0.6115$. The values for the natural landscapes were $R = 0.4206$ for the La Sal Mountains and $R = 0.4868$ for the Abajo Mountains.

Out of 38 land cover classifications, only 13 are greater than 1 % of the landscape (see Table 4.4). Using only the classes greater than one percent, we recalculated the weighted R values. All the values were slightly higher except the one for the Abajos. The random landscape still had the lowest with $R = 0.3951$ and the Rockies landscape had the highest with $R = 0.6470$. The values for the La Sals and the Abajos were $R = 0.4441$ and $R = 0.4756$, respectively.

It is interesting to note that three land cover types make up 61.12% of the study area: pinyon-juniper forest (33.96%), blackbrush shrubland (14.33%), and big sagebrush steppe (12.83%). These are very important habitats for mule deer during all times of the year [101]. Our estimated residence times from GPS data for male deer during breeding season in these habitats were 6.13, 6.2, and 8.0 min/900m^2 for pinyon-juniper forest, blackbrush shrubland, and big sagebrush steppe, respectively. These values were recovered fairly well by the simulations, with the simulation from the random landscape closely mirroring two of these values with 6.14, 6.15, and 6.4 min/900m^2.

The random landscape simulation yielded close estimations for the three dominant land cover types, but had the lowest weighted R value overall. The estimated residence times for the dominant land covers fell within the range of residence times for this simulation, 5.4-10.88 min/900m^2. The GPS data estimations show a far greater variety of residence times over the landscape with a range of 1.6 to 41.4 min/900m^2.

The resulting residence times from the Rockies simulation also spanned a smaller interval than the GPS estimates, 3.33-10.6 min/900m^2, yet this simulation had the best weighted R value. This tends to confirm our assumption that a random walk inherits correlation from the environment. The Rockies landscape was assigned land cover types by 'elevation', resulting in a correlation strikingly different than that of natural landscapes.

Although elevation plays a role in the distribution of land cover types in the La Sal

and Abajo areas, other factors contribute, such as aspect, water availability, and land use. The Abajo simulation resulted in a higher R value than the simulation over the La Sal study area. The values ranged over an interval similar to the Rockies landscape, 3.7-10.2 min/900m^2. The mid-range residence times were reflected well by the Abajo and La Sal simulations (4-7 min/900m^2) , but they did not capture the small and large residence times.

Several different strategies were evaluated during the simulations. The number of random paths simulated on the landscapes was increased from 25 to 50 and finally to 100. This did not result in better R values. The varying of spatial steps and length of paths also did not improve the results.

The simulations did not capture the high residence time estimates well. Table 4.5 contains the landcover types with estimates larger than 7 min/900m^2. These landscapes comprise a total of 29.71 % of the study area. As shown in Table 4.6 the high mean residence time estimates had large standard deviations. The predicted paths from the CTCRW model were highly variable. This may contribute to the difficulty in reproducing these numbers. A critical breeding season habitat, big sagebrush, which is 12.83% of the study area, had a mean estimated residence time of 8.0 and a standard deviation of 2.9. The simulations better approximated this value than the large residence times with large standard deviations.

Table 4.4: Simulation results for landcover types comprising greater than 1% of the study area landscape.

LANDFIRE class, EVT	**Percent**	**Estimates**	**La Sals**	**Abajos**	**Rockies**	**Random**
2016 pinyon-juniper	33.96	6.1284	5.5396	5.6153	5.1256	6.1409
2210 shrubland-blackbrush	14.33	6.1988	5.1553	5.1881	4.9690	6.1500
2080 big sagebrush	12.83	7.9882	6.0249	6.3503	6.2434	6.3979
2217 shrubland-Gambel oak	6.10	17.2963	8.1951	8.5378	10.5163	7.7320
2054 ponderosa pine woodland	5.48	6.1460	5.4697	5.5044	5.3005	6.1666
31 barren	4.97	5.8287	5.1422	5.1583	5.0195	6.1289
2011 aspen	4.75	10.4703	7.4592	6.5389	7.2476	6.7374
2159 riparian	2.97	5.7012	5.3716	5.4342	5.1601	6.0686
2181 annual grass	2.19	9.3082	6.6501	6.3365	6.1507	6.5629
2055 dry spruce-fir	1.82	2.5780	4.0319	3.9751	3.7102	5.6930
2061 aspen/mixed conifer	1.65	5.3677	5.2024	5.7521	4.5089	6.0364
2051 dry mixed conifer	1.19	12.9073	6.8212	6.9238	6.7621	7.2030
2081 salt desert scrub	1.12	6.2901	5.0093	5.5245	5.4434	6.0573
Weighted R			0.4441	0.4756	0.6470	0.3951

4.4 Discussion and conclusion

In this paper we outlined a way to estimate residence times from irregularly collected GPS movement data. We used the methods of Johnson et al. [39] to fit a CTCRW to the data and obtained the posterior predictive distribution (PPD) of animal paths between data points at 1-minute time intervals. We randomly selected 50 paths from the PPD for each deer and classified the predicted locations using the LANDFIRE data set. We calculated the mean residence time for each of 38 landcover classifications in the La Sal Mountain study area. Lastly we conducted a simulation study using breeding season residence times for male mule deer. Data were simulated using four different landscapes and residence times were estimated from the simulated data. These residence times were compared with the residence times estimated from the GPS data.

Table 4.5: Large residence times for male mule deer during breeding season compared to the simulation results.

LANDFIRE class, EVT	**Percent**	**Estimates**	**La Sals**	**Abajos**	**Rockies**	**Random**
22 dev. low intensity	0.11	41.3987	10.0692	10.1730	10.6117	10.8746
2217 shrubland-Gambel oak	6.1	17.2963	8.1951	8.5378	10.5163	7.7320
2135 semi-desert grassland	0.56	16.8702	7.1224	7.4385	8.4597	7.6052
2051 dry mixed conifer	1.19	12.9073	6.8212	6.9238	6.7621	7.2030
2062 mtn. mahogany	0.22	11.6190	5.9221	6.2949	5.4936	6.9027
2086 foothill scrub	0.27	10.9961	6.3732	6.2591	5.2638	6.8808
2011 aspen	4.75	10.4703	7.4592	6.5389	7.2476	6.7374
2181 annual grass	2.19	9.3082	6.6501	6.3365	6.1507	6.5629
2080 big sagebrush	12.83	7.9882	6.0249	6.3503	6.2434	6.3979
82 irrigated crops	0.03	7.9258	12.4117	5.0358	4.3445	6.3766
2214 shrubland-manzanita	0.11	7.8721	6.9641	7.1103	6.9690	6.2530
81 pasture/hay	0.78	7.4735	6.1251	5.7295	6.2712	6.3169
2103 semi-desert grassland	0.03	7.3856	7.5975	5.6886	3.6767	5.7342
2064 low sagebrush	0.54	7.1320	6.5440	6.2279	6.0251	6.3635
Total	29.71					

The residence time estimations from the GPS data for the most part reflect male and female seasonal behavior, especially for the land cover types that comprise the largest proportions of the study area. These residence times can be converted to motilities for use as coefficients for ecological diffusion models. The residence information gleaned from the location data links the diffusion model to the heterogeneous landscape. Many of the LANDFIRE classifications make up a very small percentage of the study area. This means

Table 4.6: The mean residence times estimated from GPS data along with the standard deviations. The long residence times have the highest standard deviations.

LANDFIRE class, EVT	Percent	Estimates	SD
22 dev. low intensity	0.11	41.3987	45.7567
2217 shrubland-Gambel oak	6.10	17.2963	29.4080
2135 semi-desert grassland	0.56	16.8702	29.1372
2051 dry mixed conifer	1.19	12.9073	12.5841
2062 mtn. mahogany	0.22	11.6190	22.3369
2086 foothill scrub	0.27	10.9961	11.3519
2011 aspen	4.75	10.4703	7.4931
2181 annual grass	2.19	9.3082	9.2458
2080 big sagebrush	12.83	7.9882	2.8950
82 irrigated crops	0.03	7.9258	8.3686
2214 shrubland-manzanita	0.11	7.8721	4.8981
81 pasture/hay	0.78	7.4735	5.3922
2103 semi-desert grassland	0.03	7.3856	4.0485
2064 low sagebrush	0.54	7.1320	6.1530
2117 ponderosa pine savanna	0.05	6.7272	2.9627
2180 intro. Riparian	0.81	6.7048	4.0302
2006 alpine sparse veg.	0.87	6.3097	4.9292
2081 salt desert scrub	1.12	6.2901	4.6732
2210 shrubland-blackbrush	14.33	6.1988	3.2592
2054 ponderosa pine woodland	5.48	6.1460	3.6089
2016 pinyon-juniper	33.96	6.1284	1.9822
31 barren	4.97	5.8287	8.2388
2159 riparian	2.97	5.7012	2.7749
2061 aspen/mixed conifer	1.65	5.3677	4.0986
21 dev. open space	0.37	4.8107	3.9945
11 open water	0.14	4.1000	5.7015
2153 greasewood flat	0.26	4.0367	3.0644
2126 sagebrush steppe	0.33	4.0139	3.4506
23 dev. med. intensity	0.01	2.8090	5.2059
2220 shrubland-big sagebrush	0.21	2.7432	1.8984
2093 sand shrubland	0.06	2.5885	2.2806
2055 dry spruce-fir	1.82	2.5780	1.7794
2107 Gambel oak	0.05	2.3265	1.6446
2160 subalpine riparian	0.31	1.9653	1.8329
2052 mixed conifer	0.21	1.7614	1.9701
2001 sparse veg.	0.27	1.7176	2.3259
2066 saltbrush scrub	0.04	1.5907	1.4736
2057 subalpine limber pine	0.06	1.5378	0.9102

that there is little data to determine how deer move thorough these habitats. It is not possible to collar all the deer in the area and keep track of all their movements, so we are without a direct way to measure motility. The methods presented here provide a way to estimate residence times from irregularly collected data that reasonably reflect seasonal behavior of male and female deer. A CWD diffusion model using motilities calculated from these residence times can connect the spread of disease with the landscape in a way that can incorporate GPS location data.

Simulation studies were conducted to examine self consistency of our estimates and the effect of landscape correlation. The residence times best matched by the simulations were those in the medium range, 4-7 min/900m^2 (see Table 4.7). This group of residence times is 67.31% of study area and includes significant habitats for mule deer such as pinyon-juniper, blackbrush shrubland and ponderosa pine woodlands. The La Sal and Abajo simulations are closer to the estimates for this range than for the large and small residence times. None of the simulations did a good job at recovering the small residence times as shown in Table 4.8. They represent only 3% of the study area and did not contain many data points.

Table 4.7: Mid-range residence times for male mule deer during breeding season compared to the simulation results.

LANDFIRE class, EVT	**Percent**	**Estimates**	**La Sals**	**Abajos**	**Rockies**	**Random**
2117 ponderosa pine savanna	0.05	6.7272	5.7592	5.6381	3.9705	6.0573
2180 intro. Riparian	0.81	6.7048	5.6766	5.6933	5.3216	6.3304
2006 alpine sparse veg.	0.87	6.3097	4.2381	7.0273	4.9201	6.1493
2081 salt desert scrub	1.12	6.2901	5.0093	5.5245	5.4434	6.0573
2210 shrubland-blackbrush	14.33	6.1988	5.1553	5.1881	4.9690	6.1500
2054 ponderosa pine woodland	5.48	6.1460	5.4697	5.5044	5.3005	6.1666
2016 pinyon-juniper	33.96	6.1284	5.5396	5.6153	5.1256	6.1409
31 barren	4.97	5.8287	5.1422	5.1583	5.0195	6.1289
2159 riparian	2.97	5.7012	5.3716	5.4342	5.1601	6.0686
2061 aspen/mixed conifer	1.65	5.3677	5.2024	5.7521	4.5089	6.0364
21 dev. open space	0.37	4.8107	5.6594	5.2826	5.1800	6.0976
11 open water	0.14	4.1	5.8648	4.1516	6.0864	5.8683
2153 greasewood flat	0.26	4.0367	4.7750	5.2311	4.4725	6.0037
2126 sagebrush steppe	0.33	4.0139	5.9668	5.9298	3.9437	5.9550
Total	67.31					

Table 4.8: Small residence times for male mule deer during breeding season compared to the simulation results.

LANDFIRE class, EVT	**Percent**	**Estimates**	**La Sals**	**Abajos**	**Rockies**	**Random**
23 dev. med. intensity	0.01	2.8090	6.7414	8.8104	3.6416	5.4073
2220 shrubland-big sagebrush	0.21	2.7432	5.5883	6.8648	4.1794	5.8685
2093 sand shrubland	0.06	2.5885	4.4541	4.7153	5.9698	5.9064
2055 dry spruce-fir	1.82	2.5780	4.0319	3.9751	3.7102	5.6930
2107 Gambel oak	0.05	2.3265	4.6019	7.5572	3.6945	5.5422
2160 subalpine riparian	0.31	1.9653	4.8881	5.6183	3.4173	5.5280
2052 mixed conifer	0.21	1.7614	4.4341	3.7039	4.4660	5.4484
2001 sparse veg.	0.27	1.7176	4.8877	4.7694	3.6360	5.4629
2066 saltbrush scrub	0.04	1.5907	4.2600	4.5788	3.3309	5.9263
2057 subalpine limber pine	0.06	1.5378	4.8033	4.4024	4.5231	5.4974
Total	3.04					

Though landscape correlation did influence the ability to recover residence times from simulated data, it was not strong enough to reproduce our original results. Future work could include finding ways to estimate residence times using a random walk model rather than a CTCRW which would be consistent with the random walk associated with ecological diffusion.

CHAPTER 5

SUMMARY AND CONCLUSION

In this dissertation we explored the use of ecological diffusion models as a way to connect the movement of animals over heterogeneous landscapes with the spread of disease. Ecological diffusion is appropriate when organisms make local decisions in response to habitat, aggregating in places with needed resources and avoiding or moving quickly through those without food and shelter, eventually giving a population distribution that is inversely proportional to the motility. This allows for solutions to be discontinuous at habitat boundaries. In order to facilitate the use of ecological diffusion models over complex environments, we derive a homogenization procedure for ecological diffusion and apply it to spatial models for the spread of CWD in mule deer populations. The averaged coefficients in the homogenized equations can be used in analysis of asymptotic speed of spread and critical population sizes.

We first illustrated the use of ecological diffusion in a simple disease model for CWD, using an SI framework with no environmental hazard and no sex-structure. We derived the homogenized equation for this model, where the motility coefficient (now the harmonic mean of motilities) is outside of the Laplacian and the reaction term coefficient is an average weighted by how long individuals spend in a particular habitat and how aggregated the population is in that habitat. Motility coefficients were estimated by taking the mean-squared displacement per time for all movements within each habitat. Other parameters, such as infection and death rates, were obtained from Miller et al. [58]. In the simulation of the spread of CWD in the La Sal Mountains of Southwest Utah, we compared the numerical solutions of the non-homogenized model and the homogenized model to demonstrate accuracy and illustrate the computational savings in using the homogenized model. It was shown that the averaged coefficients from the homogenized equation can be used to explore the asymptotic speed of spread of the disease and critical population size in order for the speed of spread to be zero.

Next, we developed a more disease-specific, sex-structured model for CWD which adds environment-to-deer transmission to the deer-to-deer transmission. Motility coefficients were computed separately for summer, breeding season, and winter for both males and females, using the methods of Johnson et al. [38, 39]. This added seasonal behavioral differences between males and females to the model. Even though this model is a system of three partial differential equations, our homogenization procedure still applied. The homogenized system was used in simulations of the spread of CWD from the La Sal Mountains to the Abajo Mountains of Southeast Utah.

Simulations explored various infection rates using population estimates for 2007, 2010, and the UDWR target population. It has taken ten years for CWD to be detected in the Abajos since its discovery in the La Sals. Our model demonstrates the plausibility of this time line for spread from the La Sals to the Abajos for reasonable infectivities for population levels near the 2007 estimates. Simulations show the spread would take longer for current population size, but CWD would devastate a population large enough to meet the UDWR goal. The number of infected deer from simulations with direct transmission and environmental transmission were double that of simulations with direct transmission only. Using seasonal, habitat-specific motilities resulted in over ten times more infected deer than using a constant motility (though the spread was far wider for the constant motility), illustrating that connecting the spread of disease to how animals move and aggregate across the landscape is essential. This idea was also demonstrated in a comparison of spread over a single season. The model with breeding season motilities yielded more new infectives per day, then with summer or winter motilities, consistent with the seasonal changes in deer behavior. The model with winter motilities resulted in wider spatial spread.

The coefficients from the homogenized equations were used to explore the asymptotic invasion speed and critical population sizes. We derived equations that can be numerically solved for asymptotic wave speed and connected them to the parameters of our homogenized model through numbers of female and male deer. We explored wave speed for different population sizes for two areas of interest, the La Sal Mountains (containing critical summer

range) and an area of critical winter range between the La Sal and Abajo Mountains. This shows an advantage of our model; it can be used to analyze CWD infected areas separately from other areas. It can also be used to see if sections of landscape act as barriers or conduits for disease spread. This is applicable to the management question of how populations may be controlled to stop disease spread from a particular area.

Lastly, we explained in more detail the methods used to estimate the motilities for the CWD model and compared the results to known mule deer behavior. We used the methods of Johnson et al. [38, 39] to fit a CTCRW model to GPS telemetry data and obtain the PPD of animal paths between data points at a desired uniform time interval. We classified the predicted locations on animal paths drawn from the PPD and estimated the amount of time spent in each land cover type. For the most part, these residence times reflect deer behavior, especially wandering behavior of males contrasted with the aggregating behavior of females. We conducted simulation studies over increasingly correlated landscapes to test the validity of these methods for estimating coefficients for ecological diffusion models. The idea that a random walk inherits correlation from the environment was reflected in our results. The estimated residence times were closest to our GPS data estimates for the landscape with the most spatial correlations and farthest for the random landscape. The simulation results were best for the landscape types that comprise the majority of the study area.

Perhaps the most significant part of this work is the development of a homogenization procedure for ecological diffusion models. This is an simple yet effective mathematical way to make large-scale predictions from small-scale data. This addresses the computational complexity of using ecological diffusion parameterized by small-scale movement data over a large domain. The computational time to numerically solve homogenized equations is far less than that need to solve non-homogenized equations.

The parameters from the homogenized equations can be used to find invasive speed of spread for different population sizes. Using this procedure can enhance the ability to examine critical, emergent behavior on large, heterogeneous landscapes. This could be important from a disease management point of view. Identification of barriers or corridors

for disease spread and population sizes needed to control spread from disease hotspots are applications that are possible with this modeling approach. It can be applied to other dispersal problems, such as invasive species, insect invasions, and escaped genetically modified organisms. It has been used for change of support in inverse implementations of statistical differential equation models [32].

Our modeling efforts for CWD in mule deer show that ecological diffusion is an effective way to connect large-scale disease spread to small-scale animal movement. Especially in the case of an environmentally transmitted disease, allowing organisms to aggregate in desirable habitats and disperse from undesirable ones is an important feature for an instructive model. Homogenization of our disease models results in averaged coefficients that are useful in analyzing the asymptotic speed of spread of the disease. This leads to a management question,"Is there a population level for an area with infected individuals, at which the disease can not spread from the area?" Having spread contingent on how organisms move through the environment, allows us to look at spread in specific areas as well as over the entire domain.

REFERENCES

[1] R. M. Anderson and R. M. May, *Population biology of infectious diseases. Part 1*, Nature **280** (1979), 361–367.

[2] D. A. Androw, P. M. Karieva, S. A. Levin, and A. Okubo, *Spread of invading organisms*, Landscape Ecology **4** (1990), 177–188.

[3] L. Arellano, J. L. Leon-Cortes, and O. Ovaskainen, *Patterns of abundance and movement in relation to landscape structure: A study of a common scarab (Canthon cyanellus cyanellus) in Southern Mexico*, Landscape Ecology **23** (2008), 69–78.

[4] L. A. Baeten, B. E. Powers, J. E. Jewell, T. R Spraker, and M. W. Miller, *A natural case of chronic wasting disease in a free-ranging moose (Alces alces shirasi)*, The Journal of Wildlife Diseases **43** (2007), 309–314.

[5] S. Bar-David, J. O. Lloyd-Smith, and W. M. Getz, *Dynamics and management of infectious disease in colonizing populations*, Ecology **87** (2006), 1215–1224.

[6] M. S. Boyce and L. L. McDonald, *Relating populations to habitats using resource selection functions*, Trends in Ecology and Evolution **14** (1999), 268–272.

[7] M. S. Boyce, P. R. Vernier, S. E. Nielsen, and F. K.A. Schmiegelow, *Evaluating resource selection functions*, Ecological Modelling **157** (1999), 281–300.

[8] C. P. Brooks, J. Antonovics, and T. H. Keitt, *Spatial and temporal heterogeneity explain disease dynamics in a spatially explicit network model*, The American Naturalist **172** (2008), 149–159.

[9] D. R. Browne, J. D. Peles, and G. W. Barrett, *Effects of landscape spatial structure on movement patterns of the hispid cotton rat (Sigmodon hispidus)*, Landscape Ecology **14** (1999), 53–65.

[10] R.S. Cantrell and C. Cosner, *Diffusion models for population dynamics incorporating individual behavior at boundaries: Applications to refuge design*, Theoretical Population Biology **55** (1999), 189–207.

[11] R. Christensen and M. D. Huffman, *Bayesian point estimation using the predictive distribution*, The American Statistician **39** (1985), 319–321.

[12] M. M. Conner, M. R. Ebinger, J. A. Blanchong, and P. C. Cross, *Infectious disease in cervids of North America: Data, models, and management challenges*, Ann. N. Y. Acad. Sci **1134** (2008), 146–172.

[13] M. M. Conner and M. W. Miller, *Movement patterns and spatial epidemiology of a prion disease in mule deer popoulation units*, Ecological Application **14** (2004), 1870–1881.

[14] L. Demaret, H. J. Eberl, M. A. Efendiev, and P. Maloszewski, *A simple bioclogging model that accounts for spatial spread of bacteria*, Electronic Journal of Differential Equations, Conference **17** (2009), 51–69.

[15] S. Dewhirst and F. Lutscher, *Dispersal in heterogeneous habitats: Thresholds, spatial scales, and approximate rates of spread*, Ecology **90** (2009), 1338–1345.

[16] T. Dobzhansky, J. R. Powell, C. E. Taylor, and M. Andregg, *Ecological variables affecting the dispersal behavior of Drosophila pseudoobscura and its relatives*, American Naturalist **114** (1979), 325–334.

[17] J. Durbin and S. Koopman, *Time Series Analysis by State Space Methods*, Oxford University Press, Oxford, UK, 2001.

[18] M. L. Farnsworth, J. A Hoeting, N. T. Hobbs, and M. W. Miller, *Linking chronic wasting disease to mule deer movement scales: A hierarchical bayesian approach*, Ecological Applications **16** (2006), 1026–1036.

[19] M. L. Farnsworth, L. L. Wolfe, N. T. Hobbs, K. P. Burnham, E. S. Williams, D. M. Theobald, M. M. Conner, and M. W. Miller, *Human land use influences chronic wasting disease prevalence in mule deer*, Ecological Applications **15** (2005), 119–126.

[20] R. A. Fisher, *The wave of advance of advantageous genes*, Annals of Eugenics **7** (1937), 355–369.

[21] W. E. Fitzgibbon, M. Langlais, and J. J. Morgan, *A mathematical model of the spread of feline leukemia virus (FeLV) through a highly heterogeneous spatial domain*, SIAM Journal on Mathematical Analysis **33** (2001), 570–588.

[22] J. D. Forester, H. K. Im, and P. J. Rathouz, *Accounting for animal movement in estimation of resource selection functions: Sampling and data analysis*, Ecology **90** (2009), 3554–3565.

[23] M. J. Garlick, J. A. Powell, M. B. Hooten, and L. R. McFarlane, *Homogenization of large-scale movement models in ecology*, Bulletin of Mathematical Biology **73** (2011), 2088–2108.

[24] V. Geist, *Behavior: Adaptive stratigies in mule deer*, Mule and black-tailed deer of North America (O. C. Wallmo, ed.), University of Nebraska Press, Lincoln, NE, pp. 157–223.

[25] G.Georgsson, S. Sigurdarson, and P. Brown, *Infectious agent of sheep scrapie may persist in the environment for a least 16 years*, Journal of General Virology **87** (2006), 3737–3740.

[26] J. E. Gross and M. W. Miller, *Chronic wasting disease in mule deer: Disease dynamics and control*, Journal of Wildlife Management **65** (2001), 205–215.

[27] E. M. Hanks, M. B. Hooten, L. R. McFarlane, and K. E. Mock, *Model-based approaches for characterizing spatial genetic flow*, JSM Proceedings, Biometrics Section, American Statistical Association, 2010.

[28] S. I. Higgins, D. M. Richardson, and R. M. Cowling, *Modeling invasive plant spread: The role of plant-environment interactions and model structure*, Ecology **77** (1996), 2043–2054.

[29] E. E. Holmes, M. A. Lewis, J. E. Banks, and R. R. Veit, *Partial differential equations in ecology: Spatial interactions and population dynamics*, Ecology **75** (1994), 17–29.

[30] M. H. Holmes, *Introduction to Perturbation Methods*, Springer-Verlag, New York, 1995.

[31] C. Homer, J. Dewitz, J. Fry, M. Coan, N. Hossain, C. Larson, N. Herold, A. McKerrow, J. N. VanDriel, and J. Wickham, *Completion of the 2001 National Land Cover Database for the conterminous United States*, Photogrammetric Engineering and Remote Sensing **73** (2007), 337–341.

[32] M. B. Hooten, M. J. Garlick, and J. A. Powell, *Advantageous change of support in inverse implementations of statistical differential equation models*, in JSM Proceedings, Section on Bayesian Statistical Science. Alexandria, VA: American Statistical Association (2009), 1847–1857.

[33] M. B. Hooten, D. S. Johnson, E. M. Hanks, and J. H. Lowry, *Agent-based inference for animal movement and selection*, Journal of Agricultural, Biological and Environmental Statistics **15** (2010), 523–538.

[34] P. R. Hosseini, A. A. Dhondt, and A. P. Dobson, *Spatial spread of an emerging infectious disease: Conjunctivitis in house finches*, Ecology **87** (2006), 3037–3046.

[35] JR. J. B. Dunning, D. J. Stewart, B. J. Danielson, B. R. Noon, T. L. Root, R. H. Lamberand, and E. E. Stevens, *Spatially explicit population models: Current forms and future uses*, Ecological Applications **5** (1995), 3–11.

[36] C. J. Johns and C. H. Mehl, *A dynamic spatial model for chronic wasting disease in Colorado*, Journal of Data Science **4** (2006), 21–37.

[37] C. J. Johnson, J. A. Pederson, R. J. Chappell, D. McKenzie, and J. M. Aiken, *Oral transmissibility of prion disease is enhanced by binding to soil particles*, Public Library of Science Pathogens **3** (2006), 874–881.

[38] D. S. Johnson, J. M. London, and C. E. Kuhn, *Bayesian inference for animal space use and other movement metrics*, Journal of Agricultural, Biological, and Environmental Statistics **16** (2011), 357–370.

[39] D. S. Johnson, J. M. London, M. Lea, and J. W. Durban, *Continuous-time correlated random walk model for animal telemetry data*, Ecology **89** (2008), 1208–1215.

[40] D. S. Johnson, D. L. Thomas, J. M. Ver Hoef, and A. Christ, *A general framework for the analysis of animal resource selection from telemetry data*, Biometrics **64** (2008), 968–976.

[41] D. O. Joly, M. D. Samuel, J. A. Langenberg, J. A. Blanchong, C. A. Batha, R. E. Rolley, D. P. Keane, and C. A. Ribic, *Spatial epidemiology of chronic wasting disease in Wisconsin white-tailed deer*, Journal of Wildlife Diseases **42** (2006), 578–588.

[42] A. Kallen, P. Arcui, and J. D. Murray, *A simple model for spatial spread and control of rabies*, Journal of Theoretical Biology **116** (1985), 377–393.

[43] P. Kareiva and G. Odell, *Swarms of predators exhibit "preytaxis" if individual predators use area-restricted search*, The American Naturalist **130** (1987), 233–270.

[44] P. M. Kareiva and N. Shigesada, *Analyzing insect movement as a correlated random walk*, Oecologia **56** (1983), 234–238.

[45] D. G. Kendall, *Mathematical Models of the Spread of Infection*, Medical Research Council, HMSO, London, 1965.

[46] H. Kierstead and L. B. Slobodkin, *The size of water masses containing plankton bloom*, Journal of Marine Research **12** (1953), 141–147.

[47] N. Kinezaki, K. Kawasaki, F. Takasu, and N. Shigesada, *Modeling biological invasions into periodically fragmented environments*, Theoretical Population Biology **64** (2003), 291–302.

[48] C. E. Krumm, M. M. Connor, and M. W. Miller, *Relative vulnerability of chronic wasting disease infected mule deer to vehicle collisions*, Journal of Wildlife Diseases **41** (2005), 503–511.

[49] T. E. Kucera, *Social behavior and breeding system of the desert mule deer*, Journal of Mammology **59** (1978), 463–476.

[50] M. A. Lewis, T. Hillen, and F. Lutscher, *Spatial dynamics in ecology*, IAS/Park City Mathematics Series **15** (2005), 3–21.

[51] J. David Logan, *Applied Mathematics*, Wiley-Interscience, New York, 2006.

[52] C. K. Mathiason, J. G. Powers, S. J. Dahmes, D. A Osborn, K. V. Miller, R. J. Warren, G. L. Mason, S. A. Hays, J. Hayes-Klug, D. M Seelig, M. A. Wild, L. L. Wolfe andf T. R Spraker, M. W. Miller andf C. J. Sigurdson, G. C. Telling, and E. A. Hoover, *Infectous prions in the saliva and blood of deer with chronic wasting disease*, Science **314** (2006), 133–136.

[53] L. R. McFarlane, *Breeding behavior and space use of male and female mule deer: An examination of potential risk differences for chronic wasting disease infection*, Master's thesis, Utah State University, 2007.

[54] ———, Personal Communication, 2012, Utah Division of Wildlife Resources.

[55] B. H. McRae, B. G. Dickson, T. H. Keitt, and V. B. Shah, *Using circuit theory to model connectivity in ecology, evolution, and conservation*, Ecology **89** (2008), 2712–2724.

[56] D. B. Meade and F. A. Milner, *SIR epidemic models with directed diffusion*, Applied Mathematics Monographs **3** (1992).

[57] M. W. Miller and M. M. Conner, *Epidemiology of chronic wasting disease in free-ranging mule deer: Spatial, temporal and demographic influences on observed prevelence patterns*, Journal of Wildlife Diseases **41** (2005), 275–290.

[58] M. W. Miller, N. Thompson Hobbs, and S. J. Tavener, *Dynamics of prion disease transmission in mule deer*, Ecological Applications **16** (2006), 2208–2214.

[59] M. W. Miller, H. M. Swanson, L.L. Wolfe, F. G. Quartarone, S. L. Huwer, C. H. Southwick, and P. M. Lukacs, *Lions, prions and deer demise*, Public Library of Science ONE **3** (2008), 1–7.

[60] M. W. Miller and M. A. Wild, *Epidemiology of chronic wasting disease in captive white-tailed and mule deer*, Journal of Wildlife Diseases **40** (2004), 320–327.

[61] M. W. Miller and E. S. Williams, *Prion disease: Horizontal prion transmission in mule deer*, Nature **425** (2003), 35–36.

[62] M. W. Miller, E. S. Williams, N. Thompson Hobbs, and L. L. Wolfe, *Environmental sources of prion transmission in mule deer*, Emerging Infectious Diseases **10** (2004), 1003–1006.

[63] M. W. Miller, E. S. Williams, C. W. McCarty, T. R. Spraker, T. J. Kreeger, C.T. Larsen, and E. T. Thorne, *Epizootiology of chronic wasting disease in free-ranging cervids in Colorado and Wyoming*, Journal of Wildlife Diseases **36** (2000), 676–690.

[64] A. R. Mitchell and D. F. Griffiths, *The Finite Difference Method in Partial Differential Equations*, John Wiley and Sons, New York, 1980.

[65] P. R. Moorcroft, M. A. Lewis, and R. L. Crabree, *Home range analysis using a mechanistic home range model*, Ecology **80** (1999), 1656–1665.

[66] J. D. Murray, *On pattern formation mechanisms for Lepidopteran wing patterns and mammalian coat markings*, Philosophical Transactions of the Royal Society Series B **295** (1980), 473–496.

[67] J. D. Murray and W. L. Seward, *On the spatial spread of rabies among foxes with immunity*, Journal of Theortical Biology **156** (1992), 327–348.

[68] J. D. Murray, E. A. Stanley, and D. L. Brown, *On the spatial spread of rabies among foxes*, Proceedings of Royal Society of London, B **229** (1986), 111–150.

[69] M. C. Nicholson, R. T. Bowyer, and J. G Kie, *Habitat selection and survival of mule deer: Tradeoffs associated with migration*, Journal of Mammology **78** (1997), 483–504.

[70] A. Okubo, *Diffusion and Ecological Problems: Mathematical Models*, Springer-Verlag, New York, 1980.

[71] A. Okubo and S. A. Levin, *Diffusion and Ecological Problems: Modern Perspective. Interdisciplinary Applied Mathematics*, Springer-Verlag, New York, 2001.

[72] R. S. Ostfeld, G. E. Glass, and F. Keesing, *Spatial epidemiology: An emerging (or re-emerging) discipline*, Trends in Ecology and Evolution **20** (2005), 328–336.

[73] O. Ovaskainen, *Habitat-specific movement parameters estimated using mark-recapture data and a diffusion model*, Ecology **85** (2004), 242–257.

[74] ———, *Analytical and numerical tools for diffusion-based movement models*, Theoretical Population Biology **73** (2008), 198–211.

[75] O. Ovaskainen and S. J. Cornell, *Biased movement at a boundary and conditional occupancy times for diffusion processes*, Journal of Applied Probability **40** (2003), 557–580.

[76] C. S. Patlak, *Random walk wtih persistence and external bias*, Bulletin of Mathematical Biophysics **15** (1953), 311–338.

[77] R. P. Pech and J. C. McIlroy, *A model of the velocity of advamce of foot and mouth disease in feral pigs*, Journal of Applied Ecology **27** (1990), 635–650.

[78] M. W. Pedersen, T. A. Patterson, U. H. Thygensen, and H. Madsen, *Estimating animal behavior and residency from movement data*, Oikos **120** (2011), 1281–1290.

[79] A. P. Plummer, D. R. Christensen, and S. B. Monsen, *Restoring big-game range in Utah*, Tech. report, Utah Division of Fish and Game, 1968.

[80] J. A. Powell and N. E. Zimmermann, *Multiscale analysis of active seed dispersal contributes to resolving Reid's Paradox*, Ecology **85** (2004), 490–506.

[81] R. Rasmussen, *Southeast Utah*, 2012, http://raysweb.net.

[82] L. A. Real and R. Biek, *Spatial dynamics and genetics of infectious diseases on heterogeneous landscapes*, Journal of the Royal Society Interface **4** (2007), 935–948.

[83] H. Risken, *The Fokker-Planck Equation: Methods of Solutions and Applications*, Springer, Berlin, 1989.

[84] C. P. Robert and G. Casella, *Monte Carlo Statistical Methods*, Springer-Verlag, New York, 1999.

[85] S. E. Saunders, S. L. Bartelt-Hunt, and J. C. Bartz, *Prions in the environment: Occurrence, fate, and mitigation*, Prion **2** (2008), 162–169.

[86] E. M. Schauber and A. Woolf, *Chronic wasting disease in deer and elk: A critique of current models and their application*, Wildlife Society Bulletin **31** (2003), 610–616.

[87] A. Sharp and J. Pastor, *Stable limit cycles and the paradox of enrichment in a model of chronic wasting disease*, Ecological Applications **21** (2011), 1024–1030.

[88] N. Shigesada and K. Kawasaki, *Biological Invasions: Theory and Practice*, Oxford University Press, Oxford-New York-Tokyo, 1997.

[89] C. J. Sigurdson, *A prion disease in cervids: Chronic wasting disease*, Veterinary Research **39** (2008), 41–53.

[90] J. G. Skellam, *Random dispersal in theoretical populations*, Biometrika **38** (1951), 196–218.

[91] D. L. Smith, B. Lucey, L. A. Waller, J. Childs, and L. A. Real, *Predicting the spatial dynamics of rabies epidemics on heterogeneous landscapes*, Proceedings of the National Academy of Sciences USA **99** (2002), 3368–3672.

[92] U.S. Geological Survey, *Multi-resolution land characteristics consortium*, 2001, http://www.mrlc.gov.

[93] ———, *The national map: LANDFIRE national existing vegetation type layer*, `http://gisdata.usgs.net/website/landfire/`, September 2006.

[94] N. W. Swindale, *A model for the formation of ocular dominance stripes*, Proceedings of the Royal Society of London Series B **208** (1980), 243–264.

[95] M. K. Tourtellot, R. D. Collins, and W. J. Bell, *The problem of movelength and turn definition in analysis of orientation data*, Journal of Theoretical Biology **150** (1991), 287–297.

[96] P. Turchin, *Translating foraging movements in heterogeneous environments into the spatial distribution of foragers*, Ecology **72** (1991), 1253–1266.

[97] ———, *Quantitative Analysis of Movement*, Sinauer Associates, Inc. Publishers, Sunderland, Massachusetts, 1998.

[98] P. Turchin and W. T. Thoeny, *Quantifying dispersal of southern pine beetles with mark-recapture experiments and a diffusion model*, Ecological Applications **3** (1993), 187–198.

[99] A. M. Turing, *The chemical basis of morphogenesis*, Philosophical transactions of the Royal Society of London Series B **237** (1952), 37–72.

[100] U.D.W.R., *Utah Division of Wildlife Resources: Chronic wasting disease in Utah*, 2012, http://wildlife.utah.gov.

[101] B. E. Watkins, C. J. Bishop, E. J. Bergman, A. Bronson, B. Hale, B. F. Wakeling, L. H. Carpenter, and D. W. Lutz, *Habitat guidelines for mule deer: Colorado plateau*

shrubland and forest ecoregion, Tech. report, Mule Deer Working Group, Western Association of Fish and Wildlife Agencies, 2007.

[102] R. C. Wiggins, *Prion stability and infectivity in the environment*, Neurochemnistry Research **34** (2009), 158–168.

[103] C. K. Wikle and M. B. Hooten, *A general science-based framework for nonlinear spatio-temporal dynamical models*, Test **19** (2010), 417–451.

[104] M. A. Wild, N. T. Hobbs, M. S. Graham, and M. W. Miller, *The role of predation in disease control: A comparison of selective and nonselective removal on prion disease dynamics in deer*, Journal of Wildlife Diseases **47** (2011), 78–93.

[105] E. S. Williams, *Chronic wasting disease*, Veterinary Pathology **42** (2005), 530–549.

[106] E. S. Williams and M. W. Miller, *Chronic wasting disease of deer and elk in North America*, O I E Revue Scientifique et Technique **21** (2002), 305–316.

[107] E. S. Williams and S. Young, *Chronic wasting disease of captive mule deer: A spongiform encephalopathy*, Journal of Wildlife Diseases **16** (1980), 90–98.

[108] K. A. With, *The landscape ecology of invasive spread*, Conservation Biology **16** (2002), 1192–1203.

APPENDIX

Numerical Method

For the non-homogenized model (2.4), let the spatial step be the same in both directions, i.e. $h = \Delta y_1 = \Delta y_2$ and let $k = \Delta\tau$. An alternating direction implicit (ADI) method for the non-homogenized model (2.4) has two equations for each time step, a discretization in the y_1 direction and a discretization in the y_2 direction:

$$\begin{aligned} I_{l,m}^{n+\frac{1}{2}} - \frac{k}{2h^2}\left(\mu_{l+1,m}I_{l+1,m}^{n+\frac{1}{2}} - 2\mu_{l,m}I_{l,m}^{n+\frac{1}{2}} + \mu_{l-1,m}I_{l-1,m}^{n+\frac{1}{2}}\right) - \frac{k}{2}\alpha_{l,m}I_{l,m}^{n+\frac{1}{2}} \\ = I_{l,m}^{n} + \frac{k}{2h^2}\left(\mu_{l,m+1}I_{l,m+1}^{n} - 2\mu_{l,m}I_{l,m}^{n} + \mu_{l,m-1}I_{l,m-1}^{n}\right) + \frac{k}{2}\alpha_{l,m}I_{l,m}^{n} \end{aligned}$$

and

$$\begin{aligned} I_{l,m}^{n+1} - \frac{k}{2h^2}\left(\mu_{l,m+1}I_{l,m+1}^{n+1} - 2\mu_{l,m}I_{l,m}^{n+1} + \mu_{l,m-1}I_{l,m-1}^{n+1}\right) - \frac{k}{2}\alpha_{l,m}I_{l,m}^{n+1} \\ = I_{l,m}^{n+\frac{1}{2}} + \frac{k}{2h^2}\left(\mu_{l+1,m}I_{l+1,m}^{n+\frac{1}{2}} - 2\mu_{l,m}I_{l,m}^{n+\frac{1}{2}} + \mu_{l-1,m}I_{l-1,m}^{n+\frac{1}{2}}\right) + \frac{k}{2}\alpha_{l,m}I_{l,m}^{n+\frac{1}{2}}. \end{aligned}$$

The superscript is the index for time, the first subscript is the index for y_1 and the second subscript is the index for y_2. Note that the motility coefficient, μ, is included inside of the central difference formula, since it is inside the Laplacian in (2.4).

For the homogenized model (2.15), let $h = \Delta x_1 = \Delta x_2$ and let $k = \Delta t$. Then the ADI method equations become

$$\begin{aligned} c_{l,m}^{n+\frac{1}{2}} - \frac{k}{2h^2}\bar{\mu}_{l,m}\left(c_{l+1,m}^{n+\frac{1}{2}} - 2c_{l,m}^{n+\frac{1}{2}} + c_{l-1,m}^{n+\frac{1}{2}}\right) - \frac{k}{2}\bar{\alpha}_{l,m}c_{l,m}^{n+\frac{1}{2}} \\ = c_{l,m}^{n} + \frac{k}{2h^2}\bar{\mu}_{l,m}\left(c_{l,m+1}^{n} - 2c_{l,m}^{n} + c_{l,m-1}^{n}\right) + \frac{k}{2}\bar{\alpha}_{l,m}c_{l,m}^{n} \end{aligned}$$

and

$$\begin{aligned} c_{l,m}^{n+1} - \frac{k}{2h^2}\bar{\mu}_{l,m}\left(c_{l,m+1}^{n+1} - 2c_{l,m}^{n+1} + c_{l,m-1}^{n+1}\right) - \frac{k}{2}\bar{\alpha}_{l,m}c_{l,m}^{n+1} \\ = c_{l,m}^{n+\frac{1}{2}} + \frac{k}{2h^2}\bar{\mu}_{l,m}\left(c_{l+1,m}^{n+\frac{1}{2}} - 2c_{l,m}^{n+\frac{1}{2}} + c_{l-1,m}^{n+\frac{1}{2}}\right) + \frac{k}{2}\bar{\alpha}_{l,m}c_{l,m}^{n+\frac{1}{2}}, \end{aligned}$$

where the coefficients, $\bar{\mu}$ and $\bar{\alpha} = \bar{\mu}\left\langle \frac{\alpha}{\mu} \right\rangle$ are the averaged coefficients in (2.15). The homogenization procedure brings the motility coefficient outside of the Laplacian, so $\bar{\mu}$ remains outside of the central difference formula.

The coupled system (3.21)-(3.23) is also solved numerically using an ADI scheme. For notational ease, let $u = c_{IF}$, $v = c_{IM}$, and $h = \langle H_0 \rangle$. The system becomes:

$$\partial_t u = \bar{\mu}_F \nabla_x^2 u + A_1 u + A_2 v + A_3 h,$$
$$\partial_t v = \bar{\mu}_M \nabla_x^2 v + B_1 v + B_2 u + B_3 h,$$

and

$$\frac{dh}{dt} = a_1 u + a_2 v - \delta h, \tag{7.1}$$

where the equations have been multiplied through by ω to return to the original time scale and the coefficients are defined as follows:

$$A_1 = \bar{\mu}_F \left\langle \left(\beta_{FF}\hat{S}_F - \omega - \phi\right)\frac{1}{\mu_F} \right\rangle, \quad B_1 = \bar{\mu}_M \left\langle \left(\beta_{MM}\hat{S}_M - \omega - \phi\right)\frac{1}{\mu_F} \right\rangle,$$

$$A_2 = \bar{\mu}_F \beta_{MF} \left\langle \frac{\hat{S}_F}{\mu_M} \right\rangle, \quad B_2 = \bar{\mu}_M \beta_{FM} \left\langle \frac{\hat{S}_M}{\mu_F} \right\rangle,$$

$$A_3 = \bar{\mu}_F \gamma_F \alpha_{DM} \left\langle \hat{S}_F \right\rangle, \quad B_3 = \bar{\mu}_M \gamma_M \alpha_{DM} \left\langle \hat{S}_M \right\rangle,$$

and

$$a_1 = \bar{\mu}_F^{-1}\left(\frac{\alpha_F}{\alpha_{DM}} + \frac{\alpha_{DF}}{\alpha_{DM}}\right), \quad a_2 = \bar{\mu}_M^{-1}\left(\frac{\alpha_M}{\alpha_{DM}} + \omega\right).$$

The method of integrating factors can be used to solve (7.1) to obtain

$$h = e^{-\delta t}\int_0^t e^{\delta s}(a_1 u + a_2 v)ds. \tag{7.2}$$

Applying the trapezoidal rule yields

$$h(t+\frac{k}{2}) = e^{\frac{-\delta k}{2}} h(t) + \frac{k}{4}\left(a_1 u\left(t+\frac{k}{2}\right) + a_2 v\left(t+\frac{k}{2}\right)\right) + \frac{k}{4} e^{\frac{-\delta k}{2}} \left(a_1 u(t) + a_2 v(t)\right) \quad (7.3)$$

Then the ADI method equations become

$$\begin{aligned} u_{l,m}^{n+\frac{1}{2}} - \frac{k}{2h^2}\bar{\mu}_{Fl,m}\left(u_{l+1,m}^{n+\frac{1}{2}} - 2u_{l,m}^{n+\frac{1}{2}} + u_{l-1,m}^{n+\frac{1}{2}}\right) - \frac{k}{2}A_{1l,m}u_{l,m}^{n+\frac{1}{2}} - \frac{k}{2}A_{2l,m}v_{l,m}^{n+\frac{1}{2}} \\ = u_{l,m}^{n} + \frac{k}{2h^2}\bar{\mu}_{Fl,m}\left(u_{l,m+1}^{n} - 2u_{l,m}^{n} + u_{l,m-1}^{n}\right) + \frac{k}{2}A_{1l,m}u_{l,m}^{n} \\ + \frac{k}{2}A_{2l,m}v_{l,m}^{n} + A_{3l,m}h_{l,m}, \end{aligned}$$

$$\begin{aligned} v_{l,m}^{n+\frac{1}{2}} - \frac{k}{2h^2}\bar{\mu}_{Ml,m}\left(v_{l+1,m}^{n+\frac{1}{2}} - 2v_{l,m}^{n+\frac{1}{2}} + v_{l-1,m}^{n+\frac{1}{2}}\right) - \frac{k}{2}B_{1l,m}v_{l,m}^{n+\frac{1}{2}} - \frac{k}{2}B_{2l,m}u_{l,m}^{n+\frac{1}{2}} \\ = v_{l,m}^{n} + \frac{k}{2h^2}\bar{\mu}_{Ml,m}\left(v_{l,m+1}^{n} - 2v_{l,m}^{n} + v_{l,m-1}^{n}\right) + \frac{k}{2}B_{1l,m}v_{l,m}^{n} \\ + \frac{k}{2}B_{2l,m}u_{l,m}^{n} + B_{3l,m}h_{l,m}, \end{aligned}$$

$$\begin{aligned} u_{l,m}^{n+1} - \frac{k}{2h^2}\bar{\mu}_{Fl,m}\left(u_{l,m+1}^{n+1} - 2u_{l,m}^{n+1} + u_{l,m-1}^{n+1}\right) - \frac{k}{2}A_{1l,m}u_{l,m}^{n+1} - \frac{k}{2}A_{2l,m}v_{l,m}^{n+1} \\ = u_{l,m}^{n+\frac{1}{2}} + \frac{k}{2h^2}\bar{\mu}_{Fl,m}\left(u_{l+1,m}^{n+\frac{1}{2}} - 2u_{l,m}^{n+\frac{1}{2}} + u_{l-1,m}^{n+\frac{1}{2}}\right) + \frac{k}{2}A_{1l,m}u_{l,m}^{n+\frac{1}{2}} \\ + \frac{k}{2}A_{2l,m}v_{l,m}^{n+\frac{1}{2}} + A_{3l,m}h_{l,m}, \end{aligned}$$

and

$$\begin{aligned} v_{l,m}^{n+1} - \frac{k}{2h^2}\bar{\mu}_{Ml,m}\left(v_{l,m+1}^{n+1} - 2v_{l,m}^{n+1} + v_{l,m-1}^{n+1}\right) - \frac{k}{2}B_{1l,m}v_{l,m}^{n+1} - \frac{k}{2}B_{2l,m}u_{l,m}^{n+1} \\ = v_{l,m}^{n+\frac{1}{2}} + \frac{k}{2h^2}\bar{\mu}_{Ml,m}\left(v_{l+1,m}^{n+\frac{1}{2}} - 2v_{l,m}^{n+\frac{1}{2}} + v_{l-1,m}^{n+\frac{1}{2}}\right) + \frac{k}{2}B_{1l,m}v_{l,m}^{n+\frac{1}{2}} \\ + \frac{k}{2}B_{2l,m}u_{l,m}^{n+\frac{1}{2}} + B_{3l,m}h_{l,m}, \end{aligned}$$

where (7.3) is treated as a forcing function.

First blank page

Second blank page

VITA

Martha J. Garlick

Contact Information:

Department of Mathematics and Statistics	Phone: 435-757-2896
Lund Hall 104	Phone (department): 435-797-2809
Utah State University	e-mail: marti.garlick@aggiemail.usu.edu
Logan, Utah	84322-3900

Education:

Degree	**Institution**	**Degree Date**
PhD, Mathematics	Utah State University	July 2012
MS, Mathematics	Utah State University	December 2007
BS, Mathematics	Utah State University	December 2003

Research Interests:

- Mathematical Biology
- Mathematical Ecology
- Applied mathematics
- Dynamical Systems

Academic Experience:

Institution	**Position**	**Dates**
Applied Biomathematics	Consultant	May 2012- Present
Setauket, NY		
Colorado College	Visiting Instructor	November-December 2011
Utah State University	Graduate Instructor	August 2005- May2008,
		May 2010-May 2012
Utah State University	Graduate Research Assistant	June-August 2007,
		May 2008-May 2010,
		May-August 2011
Utah State University	Research Assistant	January-August 2004

Publications:

1. M. Garlick, J. Powell, M. Hooten, and L. McFarlane, "A spatial model for chronic wasting disease in mule deer," In preparation for *Bulletin of Mathematical Biology*.

2. M. Hooten, M. Garlick, and J. Powell. "Computationally efficient statistical differential equation modeling using homogenization," in revision for *Computational Statistics*.

3. M. Garlick, J. Powell, M. Hooten, and L. McFarlane, "Homogenization of large-scale movement models in ecology," *Bulletin of Mathematical Biology*. 73: 2088-2108, 2011.

4. M. Garlick, J. Powell, D. Eyre, and T. Robbins, "Mathematically modeling PCR: An asymptotic approximation with potential for optimization," *Mathematical Biosciences and Engineering*. 7: 365-386, 2010.

5. M. Hooten, M. Garlick, and J. Powell, "Advantageous change of support in inverse implementations of statistical differential equation models." *JMS Proceedings*,

Section on Bayesian Statistical Science. Alexandria, BA: American Statistical Association. 1847-1857, 2009.

6. E. Stone, J. Goldes, and M. Garlick, "A multi-stage model for quantitative PCR," Technical report for the Department of Mathematical Sciences, University of Montana, 2006.

Conference Talks:

1. M. Garlick, J. Powell, M. Hooten, and L. McFarlane, "Homogenization of large-scale movement models in ecology with Application to Chronic Wasting Disease in Mule Deer," contributed talk, Joint Mathematics Meetings. Boston, MA, Jan 4, 2012.

2. B. M. Garlick, J. Powell, and M. Hooten, "Homogenization of large-scale movement models in ecology," contributed talk, 2010 Intermountain Section Meetings for the Mathematical Association of America. Logan, UT, March 26, 2010.

3. M. Garlick and J. Powell, "Mathematically modeling PCR: An asymptotic approximation," contributed talk, Joint Annual Meeting of the Society for Mathematical Biology and the Japanese Society for Mathematical Biology. San, Jose, CA, August 2, 2007.

4. M. Garlick and E. Stone, "A two-stage model for quantitative polymerase chain reaction", invited talk, SIAM Conference on Mathematics for Industry: Challenges and Frontiers, Detroit, MI, Oct 24, 2005.

Poster Presentations:

1. M. Garlick, J. Powell, and M. Hooten, "Homogenization of large-scale movement models in ecology with Application to Chronic Wasting Disease in ungulate populations," International Conference on Mathematical Biology and 2009 Annual Meeting of the Society of Mathematical Biology, Vancouver, Canada, July 30, 2009.

2. M. Garlick and J. Powell, "Mathematically modeling PCR: An asymptotic approximation," 2007 Graduate Research Symposium, Utah State University, 2007.

Courses Taught:

- Ordinary Differential Equations
- Linear Algebra and Differential Equations
- Linear Algebra
- Calculus I
- Business Calculus
- College Algebra
- Intermediate Algebra
- Beginning Algebra

I managed all aspects of teaching, including lecturing, structuring classroom learning, writing syllabi, writing exams, assigning homework, grading, holding office hours, etc.

Leadership:

USU chapter of the Association for Women in Mathematics

- President, April 2006-September 2007
- Program Chair, September 2007-April 2008.

Recognition and Awards:

- USU Department of Mathematics and Statistics PhD researcher of the year, 2012.
- The paper "Homogenization of large-scale movement models in ecology," (Bull Math Biol 2011) has been selected and evaluated by Otso Ovaskainen, a member of the Faculty of 1000 Biology, as a must read, 2011.

- USU Department of Mathematics and Statistics research writing award, 2011, 2008.
- USU College of Science Graduate Student Teacher of the Year, 2006.
- USU Department of Mathematics and Statistics teaching award, 2005, 2006, 2007.
- American Mathematical Society Travel Grant for Joint Mathematics Meetings. Boston, MA, 2012.
- Society for Mathematical Biology Travel Grant for International Conference on Mathematical Biology and 2009 Annual Meeting of the Society of Mathematical Biology, Vancouver, Canada, 2009.
- Society for Industrial and Applied Mathematics Travel Grant for SIAM Conference on Mathematics for Industry: Challenges and Frontiers, Detroit, MI, 2005.
- USU Graduate Student Senate Travel Grant, various conferences, 2007, 2009, 2012.
- USU Department of Mathematics and Statistics Travel Grant, various conferences, 2005, 2007, 2009, 2012.

Journals Reviewed For:

- *Journal of Mathematical Biology*

Professional Memberships:

- Society for Industrial and Applied Mathematics
- American Mathematical Society